A Study of the Paramagnetic Resonance and Transport Properties of Electrons in Gallium Phosphide

by

F. Thompson M.Sc.

Being a thesis

submitted to the University of Keele

for the Degree of Doctor of Philosophy

Department of Physics,
University of Keele,
Keele, Staffordshire.

September, 1969.

CONTENTS

Chapter 6 (continued)

ACKNOWLEDGEMENTS

The author would like to express his thanks to the following:

Professor D.J.E. Ingram, for providing facilities for research in his department.

Dr. G. Lancaster, for supervising the work.

Miss K.B. Davies, for her care and patience in typing this thesis.

Mrs. F. Thompson, for reading the proofs of this thesis and assisting with the diagrams.

Drs. B. Henderson and E.F. Slade, for the loan of their spectrometers.

Dr. R.D. Dowsing, for his assistance with the writing of the the computer programme.

All members of the Physics Department for their co-operation and assistance.

Mr. A.G. Smallman and other members of the Technical Staff, for their continued practical assistance.

The Plessey Company, for providing the Gallium Phosphide crystals.

The Science Research Council, for providing a maintenance grant.

INTERNATIONAL SYSTEM OF UNITS (S.I. UNITS)*

In this thesis physical quantities are generally expressed in the recommended S.I. units. There are, however, two exceptions which should be mentioned:

(i) Concentrations of impurity atoms and electrons are expressed in cm^{-3} since the cubic centimetre is, and will probably remain, a widely used unit of volume.

(ii) Electron and hole mobilities are expressed in $cm^2 volt^{-1} sec^{-1}$ since this is the unit of mobility which is used in virtually all of the relevant literature.

* Publication PD5686 (April 1967) of the British Standards Institution

ABSTRACT

The work described in this thesis is concerned with the transport properties and paramagnetic resonance of electrons from shallow donor impurities, namely, silicon, sulphur and tellurium, in gallium phosphide (GaP). The crystals of GaP, which had been grown by the epitaxial deposition from the vapour phase, were typically a few square millimeters in area and a hundred microns in thickness.

The measurement of the transport properties involved the determination of the conductivity and Hall constant for samples at temperatures in the range 4.2°K to 293°K. From the measurements on samples in the temperature range 100°K to 293°K values of the donor ionization energy and impurity concentrations have been calculated. The temperature dependence of the mobility has been discussed in terms of charge carrier scattering processes. The conductivity and Hall constant for samples at low temperatures (4.2°K to 100°K) have been interpreted in terms of impurity band conduction.

The electron paramagnetic resonance (E.P.R.) in n-type GaP has been investigated at frequencies of 10GHz, 35GHz and 70GHz for sample temperatures in the range 2.5°K to 100°K. In each case the E.P.R. spectra consisted of a single broad line and, for samples at 4.2°K, the linewidth was in the range 4.5 to 12.0mT. The g-value of

the resonance in GaP containing sulphur and tellurium impurities has been found to be 1.9996(±0.0002). To within the limits of experimental error, this g-value was found to be isotropic and independent of the sample temperature and of the impurity concentration in the sample. For the GaP sample containing silicon impurity the g-value of the resonance was found to be 1.9950(±0.0005). The measured g-values have been found to be in approximate agreement with the values calculated from the theory given by Roth. The magnitude and temperature dependence of the linewidth are discussed in terms of several relaxation processes.

CHAPTER I

INTRODUCTION

Since the discovery of the semiconducting properties of Indium Antimonide in 1950, great interest has been shown in the semiconducting Group III - V compounds which are formed from elements of Groups III and V of the Periodic Table. The prospect of commercial application of many of these compounds has led to significant advances in material preparation techniques and the production of single crystals of high purity. This availability of pure single crystals has, in turn, stimulated research into their fundamental semiconducting properties.

The transport properties of charge carriers in a semiconductor may be obtained from measurements of electrical conductivity and Hall effect. These measurements give information concerning the energy difference between the conduction and valence bands and of the energy levels associated with impurity atoms. Also, information is obtained regarding the number of charge carriers in the semiconductor and the scattering processes which effect their movement in the crystal. The experimental technique known as Electron Paramagnetic Resonance (E.P.R.) provides information about other electronic properties of semiconductors as will be described below.

In classical terms, E.P.R. is described as the resonant absorption of electromagnetic radiation, due to changes of orientation in a magnetic field of the magnetic moments associated with the spin

angular momentum of electrons. If a semiconductor is ideally pure and free from imperfections the valence electrons of the atoms are coupled so that their electron magnetic moments are aligned anti-parallel and the net magnetic moment of the material is zero. In this case the electrons are said to be "paired", the semiconductor is diamagnetic and E.P.R. can not be observed. However the presence of imperfections and impurities can give rise to situations in which the electron magnetic moments are not "paired"; in this case the semiconductor is paramagnetic and, in principle, E.P.R. may be observed.

In an intrinsic semiconductor the excitation of electrons from the valence band by thermal processes gives rise to "unpaired" electrons in the conduction band. However, practical difficulties, such as the relatively small number of conduction electrons and the short spin-lattice relaxation times, preclude their observation by E.P.R. technique and in fact E.P.R. has only been observed in extrinsic semiconductors.

The following types of impurities and imperfections in semiconductors have been investigated by E.P.R.:-

(a) The "shallow" donor and acceptor impurities.

(b) The delocalized electrons from "shallow" donor impurity atoms which are usually called "conduction electrons".

(c) Transition metal impurity atoms which often give rise to "deep" impurity centres.

(d) Localized imperfections such as interstitial atoms or vacant lattice sites.

(e) Surface imperfections which arise from incomplete bonding or chemical impurities at the surface of the crystal.

The E.P.R. spectra associated with the centres included under (c), (d) and (e) can be a source of information about the local environment of the centres. However, the spectra associated with the centres included under (a) and (b) can provide information about both the local environment of the centres and the energy band structure of the semiconductor because of the large spatial extent of the electronic wavefunctions associated with these centres.

The work described in this thesis is concerned with the study of E.P.R. and transport properties of electrons from shallow donor impurities in one of the Group III - V semiconductors, namely, Gallium Phosphide (GaP). At the time of the commencement of this work, there ~~was~~ were no data regarding the E.P.R. of electrons in n-type GaP and the measurements of the electronic transport properties had only been carried out on samples at temperatures in the range 77^{o}K to 300^{o}K. The concentration and type of impurities in some of these samples were not accurately known and discrepancies existed in the values of the donor ionization energies measured by different methods and by different workers. Also the electron scattering mechanisms were not well understood.

The aims of the present work were as follows. Firstly, the E.P.R. of electrons in n-type GaP was to be investigated and compared with the resonance of electrons from shallow donor impurities in other Group III - V compounds and the elemental semiconductors. Secondly, a study was to be made of the transport properties of electrons in samples in which the concentration of impurities had been carefully controlled in order to evaluate the donor ionization energies and elucidate the electronic scattering processes. It was also proposed to include measurements of the electronic transport properties on samples at temperatures in the range $4.2^{\circ}K$ to $300^{\circ}K$ in order to investigate the conduction processes over a wide temperature range. Thirdly, it was hoped that the above measurements would yield useful information concerning the energy band structure of GaP, in particular regarding the position in k-space of the minima of the conduction band, and also of the electronic structure of the shallow donor impurity atoms.

An outline of the relevant theory of the solid state is first given and this is followed by a short discussion on the preparation of GaP crystals and the diffusion of impurity atoms into these crystals. A brief review is then given of the experimental and theoretical information concerning the E.P.R. and transport properties of electrons from shallow donor impurities in semiconductors with specific reference to the work which has been carried out on n-type GaP.

There is then a general discussion of E.P.R. spectrometers together with a description of the modified Hilger & Watt's "Microspin" spectrometer which was used in the present work. The basic details of the low temperature cryostat and associated equipment are also described. This is followed by a short description of the apparatus used for the measurement of the electron transport properties of the GaP crystals.

Finally there is given an account and discussion of the results obtained from measurements of both E.P.R. and electron transport properties of the crystals together with recommendations for future work.

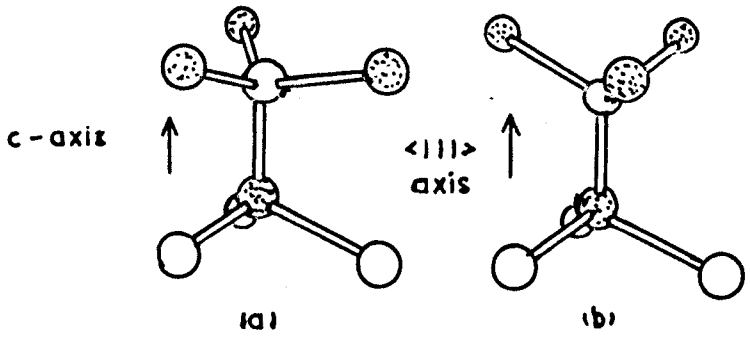

FIG. 2.1 ORIENTATION OF ADJACENT ATOMIC TETRAHEDRA SHOWING :-

(a) THE WURTZITE STRUCTURE

(b) THE ZINC BLENDE STRUCTURE.

[◎ and ○ denote atoms from different Groups.

◎——○ denotes a covalent bond.]

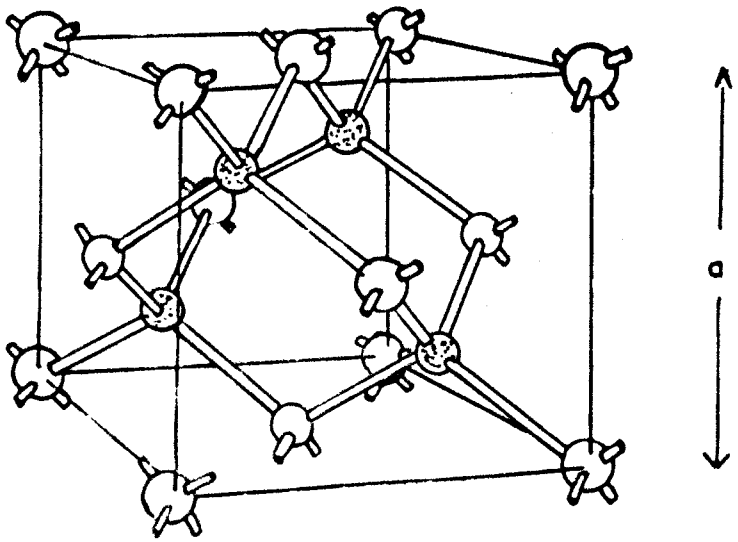

FIG. 2.2 ZINC BLENDE CRYSTAL STRUCTURE

[Lattice constant = a]

CHAPTER 2

SOME GENERAL ASPECTS OF SEMICONDUCTOR THEORY

2.1 Crystal Structure and Bonding

Nearly all the Group III - V compounds crystallize into structures in which an atom from one Group is at the centre of a regular tetrahedron formed from atoms of the other Group. These tetrahedra can be arranged in two ways as illustrated in Fig. 2.1. The arrangement shown in Fig. 2.1(a) gives rise to the wurtzite structure which has hexagonal symmetry; the arrangement shown in Fig. 2.1(b) gives rise to the zinc blende structure which has cubic symmetry and GaP has this latter crystal structure. The unit cell of the zinc blende structure is shown more clearly in Fig. 2.2.

The lattice constants at room temperature for some of the more common Group III - V compounds with the zinc blende structure are given in Table 2.1. (For comparison, the lattice constants for silicon and germanium are also given.)

Table 2.1

Lattice Constants for Silicon, Germanium and Some Group III - V Compounds (After Giesecke[1])

SEMICONDUCTOR	LATTICE CONSTANT (Å)
Boron Phosphide	4.538 (±0.001)
Boron Arsenide	4.777 (±0.001)
Gallium Phosphide	5.4505 (±0.0001)
Gallium Arsenide	5.65315 (±0.00010)
Indium Phosphide	5.86875 (±0.00010)
Indium Arsenide	6.05838 (±0.0005)
Indium Antimonide	6.47877 (±0.0005)
Silicon	5.40
Germanium	5.65

The tetrahedral coordination which occurs in semiconductors can be explained by the concept of covalent bonding. For instance, in the case of the elemental Group IV semiconductors the atoms have four valence electrons and in an isolated atom the electronic configuration of these electrons is ns^2, np^2. For the lowest energy configuration in the semiconductor crystals, however, the electrons are described by wavefunctions which are linear combinations of one atomic s-function

(or orbital) and three atomic p-functions (or orbitals) as follows:-

$$\begin{aligned} &\tfrac{1}{2}(s + p_x + p_y + p_z) \\ &\tfrac{1}{2}(s + p_x - p_y - p_z) \\ &\tfrac{1}{2}(s - p_x + p_y - p_z) \\ &\tfrac{1}{2}(s - p_x - p_y + p_z) \end{aligned} \qquad 2.1$$

These wavefunctions, which are usually referred to as "hybridized orbitals", give regions of greatest electron density in tetrahedral directions around the atom. The arrangement of the atomic cores, shown in Fig. 2.2, has the regions of high electron density along the bond directions and the covalent bond is formed by the electrostatic interaction of the neighbouring positively charged atomic cores with the regions of negative charge inbetween.

In the case of the Group III - V semiconductors the Group III and Group V atoms have three and five valence electrons respectively but covalent bonding may still take place, as outlined above, if an electron from a Group V atom is transferred to a Group III atom. This electron transfer also gives rise to ionic bonding between the atoms and it is found[2] that the bonding in Group III - V semiconductors is partly ionic and partly covalent. These compounds are therefore useful model solids in which to study the effects of bonding on physical phenomena since the bonding is intermediate between the predominantly ionic bond which occurs in the alkali halides

and the predominantly covalent bond which occurs in the elemental semiconductors.

2.2 The Band Structure of Semiconductors

Many of the electrical and optical properties of semiconductors can be explained in terms of their energy band structures. In recent years it has become increasingly important to have a detailed knowledge of semiconductor band structures for the design and analysis of the many new semiconductor devices and a great deal of effort, in both experimental and theoretical fields, has been applied to this problem. A comprehensive account of the band structures of Group IV, Group III - V and Group II - VI semiconductors has been given by Long[3].

A general statement about the wavefunctions of electrons in crystalline solids may be obtained from Group Theoretical arguments[4]. If a general lattice translation, $\underline{T}$, can be represented in the form

$$\underline{T} = m_1\underline{a}_1 + m_2\underline{a}_2 + m_3\underline{a}_3 \qquad 2.2$$

where $\underline{a}_1\ \underline{a}_2\ \underline{a}_3$ are the fundamental vectors of the direct lattice

and $m_1\ m_2\ m_3$ are integers

then the electronic wavefunctions must satisfy the equation

$$\psi_{\underline{k}}(\underline{r} + \underline{T}) = e^{i\underline{k}\cdot\underline{T}}\,\psi_{\underline{k}}(\underline{r}) \qquad 2.3$$

It can be shown[4] that the electronic wavefunctions which satisfy equation 2.3 can be of the form

$$\psi_{\underline{k}}(\underline{r}) = e^{i\underline{k}.\underline{r}}\, u_{\underline{k}}(\underline{r}) \qquad 2.4$$

where $u_{\underline{k}}(\underline{r})$ is a periodic function having the same spatial periodicity as the lattice

and $e^{i\underline{k}.\underline{r}}$ represents a plane wave with wave vector $\underline{k}$.

The wavefunctions given in equation 2.4 were first obtained by Bloch[5] and are referred to as Bloch functions.

It is convenient to represent the wave vectors $\underline{k}$ in a reciprocal lattice having basis vectors $\underline{b}_1$, $\underline{b}_2$, $\underline{b}_3$, which are defined as follows:-

$$\underline{b}_1 = \frac{2\pi(\underline{a}_2 \times \underline{a}_3)}{\underline{a}_1.(\underline{a}_2 \times \underline{a}_3)}$$

$$\underline{b}_2 = \frac{2\pi(\underline{a}_3 \times \underline{a}_1)}{\underline{a}_1.(\underline{a}_2 \times \underline{a}_3)} \qquad 2.5$$

$$\underline{b}_3 = \frac{2\pi(\underline{a}_1 \times \underline{a}_2)}{\underline{a}_1.(\underline{a}_2 \times \underline{a}_3)}$$

A general vector in reciprocal space may then be defined as

$$\underline{K} = n_1\underline{b}_1 + n_2\underline{b}_2 + n_3\underline{b}_3 \qquad 2.6$$

where n_1 n_2 n_3 are integers.

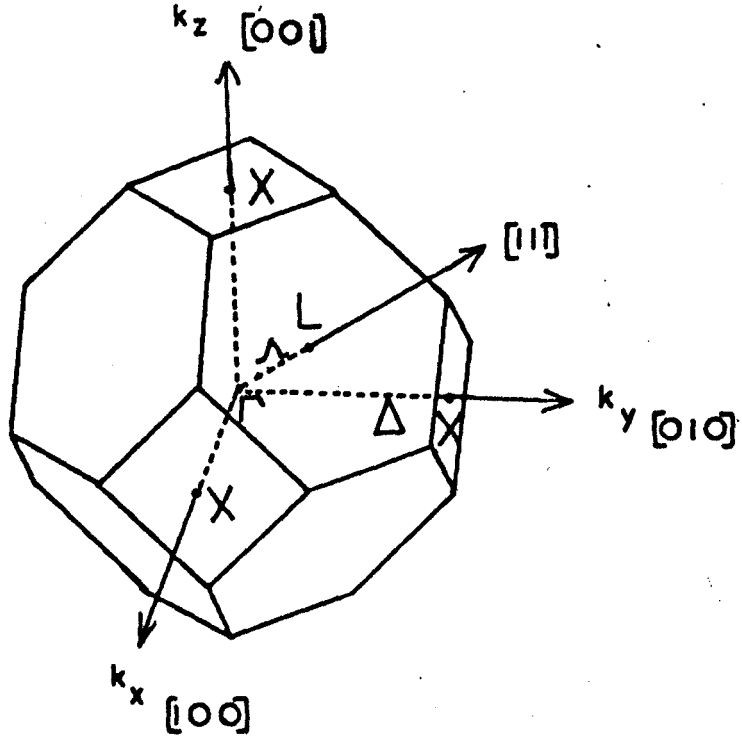

FIG. 2.3 THE FIRST BRILLOUIN ZONE FOR THE ZINC BLENDE CRYSTAL STRUCTURE.

It can be shown[4] that if two general vectors in $\underline{k}$-space, $\underline{k}_1$ and $\underline{k}_2$ satisfy the relation $\underline{k}_1 = \underline{k}_2 + \underline{K}$, then the Bloch functions $\psi_{\underline{k}_1}$ and $\psi_{\underline{k}_2}$ are physically equivalent. Consequently, the $\underline{k}$-values of all physically distinct solutions, $\psi_{\underline{k}}(\underline{r})$, can be plotted within a finite region of $\underline{k}$-space and this region is known as the first Brillouin zone. In Fig. 2.3 the first Brillouin zone for the zinc blende crystal structure is shown; the direction indices of the principal directions are given and the most important types of symmetry point and line are indicated in conventional Group Theoretical notation.

There are two different starting points in the theoretical determination of the band structures of semiconductors. Firstly, the valence electrons of the atoms may be described by the atomic orbitals of the isolated atom: calculations can then be made to see how the orbitals, and their corresponding energies, change when the atoms are placed at the lattice sites in the crystal. Secondly, the valence electrons of the atoms in the solid may be described by plane waves and the crystalline potential is then treated as a perturbation of the Hamiltonian of the free electron.

The first method, which involves the linear combination of atomic orbitals (L.C.A.O.) is useful in discussing the band structure in the region at the centre of the Brillouin zone. It was stated, in section 2.1, that the valence electrons of atoms in Group IV and Group III - V semiconductors may be described by a combination of one atomic s-orbital and three atomic p-orbitals. For an isolated atom the

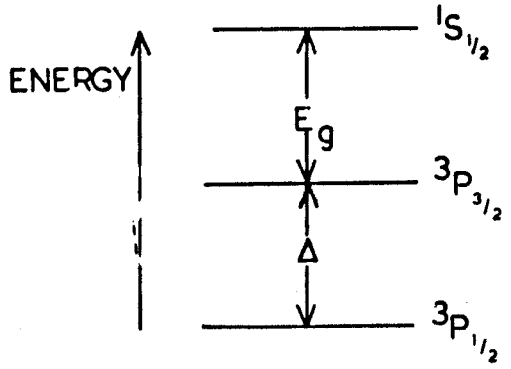

FIG. 2.4 ELECTRONIC ENERGY LEVELS FOR ELECTRONS DESCRIBED BY ATOMIC S- AND P- ORBITALS IN AN ISOLATED ATOM.

[Δ is the SPIN-ORBIT SPLITTING PARAMETER
NOMENCLATURE $^{2S+1}L_J$ is an atomic level
where S is the SPIN ANGULAR MOMENTUM quantum number
L is the ORBITAL -- -- -- --
J is the TOTAL -- -- -- --]

s-orbital gives rise to a higher electronic energy than the p-orbitals, also the p-orbitals give rise to different electronic energies because of the interaction between the spin angular momentum and the orbital angular momentum of an electron described by a p-orbital. If the assumption is made that the spin and orbital angular momenta conform to the Russell-Saunders coupling rules, the energy levels for the valence electrons in an isolated atom are as shown in Fig. 2.4.

As the isolated atoms are brought together the resultant wavefunctions of the valence electrons may be described in terms of the L.C.A.O. The energy band structure of the solid at $\underline{k} = 0$ will essentially be similar to that shown in Fig. 2.4 although the spin-orbit splitting, Δ, and the energy gap, E_g, for the solid is likely to be different from those values of the isolated atoms. It can be shown by Group Theoretical arguments[4] that the electronic level, $^1S_{\frac{1}{2}}$, of the isolated atom will become the conduction band in the solid and that the levels $^3P_{\frac{1}{2}}$, $^3P_{3/2}$ will become the "split" valence band.

For the calculation of the band structure of semiconductors at general points in the Brillouin zone, the second method, using plane wave functions, has proved more satisfactory than the L.C.A.O. method. In order to obtain the general features of energy bands in semiconductors, a fictitious lattice may be considered in which the translational periodicity is that of the actual semiconductor crystal but in which the value of the crystal potential is made vanishingly small (this is referred to as an "empty lattice"). The conduction electron energies

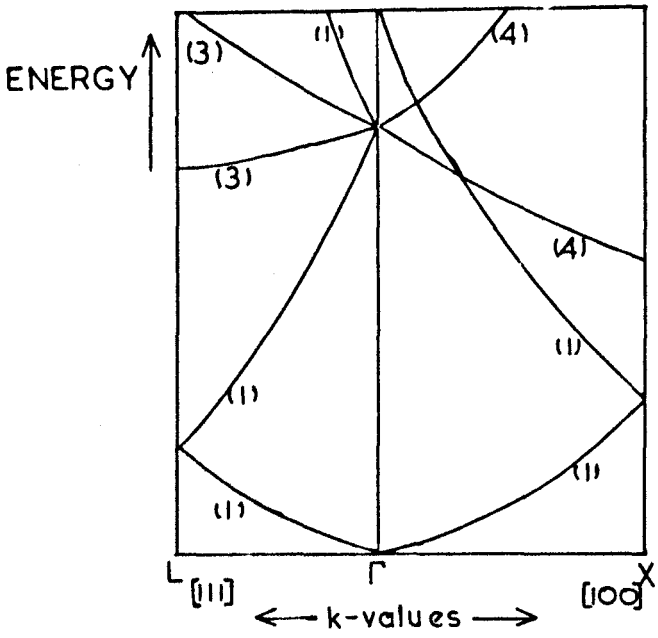

(n) indicates degeneracy

FIG. 2.5 ENERGY LEVELS FOR THE "EMPTY LATTICE" MODEL OF THE ZINC BLENDE CRYSTAL STRUCTURE.

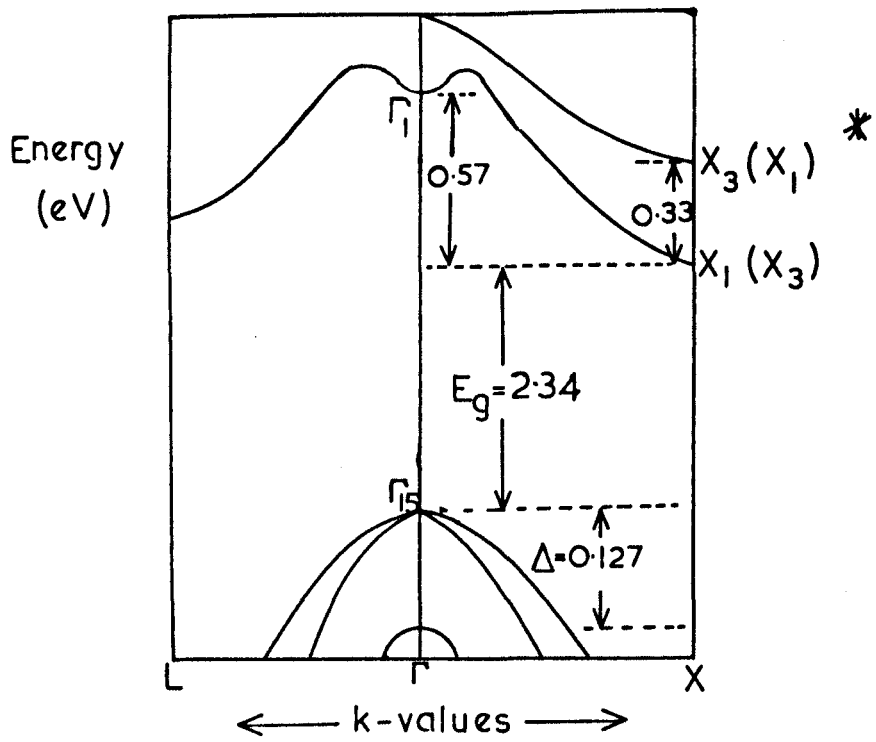

FIG. 2.6 ENERGY BAND STRUCTURE FOR GaP AT $0^{\circ}K$ (not to scale).

[*NOTATION after Morgan (10)
X_1 and X_3 are appropriate if the origin is at a Phosphorus atomic site.
(X_1) and (X_3) - - - - - - - - - - - - - - - - - - -
Gallium atomic site.]

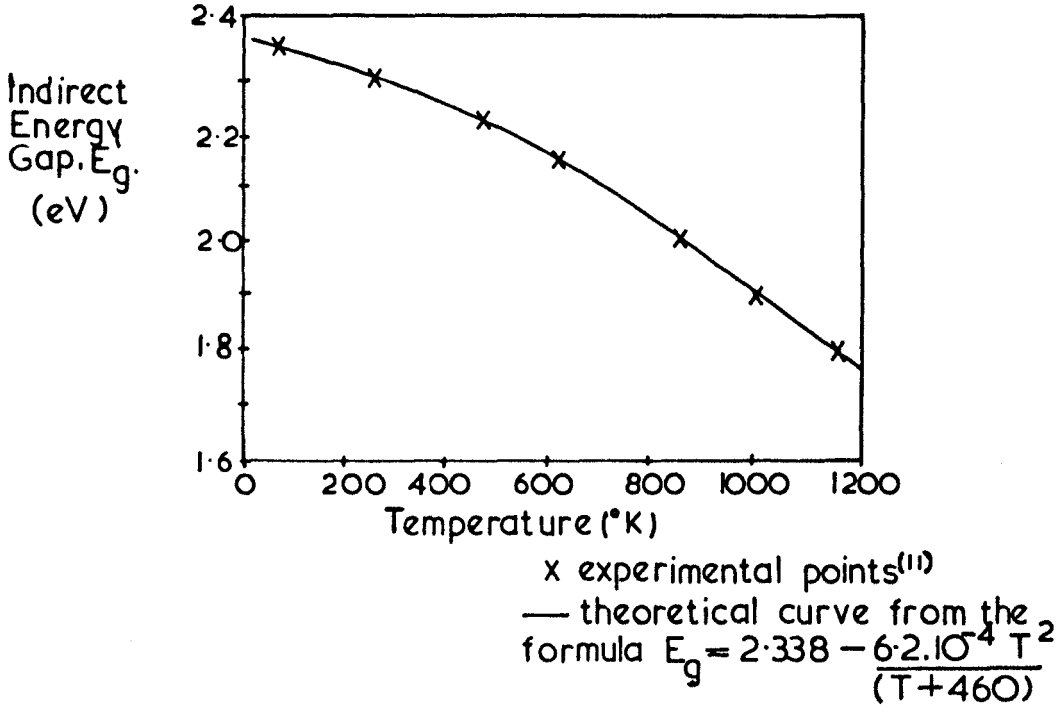

FIG. 2.7 ENERGY GAP AS A FUNCTION OF TEMPERATURE FOR GaP.

are then

$$E_{\underline{k}} = \frac{\hbar^2}{2m} |\underline{k} + \underline{K}|^2 \qquad 2.7$$

where m is the mass of a free electron

$\hbar = \frac{h}{2\pi}$ and h is Planck's constant

$\underline{K}$ is defined by equation 2.6.

and these are shown schematically in Fig. 2.5.

The introduction of the crystal potential gives rise to complex calculations for the electronic energies but the general form of the energy band diagram, shown in Fig. 2.5, remains the same although some of the degeneracies are removed. A method involving plane waves which has been particularly useful for band structure calculations in semiconductors is the orthogonalized plane wave (O.P.W.) method[6,7] and this method has recently been applied to calculations in the Group III - V compounds[8]. Other band structure calculations for the Group III - V compounds are discussed by Bassani[9].

The energy band structure for GaP is shown in Fig. 2.6 and the variation of the energy gap, Eg, with temperature is shown in Fig. 2.7. Semiconductors which have energy band structures like that of GaP, where the valence band maximum and conduction band minimum occur at different $\underline{k}$-values, are called "indirect band gap" semiconductors. Those with energy band structures where the valence band maximum and conduction band minimum occur at the same $\underline{k}$-value are called "direct band gap" semiconductors.

A comparison between various energy band parameters in GaP which have been obtained both theoretically and experimentally is given below in Table 2.2.

Table 2.2

Various Energy Band Parameters for GaP

PARAMETER	THEORETICAL VALUE[12,13]	EXPERIMENTAL VALUE
Δ	0.13eV	0.127eV[14]
$X_1 - X_3$	0.3eV	0.33eV[15]
$\Gamma_{15} - X_1$ (Eg)	2.3eV	2.34eV[11]
$m_\ell(X_1)$	1.15m	1.7m[16]
$m_t(X_1)$	0.28m	0.20m[16]
$m^*(X_1)$		0.35m[17]
	m is the mass of a free electron	

2.3 k.p Perturbation Method

Once the form of the energy band structure of a semiconductor has been established, the k.p perturbation method can be used to determine the band structure parameters more accurately at particular points in the Brillouin zone. It is also possible, by using the k.p method, to relate the various band structure parameters to each other.

A comprehensive account of this method has been given by Kane[18] and only a brief outline of the method will be given here with reference to the semiconductor Indium Antimonide.

The Schrödinger equation for an electron in a periodic potential V with the inclusion of the spin-orbit coupling term is as follows:

$$\left[\frac{\underline{p}^2}{2m} + V + \frac{\hbar}{2m^2}(\text{grad } V \times \underline{p}).\underline{\sigma}\right]\psi_{\underline{k}}(\underline{r}) = E_{\underline{k}}\psi_{\underline{k}}(\underline{r}) \qquad 2.8$$

where $\underline{p}$ is the momentum operator

$\underline{\sigma}$ is the Pauli spin operator

If the Bloch wavefunctions, as given in equation 2.4, are substituted in equation 2.8, then the following equation is obtained:-

$$\left[H_o + H_1 + H_2 + H_3\right]u_{\underline{k}}(\underline{r}) = \left[E_{\underline{k}} - \frac{\hbar^2|\underline{k}|^2}{2m}\right]u_{\underline{k}}(\underline{r}) \qquad 2.9$$

where $H_o = \frac{\underline{p}^2}{2m} + V$

$$H_1 = \frac{\hbar}{m}\underline{k}.\underline{p}$$

$$H_2 = \frac{\hbar}{4m^2}(\text{grad } V \times \underline{p}).\underline{\sigma}$$

$$H_3 = \frac{\hbar^2}{4m^2}(\text{grad } V \times \underline{k}).\underline{\sigma}$$

For small values of $\underline{k}$ the term $\frac{\hbar}{m}\underline{k}.\underline{p}$ may be treated as a spin-independent perturbation on the Hamiltonian H_o and the operators H_2 and H_3 are spin-dependent perturbations.

In the application of the $\underline{k}.\underline{p}$ perturbation method to InSb, Kane[18] represents the unperturbed wavefunctions at $\underline{k} = 0$ by an atomic s-function and three atomic p-functions. Each of these functions has associated with it two spin functions and so there are a total of eight "spin-orbital" functions.

The 8 x 8 secular determinant factorises to give:-

$$E' \left| E'(E' - E_g)(E' + \Delta) - |\underline{k}|^2 P^2 (E' + \tfrac{2}{3}\Delta) \right| = 0 \qquad 2.10$$

where $E' = E - \dfrac{\hbar^2 |\underline{k}|^2}{2m}$

E_g is the energy gap

Δ is the spin-orbit splitting parameter

P is the momentum matrix element connecting the conduction band with the valence band at $\underline{k} = 0$.

It follows from equation 2.10 that at $\underline{k} = 0$ there are four eigenvalues:

$$\begin{aligned} E_1 &= E_g \\ E_2 &= E_3 = 0 \\ E_4 &= -\Delta \end{aligned} \qquad 2.11$$

These eigenvalues may be identified with the energy level scheme shown in Fig. 2.4 with E_1 corresponding to the level $^1S_{\frac{1}{2}}$, E_2 and E_3 corresponding to the level $^3P_{3/2}$ and E_4 corresponding to the level $^3P_{\frac{1}{2}}$.

For $\underline{k}$ values close to $\underline{k} = 0$ the levels corresponding to those given in equation 2.11 are

$$E_1 = E_g + \frac{\hbar^2|\underline{k}|^2}{2m} + \frac{P^2|\underline{k}|^2}{3}\left[\frac{2}{Eg} + \frac{1}{(Eg + \Delta)}\right]$$

$$E_2 = \frac{\hbar^2|\underline{k}|^2}{2m}$$

$$E_3 = \frac{\hbar^2|\underline{k}|^2}{2m} - \frac{2P^2|\underline{k}|^2}{3Eg} \qquad 2.12$$

$$E_4 = -\Delta + \frac{\hbar^2|\underline{k}|^2}{2m} - \frac{P^2|\underline{k}|^2}{3(E_g - \Delta)}$$

Expressions for the effective mass (assumed to be isotropic) of electrons occupying these levels may be obtained from a comparison of the equations 2.12 with the following equations:

$$E_1 = Eg + \frac{\hbar^2|\underline{k}|^2}{2m_1^*}$$

$$E_2 = \frac{\hbar^2|\underline{k}|^2}{2m_2^*}$$

$$E_3 = \frac{\hbar^2|\underline{k}|^2}{2m_3^*} \qquad 2.13$$

$$E_4 = -\Delta + \frac{\hbar^2|\underline{k}|^2}{2m_4^*}$$

In particular, for the energy level E_1, the expression for the effective mass becomes

$$\frac{1}{m_1^*} = \frac{1}{m} + \frac{2P^2}{3\hbar^2}\left[\frac{2}{Eg} + \frac{1}{(Eg + \Delta)}\right] \qquad 2.14$$

The application of the k.p perturbation method to the band structure calculations of indirect band gap semiconductors is more complex than the previous analysis, but recently the method has been applied in the theoretical analysis of the band structure of GaP[13].

To summarise, it can be stated that the k.p perturbation method is semi-empirical in the sense that measured values of parameters such as Eg and Δ must be incorporated into the method if it is to yield quantitative results. However, it is most useful in providing a means of analysing experimental data in terms of an energy band structure diagram.

The k.p perturbation method will again be discussed in connection with the E.P.R. of electrons in semiconductors.

2.4 Impurities in Semiconductors

In the previous section it was assumed that the semiconductor crystals were free from any impurity. Such crystals can never be prepared in reality and, in the case of GaP, there is an atomic impurity concentration of approximately 1 part in 10^6 in the most pure crystals[19]. The effects of impurities in semiconductors will be discussed in this section.

Impurities are classified according to the positions of their electronic energy levels on the energy band diagram. The "shallow"

donor and acceptor impurities give levels close to (within the range OeV to 0.1eV) the conduction band and valence band respectively. The "deep" impurities give levels in the region towards the middle of the energy gap. A discussion of the "shallow" donor impurities will now be given in some detail since most of the work described in this thesis is concerned with this type of impurity. Only a brief reference will be made to "deep" impurities and "shallow" acceptor impurities will not be discussed.

If a Group VI atom is substituted for a Group V atom in a Group III - V semiconductor then the Group VI atom has an excess valence electron with respect to the Group V atom which it has replaced. This excess electron, which does not take part in the tetrahedral bonding, is only weakly bound to its parent atom and can move in a highly delocalized orbit with an effective mass, m^*, close to that of a conduction electron. The Coulombic attraction between the parent atom and this electron when the separation is r, can be written in terms of a potential energy, U, where

$$U = \frac{-e^2}{4\pi\varepsilon_o\varepsilon r} \qquad 2.15$$

where ε is the relative permittivity of the semiconductor

ε_o is the permittivity of free space.

The quantum mechanical description of these weakly bound electrons was first treated by Mott and Gurney[20] using the following Schrödinger equation:

$$\left[\frac{-\hbar^2 \nabla^2}{2m^*} - \frac{e^2}{4\pi\varepsilon_o \varepsilon r} \right] \psi_{\underline{k}}(\underline{r}) = E_{\underline{k}} \psi_{\underline{k}}(\underline{r}) \qquad 2.16$$

This equation is only valid if r is greater than several lattice spacings since otherwise the permittivity, ε, cannot be defined.

The equation 2.16 is of the hydrogen atom type and the eigenvalues are accordingly

$$E_n = -\frac{m^*}{m} \frac{W_H}{n^2 \varepsilon^2} \qquad 2.17$$

where E_n is the energy difference between the level and the conduction band minimum,

n takes the values 1, 2, 3 etc.

and W_H is the energy of the ground state of the hydrogen atom (W_H = 13.6eV).

If experimentally determined values of m^* and ε, for GaP[2], are substituted into equation 2.17, a ground state impurity level, E_D, of approximately -0.1eV is obtained. The parameter, E_D, is called the donor ionization energy since it represents the amount of energy needed to free an electron from its parent atom.

The wavefunctions for electrons described by equation 2.16 are obtained in terms of Wannier functions[21], denoted by F(r).

These functions are formed by making linear combinations of Bloch functions and have the property of being localized at a particular lattice site. The total electronic wavefunction is given by

$$\psi_{\underline{k}}(\underline{r}) = F(\underline{r}) \sum_{\underline{k}} \exp(i\, \underline{k}.\underline{r})\, u_{\underline{k}}(\underline{r}) \qquad 2.18$$

If only the electrons near the conduction band minima are considered, the equation 2.18 is approximated to

$$\psi_{\underline{k}}(\underline{r}) = F(\underline{r}) \exp(i\, \underline{k}_o.\underline{r})\, u_{\underline{k}_o}(\underline{r}) \qquad 2.19$$

where $\underline{k}_o$ is the value of $\underline{k}$ at which the conduction band minimum occurs.

The band structure of GaP, as illustrated in Fig. 2.6), shows that there are equivalent conduction band minima in the (100) type directions. There is an equal probability that an electron from a donor impurity in GaP may occupy states in the vicinity of any one of these minima and the complete electronic wavefunction is, therefore, of the form:

$$\psi_{\underline{k}}^{(i)}(\underline{r}) = \sum_{j} \alpha_j^{(i)} F_j(\underline{r}) e^{i\underline{k}_o{}^j.\underline{r}}\, u_{\underline{k}_o}{}^j(\underline{r}) \qquad 2.20$$

where $e^{i\underline{k}_o{}^j.\underline{r}}\, u_{\underline{k}_o}{}^j(\underline{r})$ is the Bloch wavefunction at the j^{th} minimum (valley),

$F_j(\underline{r})$ is the hydrogenic envelope function at the j^{th} valley,

$\alpha_j^{(i)}$ is a coefficient which describes the relative contribution from the j^{th} valley

and the superscript (i) have the values 1, 2 ...6.

The band structure of the elemental semiconductor, Si, also has equivalent conduction band minima in the (100) type directions and Kohn and Luttinger[22] have used wavefunctions of the form given in equation 2.20 to describe electrons from donor impurities in Si. The values of $\alpha_j^{(i)}$ are as follows:

$$
\begin{aligned}
&A_1 \text{ singlet} && \alpha_j^{\,1} = {}^1/\sqrt{6}\ (1, 1, 1, 1, 1, 1) \\
&E_1 \text{ doublet} && \alpha_j^{\,2} = {}^1/\sqrt{12}\ (1, 1, 1, 1, -2, -2) \\
& && \alpha_j^{\,3} = {}^1/_2\ \ (1, 1, -1, -1, 0, 0) \\
&T_2 \text{ triplet} && \alpha_j^{\,4} = {}^1/\sqrt{2}\ (1, -1, 0, 0, 0, 0) \\
& && \alpha_j^{\,5} = {}^1/\sqrt{2}\ (0, 0, 1, -1, 0, 0) \\
& && \alpha_j^{\,6} = {}^1/\sqrt{2}\ (0, 0, 0, 0, 1, -1)
\end{aligned}
\qquad 2.21
$$

(a detailed derivation of the values of $\alpha_j^{(i)}$ by Group Theoretical methods is given in Appendix I.)

Only the singlet state gives a non-zero electron probability density at the donor impurity nucleus and E.P.R. measurements on phosphorus-doped silicon give a clear indication that the singlet state is the ground state since an isotropic hyperfine interaction between the electron and the phosphorus nucleus is observed.

Group VI impurity atoms in GaP occupy phosphorus atomic sites and the wavefunctions corresponding to the conduction band minima have s-like symmetry (i.e. X_1 represents a conduction band minimum as shown in Fig. 2.6). There is evidence from electrical conductivity

measurements on Te-doped GaP[23] that the conduction band minima occur inside the Brillouin zone boundary as in the band structure of Si. The donor wavefunctions will, in this case, be of the form given in equation 2.21. From optical absorption data[10], however, there is evidence to suggest that the conduction band minima occur at the Brillouin zone boundary. In this latter case the values of $\alpha_j^{(i)}$ are as follows: (see Appendix I)

$$\begin{aligned} A_1 \text{ singlet} \quad & \alpha_j^{\,1} = {}^1/\sqrt{3} \quad (1, 1, 1) \\ E_1 \text{ doublet} \quad & \alpha_j^{\,2} = {}^1/_2 \quad (1, -2, 1) \\ & \alpha_j^{\,3} = {}^1/\sqrt{2} \quad (1, 0, -1) \end{aligned} \qquad 2.22$$

Group IV impurity atoms can be substituted into Group III - V compounds in three possible ways. Firstly, they can occupy only one sublattice; they then act exclusively as donor impurities when they occupy Group III atomic sites and as acceptor impurities when they occupy Group V sites. Secondly, the impurity atoms may be located on neighbouring lattice sites as pairs and thereby remain electrically neutral. Thirdly, the impurity atoms may be distributed on the two sublattices; the question of which sublattice is more heavily doped may then depend on the nature and concentration of the impurities.

In the case of Si-doped GaP with atomic impurity concentrations of less than $5 \times 10^{18} cm^{-3}$ it has been shown[24] that the silicon atoms behave as donor impurities and, presumably, occupy gallium sites.

Expressions for the wavefunctions of electrons from the silicon impurity atoms can be obtained (see Appendix I) bearing in mind that, in this situation, the wavefunctions corresponding to the conduction band minima have p-like symmetry (i.e. X_3 represents a conduction band minima as shown in Fig. 2.6). If the conduction band minima occur inside the Brillouin zone boundary then the values of $\alpha_j^{(i)}$ are of the form given in equation 2.21. However, if the conduction band minima occur at the Brillouin zone boundary, the values of $\alpha_j^{(i)}$ are as follows: (see Appendix I)

$$\begin{aligned} T_2 \text{ triplet} \quad \alpha_j^1 &= (1, 0, 0) \\ \alpha_j^2 &= (0, 1, 0) \\ \alpha_j^3 &= (0, 0, 1) \end{aligned} \qquad 2.23$$

The possible differences between the E.P.R. spectra of electrons occupying singlet and triplet states will be discussed in chapter 7.

The transition metal impurities in Group III - V semiconductors often form "deep" levels which are closer to the valence band than to the conduction band. The position of the energy levels corresponding to these impurities may be estimated theoretically using crystal field theory[25] and for the case of cobalt impurity in GaP the calculated position of the energy level is in good agreement with that given by optical measurements[25].

The positions of the energy levels of some impurities in GaP are shown below in Table 2.3; the values of E_D and E_A are taken respectively as the energy difference between the level and the conduction band minimum and the level and the valence band maximum.

Table 2.3

Positions of the Energy Levels of Some Impurities in GaP

Impurity	Energy (eV)	Type of Measurement and Reference
Sulphur	E_D = 0.093 (±0.005)	conductivity measurement[24] donor concentration $N_D = 1.0 \times 10^{18} cm^{-3}$ acceptor concentration $N_A = 1.2 \times 10^{17} cm^{-3}$
	E_D = 0.110 (±0.010)	optical measurement[26] impurity concentration not specified
Tellurium	E_D = 0.072 (±0.005)	conductivity measurement[16] $N_D = 9.8 \times 10^{17} cm^{-3}$, $N_A = 1.5 \times 10^{17} cm^{-3}$
	E_D = 0.095 (±0.010)	optical measurement[26] impurity concentration not specified
Silicon	E_D = 0.078 (±0.005)	conductivity measurement[24] $N_D = 1.2 \times 10^{18} cm^{-3}$, $N_A = 1.0 \times 10^{17}$
	E_D = 0.080 (±0.010)	optical measurement[27] impurity concentration not specified
Cobalt	E_A = 0.41 (±0.05)	theoretical calculation and optical measurement[25] impurity concentration not specified
Copper	E_A = 0.68 (±0.05)	optical measurement[2] impurity concentration not specified

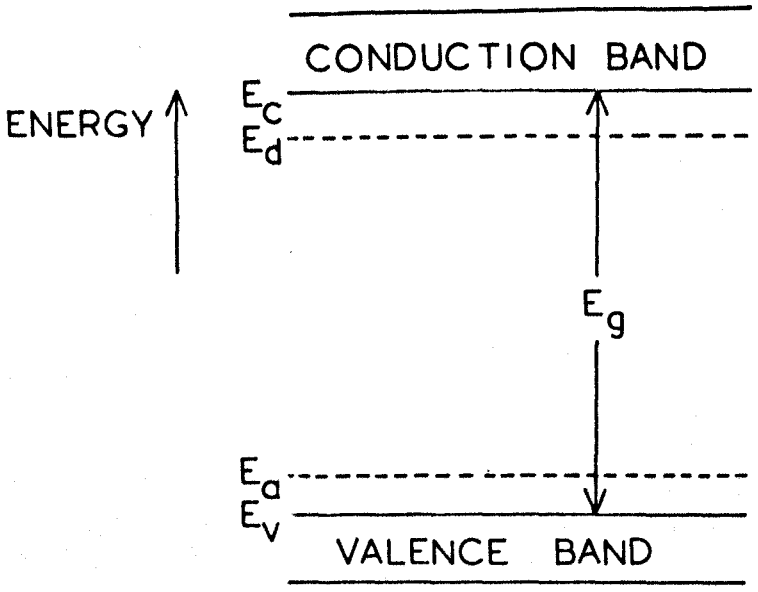

FIG.2.8 DIAGRAMATIC FORM OF THE ENERGY LEVELS IN A SEMICONDUCTOR.

E_c is the energy at the bottom of the conduction band.
E_d is the energy of a donor level.
E_a is the energy of an acceptor level.
E_v is the energy at the top of the valence band.

2.5 Fermi-Dirac Statistics

If the energy level structure of an intrinsic or extrinsic semiconductor is known, then the distribution of electrons in the energy levels may be determined by the Fermi-Dirac distribution law. The energy level structure is usually represented diagrammatically as shown in Fig. 2.8, and the value of E_g is that of the energy separation between the valence band maximum and the conduction band minimum. In the evaluation of the distribution of electrons in the energy levels of an n-type semiconductor it is convenient to choose a "zero" of energy at the bottom of the conduction band and therefore in the following discussion $E_c = 0$.

The probability that a level with energy E shall be occupied is given by F(E), the Fermi-Dirac distribution function, where

$$F(E) = \frac{1}{\exp\left(\frac{E - E_F}{kT}\right) + 1} \qquad 2.24$$

where E_F is the Fermi Energy and is defined as that energy at which the function $F(E) = \frac{1}{2}$.

If the number of electrons per unit energy range per unit volume is n(E), then the number of electrons per unit volume with energies between E and E + dE is

$$n(E)dE = F(E)\, N(E)\, dE \qquad 2.25$$

where N(E) is the electron density of states function.

For a semiconductor with an energy level structure as shown in Fig. 2.8 and with donor and acceptor impurity concentrations of N_D and N_A respectively, it can be shown[28] that charge conservation demands that

$$\frac{2N_c}{\sqrt{\pi}} F_{\frac{1}{2}}(\eta_F) = \frac{N_D}{1 + D_D^{-1}\exp(\eta_D + \eta_F)} - \frac{N_A}{1 + D_A^{-1}\exp(-\eta_A - \eta_F)} + \frac{2N_v}{\sqrt{\pi}} F_{\frac{1}{2}}(-\eta_F - \eta_G) \qquad 2.26$$

Here $\eta_F = E_F/kT$, $\eta_D = E_D/kT$, $\eta_A = E_A/kT$, $\eta_G = E_g/kT$

$$N_c = 2\left(\frac{2\pi m_n^* kT}{h^2}\right)^{3/2}$$

$$N_v = 2\left(\frac{2\pi m_p^* kT}{h^2}\right)^{3/2}$$

and m_n^* and m_p^* are respectively the "density of states" effective masses of the electrons in the conduction band and holes in the valence band.

$F_{\frac{1}{2}}(\eta_F)$ and $F_{\frac{1}{2}}(-\eta_F - \eta_G)$ are referred to as Fermi integrals for which there are tabulated values[29].

D_D and D_A are degeneracy factors which have the value 2 for isolated levels.

In the application of equation 2.26 to determine the position of the Fermi level in n-type GaP certain approximations can be made. Since the value of E_g in GaP is large the term $F_{\frac{1}{2}}(-\eta_F - \eta_G)$ is small

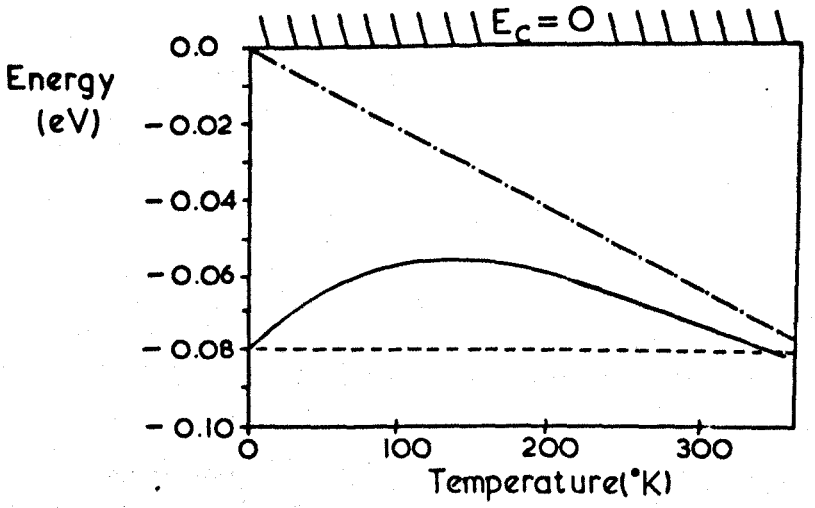

FIG. 2.9 TEMPERATURE VARIATION OF THE FERMI LEVEL IN n-TYPE GaP.

---- Impurity energy level $E_D = -.08$ eV

—·— Energy, E', given by $E' = -2kT$

——— Calculated position of the Fermi level, E_F, for the following parameters:-

$N_D = 10^{18}\ cm^{-3}$

$N_A = 10^{17}\ cm^{-3}$

compared with the other terms in equation 2.26 and therefore can be ignored. Also, if it is assumed that the acceptor level is near the valence band then the factor $\exp(-\eta_A - \eta_F)$ is small compared with unity and can be neglected. The equation 2.26 is then written as

$$\frac{2N_c}{\sqrt{\pi}} F_{\frac{1}{2}}(\eta_F) = \frac{N_D}{1 + D_D^{-1}\exp(\eta_D + \eta_F)} - N_A \qquad 2.27$$

If the values $N_D = 10^{18}cm^{-3}$, $N_A = 10^{17}cm^{-3}$, $E_D = -0.08eV$ and $D_D = 2$ are substituted into equation 2.27, the variation of the Fermi level with temperature can be obtained by numerical solution and this is shown in Fig. 2.9. It is observed from Fig. 2.9 that the energy separation between the conduction band and the Fermi level is greater than the energy corresponding to 2kT within the temperature range 300^oK to 0^oK, and the concentration of electrons in the conduction band, n, is given by the equation

$$n = N_c \exp(E_F/kT) \qquad 2.28$$

The Fermi energy, E_F, may be eliminated from equation 2.27 by substitution from equation 2.28 to give

$$\frac{n(n + N_A)}{(N_D - N_A - n)} = N_c' \, Y \exp(-E_D/kT) \qquad 2.29$$

where $N_c' = 2\left(\frac{2\pi mkT}{h}\right)^{3/2}$

$$Y = \left(\frac{m_n^*}{m}\right)^{3/2} D_D^{-1}$$

The equation 2.29 is in agreement with that given by Montgomery[23] and will be discussed again in connection with the transport properties of electrons in GaP.

The parameter E_D is taken as the energy difference between the ground state energy level of the impurity atom and the minimum of the conduction band. The effect of the excited energy levels of the impurity atom will not be discussed here but details of how to take account of these levels of the impurity atoms, when interpreting the transport properties of electrons in semiconductors, have been given elsewhere[30].

REFERENCES

1. G. Giesecke, Semiconductors and Semimetals, 2 67, "Physics of III - V Compounds" (Academic Press 1966).
2. O. Madelung, "Physics of III - V Compounds" (Wiley 1964).
3. D. Long, "Energy Bands in Semiconductors" (Interscience 1968).
4. Standard texts on the theory of solid state:
   M. Tinkham, "Group Theory" (McGraw-Hill 1964)
   J. Callaway, "Energy Band Theory" (Academic Press 1964).
5. F. Bloch, Z. Phys., 57 555 (1928).
6. C. Herring, Phys. Rev., 57 1169 (1940).
7. J.C. Slater, "Quantum Theory of Solids" (McGraw-Hill 1966).
8. F. Bassani and M. Yoshimine, Phys. Rev., 130 20 (1963).
9. F. Bassani, Semiconductors and Semimetals, 1 21, "Physics of III - V Compounds" (Academic Press 1966).
10. T.N. Morgan, Phys. Rev. Lett., 21 819 (1968).
11. M.B. Parrish and H.C. Casey, J. Appl. Phys., 40 163 (1969).
12. M.L. Cohen and T.K. Bergstresser, Phys. Rev., 141 789 (1966)
13. F.H. Pollack et al., Proc. Int. Conf. on Phys. Semiconductors (Kyoto), J. Phys. Soc. Japan, 21 (suppl.) 20 (1966).
14. J.W. Hodby, Proc. Phys. Soc. (London), 82 324 (1963).
15. R. Zallen and W. Paul, Phys. Rev., 134 1628 (1964).
16. H.C. Montgomery, J. Appl. Phys., 39 2002 (1968).
17. T.S. Moss et al., Proc. Int. Conf. on Phys. Semiconductors (Exeter) Inst. Phys. Soc., p.295 (1962).

18. E.O. Kane, Semiconductors and semimetals, 1 75, "Physics of III - V Compounds" (Academic Press 1966).

19. R. Nicklin, private communication. Plessey Company Ltd., Allen Clark Research Laboratories, Caswell, Towcester, Northants.

20. N.F. Mott and R.W. Gurney, "Electronic Processes in Ionic Crystals" (Oxford 1940).

21. G. Wannier, Phys. Rev., 52 191 (1937).

22. W. Kohn and J.M. Luttinger, Phys. Rev., 98 915 (1955).

23. H.C. Montgomery, J. Appl. Phys., 39 2002 (1968).

24. H.C. Montgomeryand W.L. Feldman, J. Appl. Phys., 36 3228 (1965).

25. J.W. Allen, Proc. Int. Conf. on Phys. of Semiconductors (Paris) p.781 (1964).

Proc. Int. Conf. on Phys. of Semiconductors (Kyoto) J. Phys. Soc. Japan, 21 239 (1966).

26. M. Gershenzon et al., Phys. Rev., 133 269 (1964).

27. P.J. Dean et al., J. Appl. Phys., 39 5631 (1968).

28. R.A. Hunter et al., Philips Res. Reports, 5 188 (1950).

29. J. McDougall and E.C. Stoner, Phil. Trans., A237 67 (1929).

30. P.T. Landsberg, Proc. Phys. Soc. (London), B69 1056 (1956).

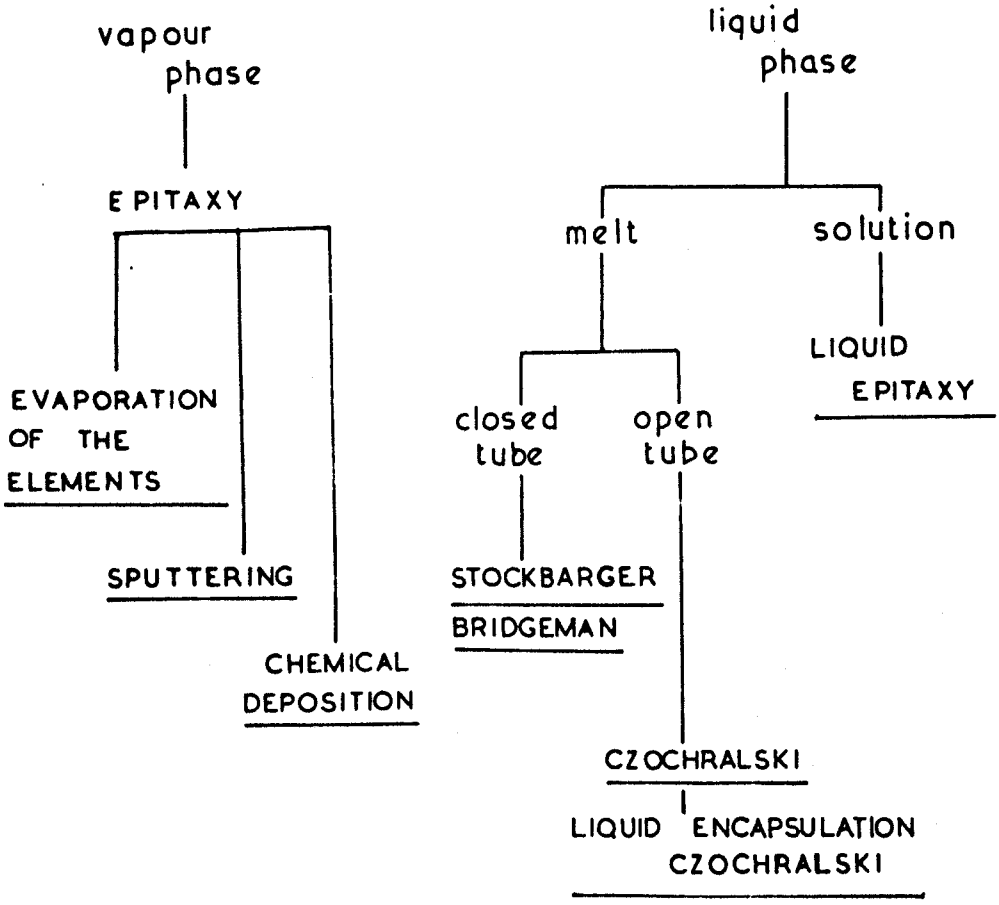

FIG. 3.1 SEMICONDUCTOR CRYSTAL GROWING TECHNIQUES.

[The METHODS are underlined]

CHAPTER 3

SEMICONDUCTOR MATERIALS

The physical properties of semiconductors are highly sensitive to the quality of the crystal structure. Therefore, from the point of view of the measurement of the basic properties of semiconductor materials it is essential to have single crystals with the greatest perfection possible. Not only should the atomic structure be of the highest order but the concentration and distribution of the electrically active impurities should likewise be accurately controlled. To these ends a variety of crystal growing techniques (methods) have been devised and some of these are shown in Fig. 3.1.

The major problem encountered in the growing of GaP crystals arises from the volatile nature of the phosphorus in GaP samples at temperatures close to their melting point. The melting point of GaP is 1743^{o}K and at this temperature the phosphorus has a vapour pressure of approximately 35 atmospheres. Two methods have been successfully used in the growth of commercial quantities of GaP crystals and these are the liquid encapsulation Czochralski method[1] and the epitaxial growth by chemical deposition[2]. In the first method the crystals are grown from the melt in furnaces which are capable of withstanding very high pressures and are designed to prevent loss of phosphorus from the melt; in the second method the crystals are formed at

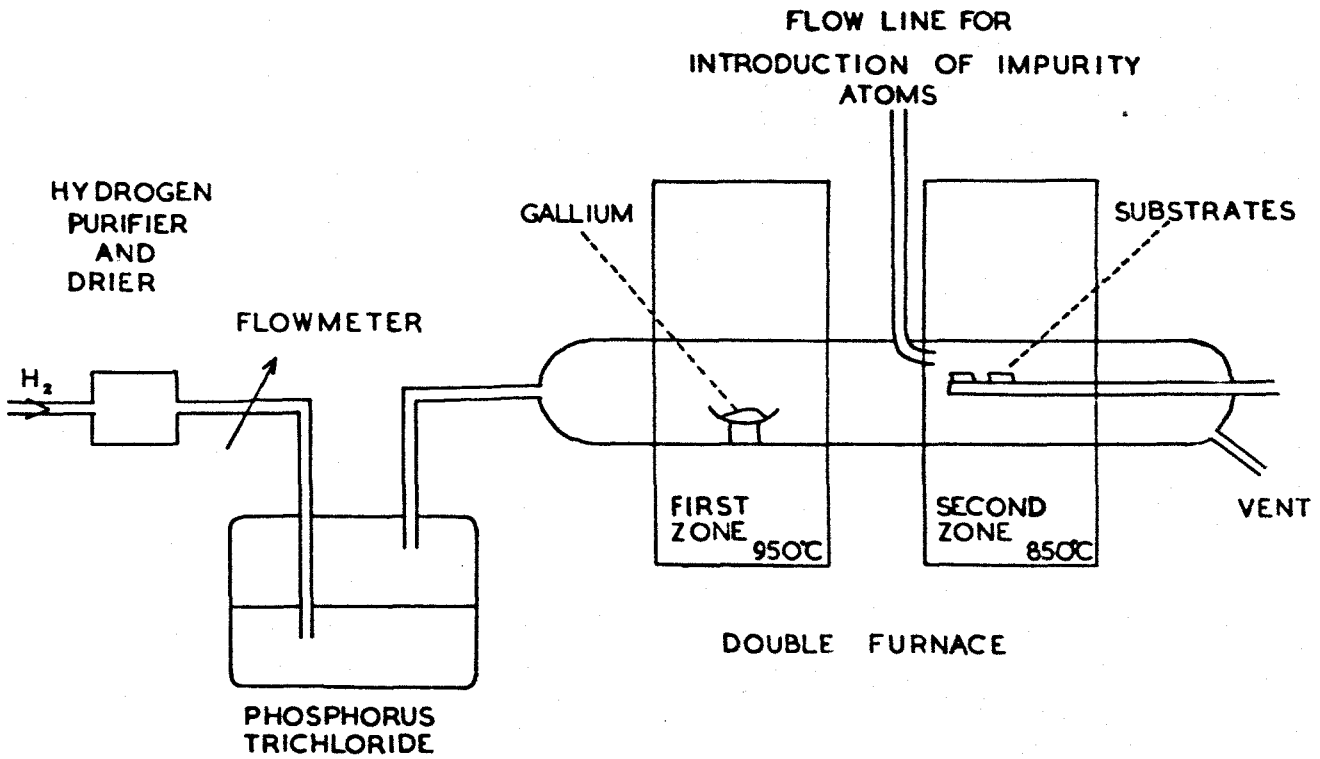

FIG. 3.2 HORIZONTAL VAPOUR DEPOSITION EPITAXY APPARATUS.

relatively low temperatures where the problem of the phosphorus vapour pressure is less important. The crystals which were used in the present work were grown by the latter method and a brief outline of epitaxial growth is now given together with a description of the GaP crystals which were available.

3.1 Epitaxial Growth of GaP

The word epitaxy has been derived from the Greek words[3], "επι" meaning "on" and "ταξις" meaning "orderly arrangement" and so the word essentially means an "oriented overgrowth". Epitaxial growing techniques have shown[4] that a crystal of one material will grow on the face of another crystal (the latter is usually termed the "substrate") and the orientation of the epitaxially grown crystal is governed by that of the substrate.

A typical apparatus which is suitable for the epitaxial growth of GaP crystals is shown diagrammatically in Fig. 3.2. The chemical reactions which occur are as follows:-

The hydrogen passes through the phosphorus trichloride to give:

$$4PCl_3 + 6H_2 \rightarrow 12HCl + P_4$$

The hydrogen chloride and phosphorus vapour pass into the reaction tube in the first zone of the furnace and the hydrogen chloride reacts with the gallium to give:

$$2HCl + 2Ga \rightarrow 2GaCl + H_2$$

In the second zone of the furnace the gallium chloride and phosphorus react as follows:

$$6GaCl + P_4 \rightleftarrows 4GaP + 2GaCl_3$$

This reaction proceeds from left to right if the substrate temperature is maintained at 1110°K and GaP is then deposited.

The choice of substrate material is clearly important in this type of crystal growing method. Ideally, the substrate crystal should be the same as the crystal that is being deposited since there is then no mismatch of the lattice spacing or difference in the thermal contraction between the crystal and substrate. However, only very recently have crystals of GaP become available[1] for the production of substrates and all the GaP crystals which were used in the present work had been grown on GaAs substrates. These crystals were kindly provided by The Plessey Company[5].

The size of the GaP crystals which were available for the present work was approximately 4mm x 4mm x 100microns. The most satisfactory crystal growth was obtained from (111) planes of the GaAs substrate[5]. In this case the stacking faults were less than 10^4 faults cm^{-2} as compared with 10^6 faults cm^{-2} in crystals grown from the (100) planes of the substrate. The dislocations per unit area in the epitaxial crystals were found to vary from $10^5 cm^{-2}$ to $10^8 cm^{-2}$[5]. For certain flow rates in the epitaxial deposition process, filamentary crystals ("whiskers") were observed to grow from the substrate[5] and

one of these crystals was available for E.P.R. studies. The approximate size of this crystal was 0.5mm x 0.5mm x 1cm.

The impurity atoms Si and S were introduced into GaP during crystal growth by the utilization of a separate flow line which is shown diagrammatically in Fig. 3.2. For the production of Si-doped GaP a mixture of hydrogen and silane (SiH_4) was passed through the impurity flow line. In the second zone of the furnace the silane dissociated to give silicon and hydrogen and the silicon was deposited on the substrate together with the GaP. The concentration of the silicon impurity in the GaP was controlled by the adjustment of the relative amounts of the hydrogen and silane. Samples of S-doped GaP were produced in a similar manner to the Si-doped GaP but in this case a mixture of hydrogen sulphide and hydrogen was passed through the impurity flow line. Impurity concentrations in the range $5 \times 10^{17}cm^{-3}$ to $5 \times 10^{18}cm^{-3}$ were obtained by this method.

3.2 Diffusion of Impurities into GaP

Impurity atoms may be introduced into semiconductor crystals during crystal growth (for example, by the method described in the previous section) or they may be diffused into semiconductor crystals after the crystal has been grown. A study of the diffusion processes in semiconductors is of considerable technological importance since diffusion processes provide a means of producing inhomogeneous impurity distributions which are necessary for many electronic devices.

A comprehensive account of diffusion processes in Group III - V semiconductors has been given by Kendall[6] and only a brief outline of diffusion processes will be given here.

The simplest mathematical formulation of the diffusion of impurity atoms in solids may be expressed as follows:

$$\frac{\partial N}{\partial t} = D \nabla^2 N \qquad 3.1$$

where D is the diffusion coefficient

N is the concentration of impurity atoms

t represents time.

The coefficient D is assumed to be independent of the concentration, N, but to have a temperature dependence of the form

$$D = D_o e^{-\Delta E/kT} \qquad 3.2$$

where ΔE is the activation energy of the diffusion process

and D_o is a constant.

For a semi-infinite wafer the impurity atom concentration profile N(x) is of the form

$$N(x) = N(o)\left[1 - \mathrm{erf}\left(\frac{x}{2\sqrt{Dt}}\right)\right] \qquad 3.3$$

where x is the depth below the surface

N(o) is the impurity atom concentration at the surface of the wafer.

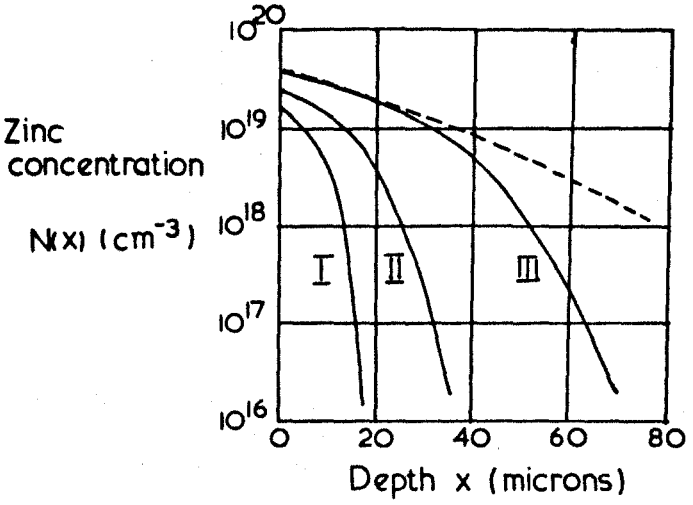

FIG. 3.3. CONCENTRATION PROFILES FOR ZINC IMPURITY ATOMS IN GaP[10]

Experimental curves ——

I T = 800°C t = 3600 seconds.
II T = 850°C t = 3600 "
III T = 900°C t = 3600 "

Theoretical curve ------

$$N(x) = N(0)\left[1 - \operatorname{erf}\left(\frac{x}{2\sqrt{Dt}}\right)\right]$$

$N(0) = 5 \cdot 10^{19}$ cm^{-3}
$D = 2 \cdot 10^{-9}$ cm^2 sec^{-1}
$t = 3600$ secs.

There are few available data concerning the diffusion of impurity atoms into GaP but the concentration profiles for the diffusion of Zn in GaP have been obtained[7] and are shown in Fig. 3.3. The diffusion coefficient has been found to be of the form[7]

$$D = 7.5 \times 10^{-6}\left[N(o)\right]^{0.45} \exp\left(-\frac{2.50}{kT}\right) \qquad 3.4$$

The discrepancies between the theoretical and experimental concentration profiles and diffusion coefficients are explained in terms of interstitial and substitutional diffusion mechanisms[7]. The majority of zinc atoms are assumed to exist in substitutional sites with only a small fraction at interstitial positions. However the interstitial diffusion occurs at a much faster rate than the substitutional diffusion and therefore the diffusion occurs by two competing processes.

Attempts were made in the course of the present work to diffuse transition metal atoms into GaP and to detect these impurities by the E.P.R. technique. However all these attempts proved to be unsuccessful and further work is in progress to obtain information concerning the diffusion of these impurities in GaP.

REFERENCES

1. S.J. Bass and P.E. Oliver, Proc. Sec. Int. Conf. on Crystal Growth (Birmingham), 3, 4 286 (1968).

2. W.G. Oldham, J. Appl. Phys., 36 2887 (1965).

3. J. Thewlis (Ed.), Encyclopaedic Dictionary of Physics, 3 1 (1964).

4. D.W. Pashley, Adv. in Phys., 14 327 (1965).

5. R. Nicklin, private communication. The Plessey Company Ltd., Allen Clark Laboratories, Caswell, Towcester, Northants.

6. D.L. Kendall, Semiconductors and Semimetals, 4 163 "Physics of III - V Compounds" (Academic Press 1968).

7. L.L. Change and G.L. Pearson, J. Appl. Phys., 35 375, 1960 (1964).

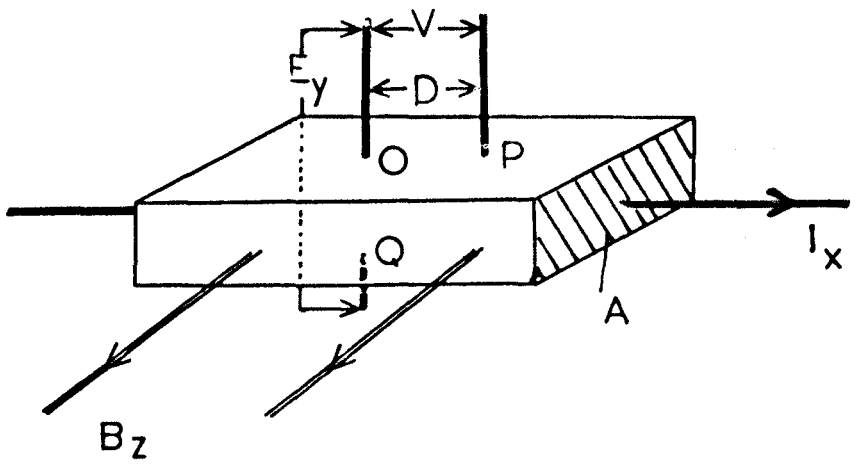

FIG. 4.1. DIAGRAM OF THE SAMPLE ARRANGEMENT FOR CONDUCTIVITY AND HALL EFFECT MEASUREMENTS.

[I_x is the current
A is the uniform area
B_z is the magnetic field
E_y is the electric field between the contacts O and Q
V is the potential difference
and D is the distance] between the contacts O and P .

CHAPTER 4

ELECTRON TRANSPORT PROPERTIES OF n-TYPE SEMICONDUCTORS

The transport properties of electrons in a semiconductor describe the movement of charge carriers under the influence of external electrical and magnetic fields and temperature gradients within the semiconductor. Comprehensive accounts of these properties are given in standard texts[1] and here the discussion is restricted to the phenomena of the Hall effect and electrical conductivity. The influence of electromagnetic radiation, which produces photo-electric effects, will not be discussed.

4.1 Hall Effect and Conductivity

The measurements of Hall effect and conductivity are commonly carried out with a test bar as illustrated in Fig. 4.1. The conductivity, σ, is given as:-

$$\sigma = \frac{D.I_X}{V.A} \qquad 4.1$$

and the Hall constant R_H is given as:-

$$R_H \doteq \frac{E_Y.A}{B_Z.I_X} \qquad 4.2$$

For n-type semiconductors the Hall constant may be written in terms of the concentration of conduction electrons, n, to give

$$R_H = -\frac{r}{ne} \qquad 4.3$$

where r is called the Hall factor.

The value of r depends on the type of electron scattering process, as shown in Table 4.1.

Table 4.1

The Dependence of the Hall Factor, r, on the Electron Scattering Processes (after Hilsum[2])

SCATTERING PROCESS	VALUE OF r
Acoustic phonon	$3\pi/8$
Optical phonon	1 to 1.14
Ionized impurity	$315\pi/512$
Neutral impurity	1

The Hall constant is related to the drift mobility, μ_D, as follows:

$$R_H\sigma = r\mu_D \qquad 4.4$$

and this equation can be rewritten in the form

$$R_H\sigma = \mu_H \qquad 4.5$$

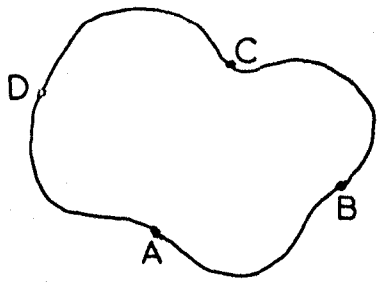

(a) An arbitrary shaped sample with four point contacts, A,B,C,D, at the circumference.

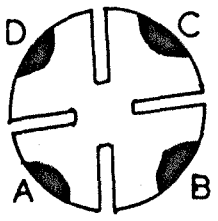

(b) A "clover-leaf" sample with four contacts of finite area, A,B,C,D, at the circumference.

FIG. 4.2. SAMPLE ARRANGEMENTS FOR THE MEASUREMENTS OF HALL EFFECT AND CONDUCTIVITY BY THE Van der Pauw METHOD[3].

where the quantity μ_H has the dimensions of mobility and is called the Hall mobility.

The Hall factor then becomes

$$r = \frac{\mu_H}{\mu_D} \qquad 4.6$$

4.2 Hall Effect and Conductivity Measurements on Small Samples

If only small thin samples of semiconducting material are available it is difficult to produce a sample in the form shown in Fig. 4.1. Van der Pauw[3] has suggested a method of measuring the Hall effect and conductivity of thin slices of material of an arbitrary shape in the arrangement as shown in Fig. 4.2(a). For such measurements the following conditions must be fulfilled:-

(a) the contacts must be placed at the circumference of the sample;

(b) the contacts must be small in area compared to the area of the sample;

(c) the sample must be of uniform thickness;

(d) the surface of the sample must be singly connected, i.e. the sample must not contain holes.

If a current i_{AB} flows from contact A to contact B and the potential difference between contacts C and D is $V_D - V_C$, then a resistance, R_{ABCD}, may be defined such that

$$R_{ABCD} = \frac{V_D - V_C}{i_{AB}} \qquad 4.7$$

Similarly R_{BCDA} may be defined as

$$R_{BCDA} = \frac{V_A - V_D}{i_{BC}} \qquad 4.8$$

The conductivity is then given as[3]:-

$$\sigma = \frac{2 \ln 2}{\pi . d . (R_{ABCD} + R_{BCDA}) f(\frac{R_{ABCD}}{R_{BCDA}})} \qquad 4.9$$

where d is the thickness of the sample

and $f(\frac{R_{ABCD}}{R_{BCDA}})$ has been given graphically[3].

The Hall constant, R_H, may be obtained by the following relationship:-

$$R_H = \frac{d}{B} . \Delta R_{BDAC} \qquad 4.10$$

where ΔR_{BDAC} is the change in the resistance R_{BDAC} which occurs when a magnetic field B is applied perpendicular to the plane of the sample.

The errors in the measurements of the conductivity and Hall effect due to large area contacts have been discussed[3] and it is shown that these errors may be substantially reduced with the "clover-leaf" sample arrangement as shown in Fig. 4.2(b).

4.3 Conduction Processes

The current in an impure semiconductor (for example, n-type material) may arise from two competing conduction processes. In the first process the current is carried by electrons which are excited from a donor level into the conduction band by thermal processes. The second process arises as follows: an electron occupying a donor level has a wavefunction localized about the impurity atom. Because there is a small but finite overlap of the electronic wavefunctions from neighbouring impurity atoms, a conduction process is possible in which the electron moves between centres without activation into the conduction band. This latter process, called impurity conduction, has been discussed by Mott and Twose[4] and observed in Ge[5], Si[6], InSb[7] and GaAs[8]. It is a process which only becomes significant at low temperatures since then the condition, $kT < E_D$ is satisfied and there are few electrons in the conduction band.

In the hydrogen-like model for donor impurities in semiconductors, the electronic wavefunction is assumed to give a region of high electron density at a radius a_i from the donor impurity ion where

$$a_i = \epsilon\left(\frac{m}{m^*}\right) a_H \qquad 4.11$$

Here m^* is the effective mass (assumed isotropic)

and a_H is the Bohr radius ($a_H = 0.54\text{Å}$).

An average inter-impurity spacing, r_i, may be obtained from the donor impurity concentration, N_D, as follows:

$$r_i = \left[\frac{3}{4\pi N_D}\right]^{1/3} \qquad 4.12$$

Mott and Twose[4] have shown that significant overlap of the electronic wavefunctions of the donor impurities occurs when $r_i = 3a_i$ and have defined a critical donor concentration, N_c, by the relationship

$$\left[\frac{3}{4\pi N_c}\right]^{1/3} = 3a_i \qquad 4.13$$

Three different mechanisms of impurity conduction have been identified generally in semiconductors according to the impurity concentration.

(a) Phonon-assisted hopping

If only donor impurities are present in a semiconductor and the donor concentration, N_D, is less than N_c, electronic conduction is unlikely to take place. However, if a small concentration of acceptor centres, N_A, are present (where $N_A < N_D$) electrons from some of the donor centres may occupy the acceptor levels (the semiconductor is said to be compensated). Electronic conduction is then possible by electrons hopping from occupied to unoccupied donor sites. The energy associated with the hopping process comes from the interaction of the electrons with the lattice phonons. An expression for the hopping frequency, W, which was first obtained by Miller and Abrahams[9], is:-

$$W = \frac{1}{(4\pi\varepsilon_o)^2} \cdot \left(\frac{e}{h}\right)^4 \cdot \left(\frac{D_u}{\varepsilon}\right)^2 \cdot \frac{1}{\rho u^5 a_i^2} \cdot \left(\frac{R}{a_i}\right)^{3/2}$$

$$\times \exp\left(-\frac{2R}{a_i}\right) \cdot E_h \cdot \coth\left(\frac{E_h}{2kT} + 1\right) \qquad 4.14$$

where R is the average separation of donor centres

E_h is the activation energy for hopping

a_i is the effective radius of the electronic orbit at the impurity

D_u is the deformation potential (conduction band)

ρ is the density

u is the velocity of sound.

E_h is given by

$$E_h = \frac{e}{4\pi\varepsilon_o\varepsilon}\left(\frac{4\pi N_D}{3}\right)^{1/3}(1 - 1.35\ K^{1/3}) \qquad 4.15$$

where $K \equiv \frac{N_A}{N_D}$ is the compensation ratio.

For this type of conduction mechanism the existence of the Hall effect has not been firmly established[4,10].

(b) Impurity band conduction

For donor concentrations of the order of N_c the donor wavefunctions have a significant overlap and the electronic levels are no longer isolated but form an impurity band. Electronic conduction can occur via this impurity band. The delocalized electrons in the

crystal can be divided into two groups having concentrations n_c and n_i, each of which is characterised by its own mobility, μ_c or μ_i; (the subscripts c and i correspond to the conduction and impurity bands respectively).

The conductivity may be written as[4]:-

$$\sigma = n_c e\mu_c + n_i e\mu_i \qquad 4.16$$

and the Hall constant R_H becomes[4]:-

$$R_H = \frac{1}{e}\left[\frac{n_c\mu_c(\mu_H)_c + n_i\mu_i(\mu_H)_i}{(n_c\mu_c + n_i\mu_i)^2}\right] \qquad 4.17$$

The value of the Hall constant has a maximum when

$$n_c\mu_c = n_i\mu_i \qquad 4.18$$

At high temperatures, such that $kT >> E_D$, it is found that $n_c\mu_c >> n_i\mu_i$ and the equations 4.16 and 4.17 reduce to

$$\sigma = n_c e\mu_c \quad , \quad R_H = \frac{1}{en_c}\left[\frac{(\mu_H)_c}{\mu_c}\right] \qquad 4.19$$

However at low temperatures, such that $kT << E_D$, the equations 4.16 and 4.17 reduce to

$$\sigma = n_i e\mu_i \quad , \quad R_H = \frac{1}{en_i}\left[\frac{(\mu_H)_i}{\mu_i}\right] \qquad 4.20$$

crystal can be divided into two groups having concentrations n_c and n_i, each of which is characterised by its own mobility, μ_c or μ_i; (the subscripts c and i correspond to the conduction and impurity bands respectively).

The conductivity may be written as[4]:-

$$\sigma = n_c e\mu_c + n_i e\mu_i \qquad 4.16$$

and the Hall constant R_H becomes[4]:-

$$R_H = \frac{1}{e}\left[\frac{n_c\mu_c(\mu_H)_c + n_i\mu_i(\mu_H)_i}{(n_c\mu_c + n_i\mu_i)^2}\right] \qquad 4.17$$

The value of the Hall constant has a maximum when

$$n_c\mu_c = n_i\mu_i \qquad 4.18$$

At high temperatures, such that $kT >> E_D$, it is found that $n_c\mu_c >> n_i\mu_i$ and the equations 4.16 and 4.17 reduce to

$$\sigma = n_c e\mu_c \quad , \quad R_H = \frac{1}{en_c}\left[\frac{(\mu_H)_c}{\mu_c}\right] \qquad 4.19$$

However at low temperatures, such that $kT << E_D$, the equations 4.16 and 4.17 reduce to

$$\sigma = n_i e\mu_i \quad , \quad R_H = \frac{1}{en_i}\left[\frac{(\mu_H)_i}{\mu_i}\right] \qquad 4.20$$

and the Hall constant will not be expected to vary greatly with temperature since n_i is constant at low temperatures.

(c) "Metallic-like" conduction

If the donor impurity concentration is very much larger than N_c the impurity band extends to the conduction band. The Fermi level lies in the conduction band and the semiconductor exhibits "metallic-like" conduction.

4.4 Electron Scattering Processes

The mobility of electrons travelling through a crystal is limited by several scattering mechanisms. In this section some of these mechanisms will be listed; more detailed accounts have been given elsewhere[1,2].

(a) Scattering by acoustic lattice phonons

It has been shown that the interaction of electrons with acoustic lattice phonons limits the mobility to a value μ_A[11] where

$$\mu_A = \frac{2^{3/2}.(\pi)^{\frac{1}{2}}.e.\bar{h}^4.\rho.u^2}{3.D_u^2.(m^*)^{5/2}.(kT)^{3/2}} \qquad 4.21$$

i.e. μ_A is proportional to $T^{-3/2}$.

(b) Scattering by optical lattice phonons

In Group III - V compounds, optical mode phonons give rise to strong interactions between electrons and the lattice because the relative movements of the two different types of atoms cause a polarization in the crystal. An expression for the mobility limited by optical mode phonon scattering, μ_o, is of the form[12]:-

$$\mu_o = \frac{2\sqrt{2}\hbar(kT)^{\frac{1}{2}}Mv}{3(e^*)^2(m^*)^{\frac{3}{2}}}\left(\frac{\omega_\ell}{2\pi}\right)F\left(\frac{\theta_\ell}{T}\right)\left[\exp\left(\frac{\theta_\ell}{T}\right) - 1\right] \qquad 4.22$$

where M is the reduced mass of the atoms,

v is the volume of the unit cell,

e^* is an effective charge defined by Callen[13] which can be considered to be a measure of the heteropolar contribution to the lattice bonding,

θ_ℓ is the Debye temperature for longitudinally polarized optical vibrations,

$F\left(\frac{\theta_\ell}{T}\right)$ is a slowly varying function with respect to temperature and is defined by Howarth and Sondheimer[14].

From the equation 4.22 it can be seen that μ_o has an exponential dependence on temperature.

(c) Scattering by ionized impurities

The scattering of an electron in the Coulomb field of an ionized impurity has been discussed by Dingle[15]. If the electron distribution can be described by Maxwell-Boltzmann statistics, the

mobility, μ_I, has the form:-

$$\mu_I = \frac{2^{7/2}\varepsilon^2\varepsilon_o^2(kT)^{3/2}}{N_I\pi^{3/2}e^3(m^*)^{\frac{1}{2}}f(y)} \qquad 4.23$$

where $f(y) = \ln(1 + b) - \frac{b}{1 + b}$

and $b = \frac{6\varepsilon\varepsilon_o m^*(kT)^2}{\pi N\hbar^2 e^2}$

N_I is the concentration of ionized impurities

N is the concentration of free charge carriers.

Other forms of μ_I have been given[1] which are appropriate for degenerate electron distributions.

The function $f(y)$ is a slowly varying function of temperature and so μ_I is approximately proportional to $T^{3/2}$.

(d) Scattering by neutral impurities

The mobility μ_N of charge carriers limited by neutral impurity scattering has the form[16]:-

$$\mu_N = \frac{m^*e^3}{20\varepsilon\varepsilon_o N_o\hbar^3} \qquad 4.24$$

and is independent of temperature. Here N_o is the concentration of neutral impurities.

(e) Scattering by lattice imperfections

It has been suggested by Weisberg[17] that inhomogeneities in a crystal can give rise to the scattering of charge carriers. For example, large inhomogeneous distributions of acceptor and donor impurity atoms can give regions within the crystal which are non-conducting and these regions will scatter the charge carriers. If the scattering region has an effective area A and the concentration of these regions is N_s, then the mobility, μ_s, has the form[17]:-

$$\mu_s = e\left[N_s(2m^*kT)^{\frac{1}{2}}A \right]^{-1} \qquad 4.25$$

The scattering of charge carriers by dislocations has also been investigated[18]. In an n-type crystal a dislocation behaves as a negative line charge which is surrounded by a positive space charge; this latter region repels incident electrons and so causes electron scattering. If the dislocations are regarded as cylinders of radius R and if there are N dislocations per unit area, then the mobility, μ_D, has the form[18]:-

$$\mu_D = \frac{3e}{8}\left[RN(2m^*kT)^{\frac{1}{2}} \right]^{-1} \qquad 4.26$$

From both equations 4.25 and 4.26 it is seen that the mobility limited by lattice imperfections is proportional to $T^{-\frac{1}{2}}$.

(f) "Inter-valley" scattering

Another form of scattering which is of importance in semi-conductors which have several equivalent minima in the conduction band

is known as "inter-valley" scattering. If the $\underline{k}$-values corresponding to two of the minima are $\underline{k}_1$ and $\underline{k}_2$, then an electron with wave vector $\underline{k}$ nearly equal to $\underline{k}_1$ may change its wave vector to $\underline{k}'$ which is nearly equal to $\underline{k}_2$ by an interaction with a lattice phonon. However, if $|\underline{k}_1|$ and $|\underline{k}_2|$ are not nearly equal quite a large change in crystal momentum will be involved, approximately $\hbar(|\underline{k}_1| - |\underline{k}_2|)$, and the emission or absorption of an energetic phonon is necessary. The scattering will therefore be highly inelastic and is unlikely to take place at low temperatures. The effect of this kind of scattering on the mobility of electrons in n-type Si and Ge has been discussed by Herring[19].

(g) Combined scattering

When several of the scattering mechanisms, listed under sections 4.4(a) to 4.4(f), occur at the same time, the resultant mobility, μ, may be derived from the formula

$$\frac{1}{\mu} = \sum_i \frac{1}{\mu_i} \qquad 4.27$$

where μ_i represents the mobility limited by one type of scattering mechanism.

4.5 Transport Properties of Electrons in n-Type GaP

The resistivity and Hall effect measurements on n-type GaP have been reported by several workers[20-29] and some details of these measurements have been given in Table 4.2. The crystals used for these measurements have been grown from solution by the method outlined by Miller[30] or grown by the epitaxial deposition on GaAs substrates by the method outlined in Chapter 3. No data concerning the electron transport properties has yet been reported for GaP crystals grown by the liquid encapsulation technique. Details of the different types of impurity in the samples are given in Table 4.2.

It can be seen from Table 4.2 that the type of electron scattering mechanism in n-type GaP in the temperature range 77°K to 400°K is in some doubt and that the low temperature conduction processes are not firmly established. Measurements of conductivity and Hall effect on n-type GaP samples grown by the epitaxial technique are reported in chapter 7 and the electron scattering mechanisms and conduction processes are discussed.

Table 4.2

Conductivity Data for n-Type GaP

Author & Reference	Type of Crystal	Type of Impurity	Temperature Range of the Measurement	Comments
Frosch et al. (20)	Solution grown	Unknown	77°K to 400°K	$\mu_H \propto T^{-3/2}$ in the temperature range 200°K to 400°K. No analysis of scattering processes.
Nasledov et al. (21)	Solution grown	Unknown	77°K to 300°K	μ_H limited by optical phonon scattering in the temperature range 120°K to 300°K.
Flicker et al. (22)	Epitaxially grown	Unknown	77°K to 300°K	$\mu_H \propto T^{-3/2}$ in the temperature range 150°K to 300°K
Nasledov et al. (23)	Solution grown	Tellurium	77°K to 500°K	$\mu_H \propto T^{-3/2}$ in the temperature range 200°K to 500°K.
Montgomery (24)	Epitaxially grown	Silicon Sulphur Tellurium	77°K to 500°K	Values of the donor ionization energies for S, Te, Si were given (see Table 2.3).
Epstein (25)	Epitaxially grown	Silicon Sulphur Tellurium	77°K to 400°K	μ_H limited by optical phonon scattering in the temperature range 150°K to 400°K.
Hilsum et al. (26)	THEORETICAL INVESTIGATION			μ_H calculated for combined scattering processes.
Miyauchi et al. (27)	Solution grown	Silicon Sulphur	4.2°K to 300°K	μ_H limited by acoustic phonon scattering in the temperature range 100°K to 300°K.
Hara et al. (28)	Epitaxially grown	Sulphur	4.2°K to 400°K	μ_H limited by optical phonon scattering in the temperature range 200°K to 400°K.
Montgomery (29)	Epitaxially grown	Tellurium	80°K to 350°K	No discussion on electron scattering process. Investigation of the effective mass parameters.

REFERENCES

1. R.A. Smith, "Semiconductors" (C.U.P. 1961).
   E.H. Putley, "The Hall Effect and Related Phenomenon" (Butterworth 1960).
2. C. Hilsum and A.C. Rose-Innes, "Semiconducting III - V Compounds" (Pergamon 1961).
3. C.J. Van der Pauw, Philips Res. Repts., 13 1 (1958).
4. N.F. Mott and W.D. Twose, Adv. in Phys., 10 107 (1961).
5. C.S. Hung and J.R. Gliessman, Phys. Rev., 96 1226 (1954).
6. T.A. Longo et al., J. Phys. Chem. Solids, 8 259 (1959).
7. E.H. Putley, Solid State Phys. Electron. Telecom., 2 751 (1960).
8. D.J. Oliver, Phys. Rev., 8 259 (1962).
9. A. Miller and E. Abrahams, Phys. Rev., 120 745 (1960).
10. M. Pollack et al., Proc. Int. Conf. on Phys. Semiconductors (Kyoto), J. Phys. Soc. Japan, 21 (Suppl.) 549 (1966).
11. J. Bardeen and W. Shockley, Phys. Rev., 80 72 (1950).
12. H. Ehrenreich, J. Phys. Chem. Solids, 2 131 (1957).
13. H.B. Callen, Phys. Rev., 76 1394 (1949).
14. D.J. Howarth and E.H. Sondheimer, Proc. Roy. Soc., A219 53 (1953).
15. R.B. Dingle, Phil. Mag., 46 831 (1955).
16. C. Erginsoy, Phys. Rev., 79 1013 (1950).
17. C.R. Weisberg, J. Appl. Phys., 33 1817 (1962).
18. W.T. Read, Phil. Mag., 45 119,775 (1954).

19. C. Herring, Bell. Syst. Tech. J., 34 237 (1955).

20. C. Frosch et al., Symposium Battelle Memorial Institute (1959).

21. D.N. Nasledov and S.W. Slobodchikov, Soviet Phys. Sol. State, 4 2021 (1963).

22. H.F. Flicker et al., J. Appl. Phys., 35 2959 (1964).

23. D.N. Nasledov et al., Soviet Phys. Sol. State, 7 1549 (1965).

24. H.C. Montgomery et al., J. Appl. Phys., 36 3228 (1965).

25. A.S. Epstein, J. Phys. Chem. Sol., 27 1611 (1966).

26. C. Hilsum and J. Welborn, Proc. Int. Conf. on Phys. Semiconductors (Kyoto), J. Phys. Soc. Jap., 21 (suppl) 532 (1966).

27. T. Miyauchi et al., Jap. J. of Appl. Phys., 6 1409 (1967).

28. T. Hara et al., J. Appl. Phys., 39 285 (1968).

29. H.C. Montgomery, J. Appl. Phys., 39 2002 (1968).

30. J.F. Miller, Compound Semiconductors 1 194, "Preparation of III - V Compounds" (Reinhold 1962).

CHAPTER 5

ELECTRON PARAMAGNETIC RESONANCE OF ELECTRONS IN n-TYPE SEMICONDUCTORS

The experimental techniques of E.P.R. has been used to examine the properties of impurities and imperfections in a considerable range of semiconductors; silicon, germanium and the Group III - V and Group II - VI semiconductors. However, only shallow donor impurities in GaP are considered here and more detailed accounts of E.P.R. in semiconductors are found elsewhere[1,2,3,4]. In order to understand the basic principles underlying the E.P.R. of electrons from shallow donor impurities in semiconductors, the motion of a free electron in a magnetic field will first be discussed.

5.1 The g-Value for a Free Electron

If the spin angular momentum of an electron is neglected, then the non-relativistic Schrödinger equation for an electron in a magnetic field is:-

$$\frac{1}{2m}(i\hbar\nabla + e\underline{A})^2 \psi_{\underline{k}}(\underline{r}) = E \psi_{\underline{k}}(\underline{r}) \qquad 5.1$$

where $\underline{A}$ is the vector potential of the magnetic field $\underline{B}$.

The solution of equation 5.1 was first given by Landau[5]. If the magnetic field is in the z-direction, the energy of the electron is given by

$$E_{\underline{k},n} = (n + \tfrac{1}{2})\hbar\omega_c + \frac{\hbar^2 k_z^2}{2m} \qquad 5.2$$

where $\omega_c = \dfrac{e|\underline{B}|}{m}$

k_z is the z-component of the wave vector of the electron

n is an integer taking values 0, 1, 2, 3 .... etc.

The discrete energy levels labelled by the integral values of n are referred to as Landau levels. Electric dipole transitions, governed by the selection rule $\Delta n = \pm 1$, can occur between neighbouring Landau levels to give the so-called cyclotron resonance transitions.

If the spin angular momentum of the electron is taken into account, the motion of the electron is treated by the Dirac relativistic equation[6]. Assuming that the electron kinetic energy is small compared with the term mc^2, the energy of the electron is given by:-

$$E_{\underline{k},n,m_s} = \frac{\hbar^2 k_z^2}{2m} + (n + \tfrac{1}{2})\hbar\omega_c + g_s\beta|\underline{B}|m_s \qquad 5.3$$

where β is the Bohr magneton, $\beta = e\hbar/2m$

g_s is the g-value for the free electron

m_s is the spin angular momentum quantum number ($\pm\frac{1}{2}$ for a free electron).

From the Dirac equation the value of g_s is exactly 2 and hence, in a magnetic field, the energy difference between the levels $m_s = \pm\frac{1}{2}$ is exactly equal to the splitting between neighbouring Landau levels, i.e. $e|\underline{B}|\hbar/m$. However the departure of the free electron g-value

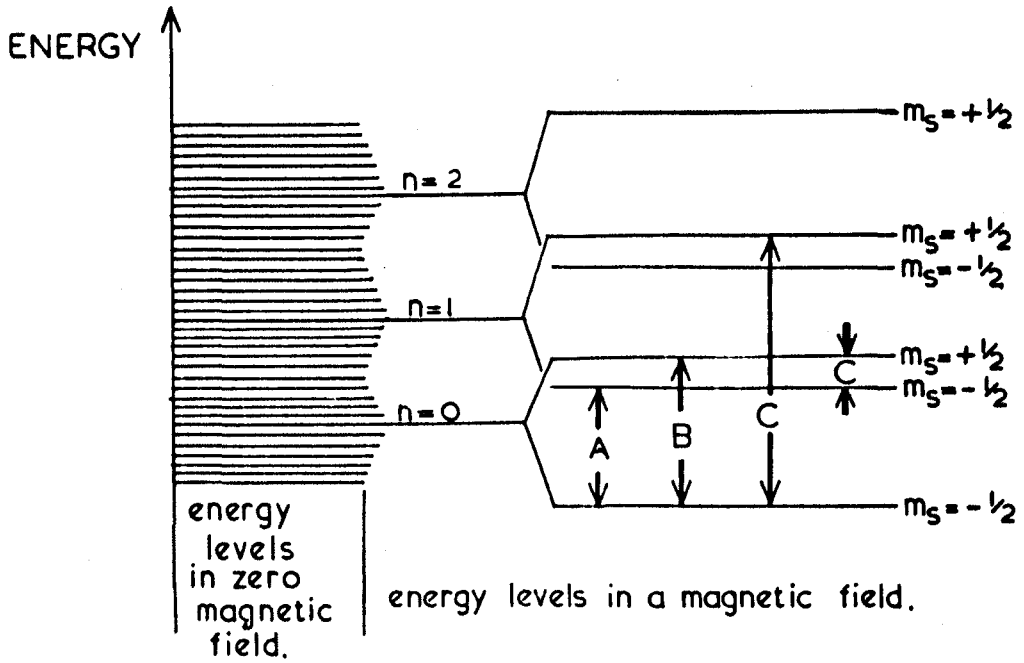

FIG. 5.1. THE SPLITTING OF THE ENERGY LEVELS OF A FREE ELECTRON IN A MAGNETIC FIELD.

A ≡ cyclotron resonance transition
B ≡ paramagnetic " "
C ≡ combined " "

from 2 has been determined using quantum electrodynamical calculations and the present accepted value of g_s has been given as[7] $g_s = 2.002319$ ($\pm$ 0.000001).

The energy levels arising from equation 5.3 are shown schematically in Fig. 5.1. The following types of resonant absorption can be observed:-

(a) Cyclotron resonance which results from electric dipole transitions between adjacent Landau levels. The selection rules are $\Delta n = \pm 1$, $\Delta m_s = 0$ and the resonance condition is $\hbar\omega_c = e|\underline{B}|\hbar/m$.

(b) Electron paramagnetic resonance in which magnetic dipole transitions occur between the two sub-states, $m_s = \pm\frac{1}{2}$, of a particular Landau level. The selection rules are $\Delta n = 0$, $\Delta m_s = \pm 1$ and the resonance condition is $\hbar\omega = g_s\beta|\underline{B}|$.

(c) Combined resonance which results from both magnetic and electric dipole transitions with selection rules $\Delta n = \pm 1$, $\Delta m_s = \pm 1$.

This type of resonance has only been observed for conduction electrons in InSb[8].

5.2 The g-Values of Electrons Bound to Shallow Donor Impurities

The $\underline{k}.p$ perturbation method, described in section 2.3, has been extended by Bowers and Yafet[9] for the treatment of valence electrons in InSb under the influence of an external magnetic field. In this latter treatment the secular determinant factorizes to give:-

$$E'\left[E'(E'-E_g)(E'+\Delta) - P^2\{k_z^2 + S(2n+1)\}\{E'+\tfrac{2}{3}\Delta\} \pm \tfrac{1}{3}P^2.\Delta.S\right] = 0 \qquad 5.4$$

where $S = e|\underline{B}|/\hbar$.

This is a two band approximation (i.e. only the momentum matrix element between the conduction band and the valence band are considered) and it has been found[10,11] that the energy of an electron in the conduction band has the same form as that given by equation 5.3 and that the g-value of the electron is:-

$$g = 2\left[1 - (\frac{m}{m^*}) - 1)(\frac{\Delta}{3E_g + 2\Delta})\right] \qquad 5.5$$

Also $\omega_c = \frac{e|\underline{B}|}{m^*}$

and m^* is given by the equation 2.14.

The calculated g-values, obtained from equation 5.5, for conduction electrons in some Group III - V semiconductors, together with values obtained from E.P.R. measurements, are shown in Table 5.1.

Table 5.1

The g-Value of Conduction Electrons in Some Group III - V Semiconductors

SEMICONDUCTOR	THEORETICAL g-VALUE	g-VALUE DETERMINED FROM E.P.R. MEASUREMENT
GaP	2.0 (±0.5)	1.9976 (±0.0008) at 77°K[12]
InP	0.60 (±0.10)	
GaAs	0.40 (±0.14)	0.5228 (±0.0001) at 4.2°K[13]
InAs	-12.0 (±3.0)	-14.75 (±0.01) at 4.2°K[14]
AlSb	0.40 (±0.10)	
GaSb	-6.1 (±2.0)	
InSb	-45 (±5)	At 4.2°K the g-value is within the range 48.8 to 50.7 and is dependent on the electron concentration[15].

From Table 5.1 it can be seen that the experimentally measured g-values agree with the calculated values to within the ranges produced by the uncertainties in the values of m^*, Δ, and E_g. Variations of the experimentally determined g-values with respect to changes in temperature and electron concentration have been observed in GaAs[13], InAs[14] and InSb[15]. These variations have been explained in terms of changes in the value of m^* with temperature and electron concentration.

The value of m^* in equation 5.5 is assumed to be isotropic and Roth[16] has extended the $\underline{k}.\underline{p}$ perturbation method to obtain expressions for the g-values of conduction electrons in terms of the longitudinal and transverse effective masses of the electrons.
On the basis of the two band model the g-values for conduction electrons in Ge are[16]:-

$$g_{\parallel} - 2 = -2_3(\frac{\Delta}{E_g})\left[\left|\frac{m}{m_t} - 1\right.\right] \qquad 5.6$$

$$g_{\perp} - 2 = -2/3(\frac{\Delta}{E_g})\left[\frac{m}{m_{\ell}} - 1\right] + \Delta g_{\perp}' \qquad 5.7$$

where Δ is the spin-orbit splitting of the valence band at $k = 0$

E_g is the energy gap

m_{ℓ}, m_t are respectively the longitudinal and transverse electron effective masses

$\Delta g_{\perp}'$ is a small correction term.

E.P.R. measurements on conduction electrons in phosphorus-doped silicon have shown discrepancies between the experimentally determined g-values and those calculated in terms of the two band model[17]. However, Liu[18] has shown that a dominant contribution to the calculated g-values of conduction electrons in silicon comes from a deep-lying 2p state, because of its large spin-orbit splitting and his values show good agreement with the experimental results[17].

5.3 The Magnetic Resonance Phenomenon for a Free Electron

The energy levels for a free electron in a magnetic field have been shown in Fig. 5.1. If the energy levels, $m_s = \pm\frac{1}{2}$, of the lowest Landau level are considered, an effective Hamiltonian $\mathcal{H}_o$ (or Spin Hamiltonian) may be used to obtain the eigenvalues of these levels where

$$\mathcal{H}_o = g_s \beta B_z \hat{S}_z \qquad 5.8$$

$\hat{S}_z$ is a spin angular momentum operator

B_z is the steady magnetic field in the z-direction.

The phenomenon of E.P.R. arises from the transition of an electron between the energy levels caused by the application of an oscillating magnetic field. If the components of magnetic field are $(2b \cos \omega t, 0, B_z)$ then the additional interaction due to the oscillating magnetic field, of angular frequency ω, is described by an additional term, $\mathcal{H}'$, in the Spin Hamiltonian where

$$\mathcal{H}' = 2g_s \beta b \cos \omega t \, \hat{S}_x \qquad 5.9$$

For the condition $b \ll B_z$, first order perturbation theory can be used to show that the probability, $P_{\pm\frac{1}{2}\rightarrow\mp\frac{1}{2}}$, of an electronic transition between the energy levels having spin magnetic quantum numbers $m_s = \pm\frac{1}{2}$ is

$$P_{\pm\frac{1}{2}\rightarrow\mp\frac{1}{2}} = \frac{g_s{}^2\beta^2}{\hbar^2} \, 4b^2 \, |\langle \pm\tfrac{1}{2}|\hat{S}_x|\mp\tfrac{1}{2}\rangle|^2 \times \left[\frac{\sin^2\{(\theta-\omega)t/2\}}{(\theta-\omega)^2}\right] \qquad 5.10$$

where $\theta = \dfrac{E_{+\frac{1}{2}} - E_{-\frac{1}{2}}}{\hbar}$

and $E_{+\frac{1}{2}}$, $E_{-\frac{1}{2}}$ are the energies of the levels having spin magnetic quantum numbers $m_s = +\frac{1}{2}$ and $m_s = -\frac{1}{2}$ respectively.

The transition probability given by equation 5.10 has a maximum when $\theta = \omega$ and this leads to the resonance condition $\hbar\omega = g_s \beta B_z$.

An electron transition from the level $m_s = +\frac{1}{2}$ to level $m_s = -\frac{1}{2}$ can also occur by spontaneous emission but the probability for this transition can be shown[19] to be very small compared with $P_{\pm\frac{1}{2}\rightarrow\frac{-1}{+2}}$ if the frequency corresponding to the transition is of the order of 100 GHz or less. (E.P.R. spectrometers operate at frequencies of up to approximately 100 GHz). Therefore, if an assembly of free electrons in a homogeneous steady magnetic field, B_z, is subjected to an oscillating magnetic field, of angular frequency ω, (where $\omega = g_s \beta B_z / \hbar$) the number of electrons in each of the levels, $m_s = \pm\frac{1}{2}$, will become equalized. However, in practice, E.P.R. is concerned with the electronic transitions of an assembly of electrons contained in a solid, liquid or gas which can be referred to generally as the "lattice" and the electrons can interact with the "lattice" and with each other. These interactions, which cause a relaxation of the non-equilibrium electron distribution to a distribution corresponding to thermal equilibrium with the "lattice", will now be discussed.

5.4 The Phenomenological Equations of Bloch

The quantum mechanical treatment for a single free electron, which has been described in section 5.3 can be extended to the treatment of an assembly of electrons in a "lattice" but the basic principles underlying E.P.R. may be obtained from a classical treatment proposed by Bloch[20].

In a paramagnetic sample in zero magnetic field the magnetic moments, μ_i, associated with the unpaired electrons are randomly orientated and the total magnetization, $\underline{M}$ ($= \Sigma\underline{\mu_i}$), of the sample is zero. When a magnetic field, B_z, is suddenly applied to the sample, the individual magnetic moments ,μ_i, precess about axes parallel to B_z (the precessional frequency is called the Larmor frequency), and give rise to a magnetization, $\underline{M}$. If the components of $\underline{M}$ are M_x, M_y, M_z, then the value of M_z tends exponentially towards its thermal equilibrium value M_o due to interactions between the electrons and the "lattice". The time constant, T_1, for this process is known as the "spin-lattice" or "longitudinal" relaxation time. The values of M_x and M_y decay exponentially to zero due to interactions between the individual magnetic moments and the time constant, T_2, for this process is known as the "spin-spin" or "transverse" relaxation time.

If an oscillating magnetic field is applied to the sample in addition to B_z, then the Bloch equations describing the dynamical behaviour of the magnetization are as follows:-

$$\frac{dM_x}{dt} = \gamma(\underline{M} \times \underline{B})_x - \frac{M_x}{T_2}$$

$$\frac{dM_y}{dt} = \gamma(\underline{M} \times \underline{B})_y - \frac{M_y}{T_2} \qquad 5.11$$

$$\frac{dM_z}{dt} = \gamma(\underline{M} \times \underline{B})_z - \frac{M_z - M_o}{T_1}$$

$\underline{B}$ is the total magnetic field having components $(2b \cos \omega t, 0, B_z)$ and $\gamma = g\beta/\hbar$.

It is difficult to solve equations 5.11 generally and only one solution will be given here which is based on the assumption that changes in the value of magnetic field are sufficiently slow such that the value of M_z is constant at alltimes. This is called the "slow-passage" solution.

If the complex magnetic susceptibility is defined as $\chi(\omega) = \chi'(\omega) + i\chi''(\omega)$ it can be shown that[21]:-

$$\chi'(\omega) = \tfrac{1}{2}\chi_o\omega_o T_2 \left[\frac{T_2(\omega_o-\omega)}{1 + T_2^2(\omega_o-\omega)^2 + \gamma^2 b^2 T_1 T_2} \right]$$

$$\chi''(\omega) = \tfrac{1}{2}\chi_o\omega_o T_2 \left[\frac{1}{1 + T_2^2(\omega_o-\omega)^2 + \gamma^2 b^2 T_1 T_2} \right] \qquad 5.12$$

where χ_o is the static magnetic susceptibility

and $\omega_o = \gamma|\underline{B}|$.

The power absorbed, P, from the oscillating magnetic field when resonance occurs can be shown to be:-

$$P = 2\omega_o \chi'' \frac{b^2}{\mu_o} \qquad 5.13$$

and substitution from equation 5.12 into 5.13 gives a value for the power absorption at resonance as:-

$$P = \frac{1}{\mu_o} \left[\frac{\omega_o(\omega_o T_2)\chi_o b^2}{1 + T_2 (\omega_o - \omega)^2 + \gamma^2 b^2 T_1 T_2} \right] \qquad 5.14$$

For small values of b the term $\gamma^2 b^2 T_1 T_2$ may be neglected in equation 5.14 to give:-

$$P = \frac{1}{\mu_o} \left[\frac{\omega_o(\omega_o T_2)\chi_o b^2}{1 + T_2^2(\omega_o - \omega)^2} \right] \qquad 5.15$$

It is usual practice in E.P.R. experiments to use a fixed frequency oscillating magnetic field and vary the value of B_z to observe the resonant absorption. The equation 5.15 may be rewritten in terms of values of the steady magnetic field to give:-

$$P = \frac{\text{constant}}{\Delta B_z^2 + (B_{res} - B_z)^2} \qquad 5.16$$

where ΔB_z is the magnetic field difference between the points of maximum slope on the absorption curve

and B_{res} is the magnetic field value at resonance.

A collection of electrons (a spin-packet) whose spin magnetic moments obey Bloch's equations give an absorption curve (or absorption line) described by equation 5.16 which is said to have a Lorentzian form and be homogeneously broadened. However, other interactions are commonly encountered in solids which, by producing spatially varying local magnetic fields, produce a collection of spin-packets. The absorption line can then be considered to be composed of a collection of homogeneously broadened lines belonging to each spin-packet and is described by the equation

$$P = \text{constant} \times \exp -\left[\frac{(B_{res} - B_z)^2}{\Delta B_z^2} \right] \qquad 5.17$$

This absorption line is said to be inhomogeneously broadened and has a Gaussian form.

The "skin-effect" can further complicate the shape of the absorption line of the E.P.R. in semiconductors and metals. Dyson[22] has formulated a solution to this problem in terms of the skin-depth, δ, and the rate of diffusion of electrons across the material contained within the skin depth. If the sample thickness is much greater than 4δ then the line shape becomes significantly asymmetrical. Further details on E.P.R. line shapes have been discussed by Poole[23].

5.5 Relaxation Processes in General

In the previous section the relaxation times T_1, T_2 were introduced phenomenologically to describe the dynamical behaviour of an assembly of magnetic moments. In this section the general relaxation processes which determine T_1 and T_2 will be described briefly and in section 5.6 the relaxation processes which occur in semiconductors will be discussed.

(a) "Spin-Spin" relaxation

The "spin-spin" relaxation time T_2, as defined by equation 5.11, characterizes the decay of the transverse magnetization of an assembly of magnetic moments in a magnetic field. From a classical viewpoint this decay is due to the loss of phase coherence between the precessing magnetic moments and two mechanisms by which this may occur are described. Firstly, the local steady magnetic field at each magnetic moment will depend on the spatial orientation of neighbouring magnetic moments and this can cause individual magnetic moments to precess at different rates. Secondly, by a mutual interaction neighbouring magnetic moments may be reorientated by a "flip-flop" process. This process does not change the value of M_z and so does not contribute to T_1 but serves to destroy the transverse precessional coherence. These two mechanisms, however, can be considerably modified if the magnetic moments are in rapid relative motion[21].

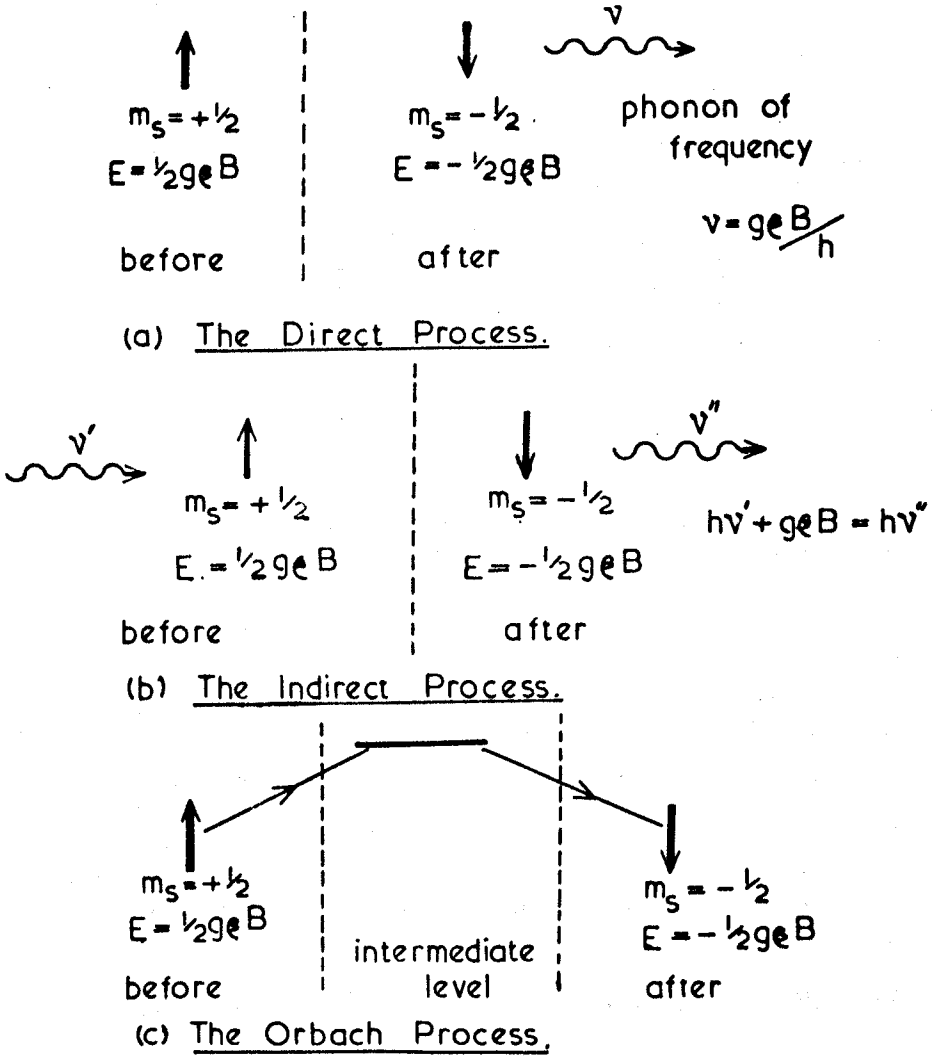

FIG. 5.2. DIAGRAM ILLUSTRATING "SPIN-LATTICE" RELAXATION MECHANISMS

(b) "Spin-lattice" relaxation

The "spin-lattice" relaxation is the process by which the distribution of electron spin magnetic moments (dipoles) returns to that corresponding to thermal equilibrium with the lattice.

One mechanism by which the dipoles and "lattice" may interact is due to dipole-dipole interaction[24]. The magnetic field at one dipole, due to a neighbouring dipole, varies as $1/R^3$, where R is the separation. The "lattice" vibrations (phonons) modulate R and so give rise to oscillating magnetic fields at the dipole sites. If the frequency of a phonon coincides with the precessional frequency of a dipole then there is a finite probability that a transition can take place as illustrated schematically in Fig. 5.2(a). This relaxation process is called a "Direct" process. An "Indirect" or "Raman" process, illustrated in Fig. 5.2(b), can also occur and this latter process involves the interaction of a dipole with two phonons.

The dipoles and "lattice" may also interact through the modulation of the crystalline electric field by phonons[25]. The oscillating electric field influences the dipoles by virtue of the spin-orbit coupling and again "Direct" and "Indirect" processes can occur.

As an extension to the "Direct" and "Indirect" processes, the dipoles and "lattice" may interact by the so-called Orbach process[26]. In this process a change of spin magnetic moment quantum number occurs

as a result of the interaction of a dipole and the "lattice" at some intermediate energy level above the ground state, as illustrated schematically in Fig. 5.2(c).

5.6 Some Characteristics of the E.P.R. Lines of Electrons Associated With Shallow Donor Impurities in Semiconductors

A brief account of the lineshapes and linewidths of resonance lines of electrons associated with shallow donor impurity atoms in semiconductors will now be given with specific reference being made to phosphorus doped silicon and n-type Group III - V semiconductors.

5.6.1 Phosphorus-doped silicon

(a) Localized electrons

Fletcher et al.[27,28] observed E.P.R. spectra in phosphorus-, arsenic- and antimony-doped silicon ($N_D \lesssim 5 \times 10^{16} cm^{-3}$) at 4.2°K. The spectra were identified with electrons localized at parent donor nuclei by means of the characteristic hyperfine splitting into $(2I + 1)$ lines (I is the nuclear spin magnetic quantum number). The hyperfine lines were found to be inhomogeneously broadened (i.e. the lineshape was Gaussian) and the source of this broadening was assumed to be due to the hyperfine interaction between the electron and the 4.7 per cent abundant Si^{29} nuclei ($I = \frac{1}{2}$) within its orbit. This assumption was confirmed by a further E.P.R. experiment[29] on a P-doped silicon sample containing approximately 99.88 per cent Si^{28} nuclei ($I = 0$);

the linewidth, ΔB_{hfs}, was reduced by about an order of magnitude to 0.022mT.

The theoretical value of ΔB_{hfs} was evaluated by Kohn[30] from the equation

$$\Delta B_{hfs} = \left(\frac{\mu_o}{4\pi}\right).\frac{12}{g}.\frac{\mu_N}{I}.\ m_{rms}.\ f^{\frac{1}{2}}.\ \eta.\ \frac{C}{(a\ a_i)^{3/2}} \qquad 5.18$$

where μ_N is the magnetic moment of the nucleus

m_{rms} is the root mean square value of I at all the lattice sites

f is the relative abundance of the nuclear species

η is a factor describing the "peaking" of the conduction band wavefunction at a lattice site

C is a factor which depends on the position of the conduction band minima

a is the lattice constant.

Agreement between the calculated and observed linewidth was obtained when a value of C was used which corresponded to a position of the conduction band minima at 70 per cent of the distance from the centre to the edge of the Brillouin zone in (100)-type directions.

(b) Interaction of electrons from donor impurity atoms

In the E.P.R. experiments on samples of P-doped silicon at liquid helium temperatures with impurity concentrations in the range $1 \times 10^{18} \geq N_D \geq 6 \times 10^{16} cm^{-3}$ "satellite" lines were observed between

the main hyperfine lines[31,32]. The "satellite" lines were attributed to exchange-coupled pairs of electrons from donor impurities lying particularly close together[31,32]. Motional narrowing of these E.P.R. lines has been observed in samples at temperatures in the range $30^{\circ}K$ to $45^{\circ}K$ and has been explained in terms of electron hopping processes[33]. From the theory of Anderson and Weiss[34] the width of an E.P.R. line, ΔB, which is motionally narrowed is given by

$$\Delta B = \frac{g\beta}{h} \frac{(\Delta B_{hfs})^2}{W} \qquad 5.19$$

where W is given in equation 4.14.

Such a motionally narrowed line has a Lorentzian lineshape.

(c) Non-localized electrons

The E.P.R. of electrons in P-doped silicon with $N_D \geq 2 \times 10^{18}$ consists of a single line which has been attributed to conduction electrons[35]. The line is homogeneously broadened and has a Lorentzian lineshape. It was suggested by Overhauser[36] that the hyperfine interaction which causes inhomogeneous broadening of an E.P.R. line without producing energy relaxation should not be important for conduction electrons since the high speed of the electrons causes motional narrowing. A more detailed investigation of the motional effects on the relaxation processes of conduction electrons in metals and semiconductors has been given by Pines and Slichter[37]. These authors have shown that when the correlation time τ_c (this is the reciprocal of the collision frequency) is short compared with the

reciprocal of the Larmor frequency then the relaxation times T_1 and T_2 are equal. This condition is found to be satisfied for conduction electrons in semiconductors. Various relaxation processes will now be discussed.

(i) Relaxation by lattice scattering

It has been suggested by Elliott[38] that the relaxation of conduction electrons by lattice vibrations results from spin-orbit interaction. The relaxation time, T_1, is given approximately as

$$T_1 \simeq \frac{\tau}{(\Delta g)^2} \qquad 5.20$$

where Δg is the difference between the observed and free electron g-values

and τ is related to the electrical mobility, μ, as follows

$$\mu = \frac{e\tau}{m^*} \qquad 5.21$$

If the electron mobility is limited by acoustic phonon scattering then $\mu \propto T^{-3/2}$ and

$$\Delta B \propto \frac{1}{T_1} \propto T^{3/2}$$

Early work by Lancaster and Schneider[39] on the E.P.R. of conduction electrons in P-doped silicon appeared to support this theory, but further measurements by Lancaster et al.[40] showed that $\Delta B \propto T^{5/2}$. This latter temperature dependence was in agreement with that given

by Yafet[41] who obtained the following expression:

$$\frac{1}{T_1} = \frac{2}{\pi^{2/3}\hbar} \frac{D^2}{\rho u^2} \frac{2m^*kT^{5/2}}{\hbar} \qquad 5.22$$

where ρ is the density

u is the velocity of sound

$D = D_u a \Delta_g$

where a is the length of the order of the lattice constant

D_u is the deformation potential

Relaxation arising from the modulation by lattice phonons of the hyperfine coupling between electrons and the Si^{29} nuclei has been investigated by Pines et al.[42]. The relaxation time due to this mechanism has been found to be approximately two to three orders of magnitude longer than that calculated on the basis of the Elliott/Yafet theories.

(ii) Relaxation by the Orbach process

Shallow donor impurities in semiconductors have energy levels which are approximately 10^{-1}eV, or less, below the conduction band. Electrons occupying the ground state level can be excited into higher levels by phonons and there is a finite probability that the spin magnetic quantum number of the electron will be changed before the electron returns to the ground state level. An expression for T_1, obtained by Orbach[26], is:

$$T_1^{-1} = R \exp(-\frac{\Delta E}{kT}) \qquad 5.23$$

where R is the rate constant for the process

ΔE is the energy difference between the ground state and the relevant excited state.

Castner[43] has found that this process occurs in P-doped silicon.

(iii) Relaxation by impurity scattering

A further interaction between the conduction electrons and the lattice is by the spin-orbit coupling between the electrons and their parent impurity atoms. Pines and Slichter[37] have shown that the spin-lattice relaxation rate is of the form

$$T_1^{-1} = \alpha\tau_c(\lambda)^2/\hbar^2 \qquad 5.24$$

where α is the fractional concentration of impurities

λ is the spin-orbit interaction parameter

$\tau_c = \frac{2a_o}{v}$

a_o is the atomic radius of the impurity atom

v is the mean electron velocity.

The relaxation of electrons in P-doped silicon ($N_D \sim 10^{19}cm^{-3}$) has been discussed in terms of this type of scattering mechanism[44,45].

5.6.2 n-type Group III - V semiconductors

At the present time E.P.R. has only been reported for non-localized electrons in n-type Group III - V semiconductors[12,13,14,15].

The lineshapes and linewidths of the resonance lines in n-type GaP, n-type InAs and n-type InSb have not been analysed in great detail but the linewidth of the E.P.R. of electrons in n-type GaAs has been explained by assuming that the active electrons have a range of k-values and that the consequent spread of effective masses produces a spread of g-values. A discussion of the characteristics of the resonance line in n-type GaP will be given in chapter 7.

5.7 E.P.R. of Electrons from Shallow Donor Impurities in GaP

A single E.P.R. line has been observed by Title[12] in solution-grown crystals of GaP. The linewidths and g-values were measured at X-band (9.5 GHz) on samples at a temperature of 77°K. For S-, Se- and Te-doped crystals the g-values were as follows:

GaP : S 1.9975 (± 0.0008)

GaP : Se 1.9983 (± 0.0007)

GaP : Te 1.9978 (± 0.0010)

These values were interpreted in terms of the theory given by Roth[16].

The linewidth of the resonance line was found to vary between 5 mT and 13 mT and could be correlated with the donor concentration. The lineshape was found to be Lorentzian and it was suggested that this was due to some kind of motional effect caused by the hopping of electrons between donor impurity atoms.

Further studies have been made by Taylor and Title[46] on epitaxially grown n-type GaP. The resonance from electrons from S and Se impurities were again reported and, in some samples, a resonance was obtained which was thought to be due to Fe^{+++}. These resonances were observed to show a dependence on the substrate orientation as follows. If the GaP samples were grown on a 111 B face of GaAs substrate, the samples were found to be n-type and to give a resonance of the form outlined previously[12]. But the GaP samples which had been grown on a 111 A face of GaAs had a high resistivity, exhibiting only a weak resonance corresponding to electrons from donor impurity atoms and a further resonance which was thought to be due to Fe^{+++}.

REFERENCES

1. G. Lancaster, "Electron Spin Resonance in Semiconductors" (Hilger & Watts Monograph 1966).
2. G.W. Ludwig and H.H. Woodbury, Solid State Physics, 13 223 (Academic Press 1962).
3. B. Goldstein, Semiconductors and semimetals, 2 189. "Physics of III - V Compounds" (Academic Press 1966).
4. R.S. Title, "Physics and Chemistry of II - VI Compounds" (North Holland 1967).
5. L. Landau, Z. Phys., 64 629 (1930).
6. L.D. Huff, Phys. Rev., 38 501 (1931).
7. C.M. Sommerfield, Phys. Rev., 107 328 (1957).
8. B.D. M^{c}Combe et al., Phys. Rev. Lett., 18 748 (1967).
9. R. Bowers and Y. Yafet, Phys. Rev., 115 1165 (1959).
10. E.J. Johnson, Semiconductors and semimetals, 3 153 "Optical Properties of III - V Compounds" (Academic Press 1967).
11. L.M. Roth et al., Phys. Rev., 114 90 (1959).
12. R.S. Title, Phys. Rev., 154 668 (1967).
13. W. Duncan and E.E. Schneider, Phys. Lett., 7 23 (1964), Proc. Int. Conf. on Phys. Semi. (Paris).
14. J. Konopka, Phys. Lett., 26 29 (1967).
15. G. Bemski, Phys. Rev. Lett., 4 62 (1960).

16. L. Roth, Phys. Rev., 118 1534 (1960).

17. D.K. Wilson and G. Feher, Phys. Rev., 124 1068 (1961).

18. L. Liu, Phys. Rev., 126 1317 (1962).

19. A. Yariv, "Quantum Electronics" (Wiley 1967).

20. F. Bloch, Phys. Rev., 70 460 (1946).

21. G.E. Pake, "Paramagnetic Resonance" (Benjamin 1962).

22. F. Dyson, Phys. Rev., 98 349 (1955).

23. C.P. Poole, "Electron Spin Resonance" (Interscience 1967).

24. J. Waller, Z. Phys., 79 370 (1932).

25. J.H. Van Vleck, J. Chem. Phys., 7 72 (1939).

26. R. Orbach, Proc. Phys. Soc. (London) A77 821 (1960).

27. R.C. Fletcher et al., Phys. Rev., 94 1392 (1954).

28. R.C. Fletcher et al., Phys. Rev., 95 944 (1954).

29. G. Feher, Phys. Rev., 109 221 (1958).

30. W. Kohn, Solid State Physics, 5 258 (Academic Press 1957).

31. C.P. Slichter, Phys. Rev., 99 479 (1955).

32. D. Jérome and J.M. Winter, Phys. Rev., 134 A1001 (1964).

33. S.D. Lacey and G. Lancaster, Phys. Lett., 22 386 (1966).

34. P.W. Anderson and P.R. Weiss, Rev. Mod. Phys., 25 269 (1953).

35. A.M. Portis et al., Phys. Rev., 90 488 (1953).

36. A.W. Overhauser, Phys. Rev., 89 689 (1953).

37. D. Pines and C.P. Slichter, Phys. Rev., 100 1014 (1955).

38. R.J. Elliott, Phys. Rev., 96 266 (1954).

39. G. Lancaster and E.E. Schneider, Proc. Int. Conf. on Semi. Phys., p.589 (Prague 1962).

40. G. Lancaster, J.A. Van Wyk and E.E. Schneider, Proc. Phys. Soc., 84 19 (1964).

41. Y. Yafet, Solid State Physics, 14 90 (Academic Press 1963).

42. D. Pines et al., Phys. Rev., 106 489 (1957).

43. T.G. Castner, Phys. Rev., 130 58 (1963).

44. H. Kodera, J. Phys. Soc. Jap., 21 1040 (1966).

45. I. Granacher and W. Czaja, J. Phys. Chem. Solids, 28 231 (1967).

46. R.C. Taylor and R.S. Title, Appl. Phys. Lett., 11 355 (1967).

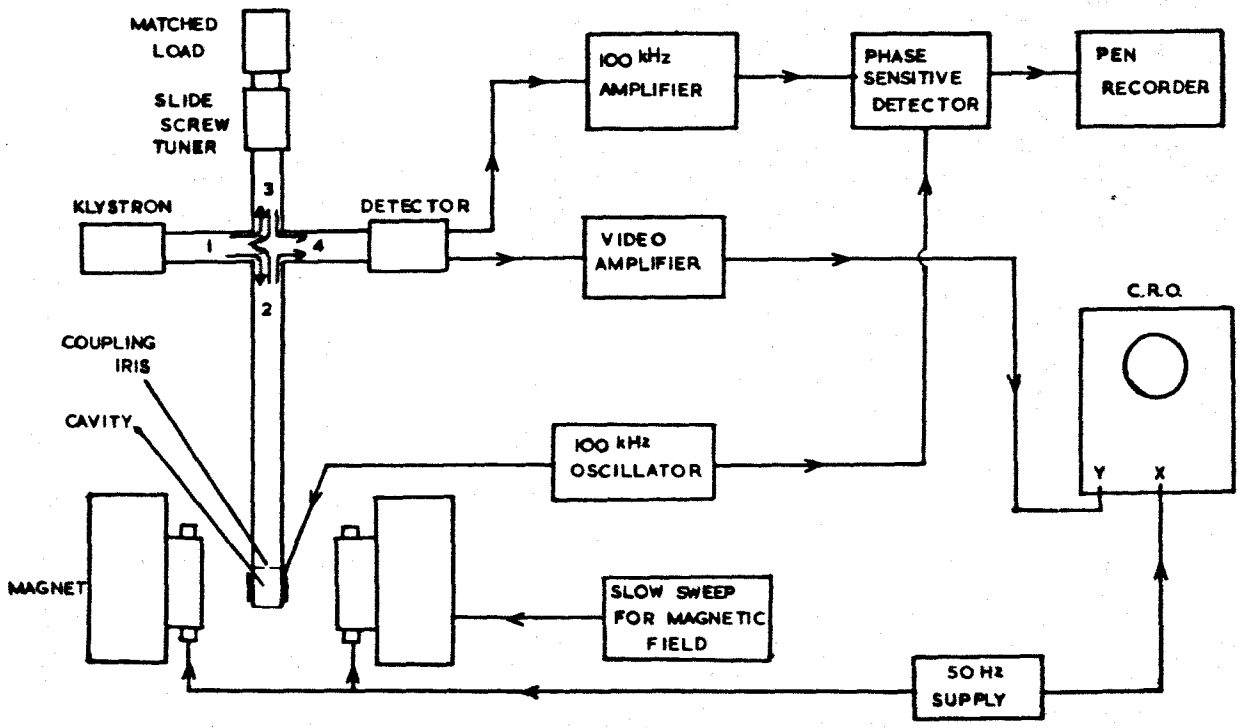

FIG. 6.1. A DIAGRAM OF A REFLECTION-CAVITY SPECTROMETER WITH FACILITIES FOR CRYSTAL-VIDEO DISPLAY OR OPERATION WITH HIGH FREQUENCY (100kHz) MAGNETIC FIELD MODULATION.

CHAPTER 6

EXPERIMENTAL TECHNIQUES

6.1 E.P.R. Spectrometers

The experimental techniques of E.P.R. have been described by a number of authors[1,2,3] and in this section only a few selected topics will be discussed. Most of the E.P.R. results described in this thesis were obtained with a Q-band (35 GHz) "Microspin" spectrometer manufactured by Hilger and Watts Ltd. Other results were obtained with an X-band (9.5 GHz) spectrometer manufactured by Varian Associates Ltd. and a spectrometer operating at a wavelength of 4 mm which had been constructed in the Physics Department.

6.1.1 A basic spectrometer

The basic features of an E.P.R. spectrometer using a reflection cavity are shown schematically in Fig. 6.1. In this thesis it is assumed that microwave radiation is obtained from a klystron, the microwave bridge circuit employs a magic tee, and the detector is a point-contact semiconductor diode (usually referred to as a detector crystal). However, bolometers and backward diodes are also used as detectors[3] and Faulkner[4] has shown that the use of a circulator instead of a magic-tee gives an increase in sensitivity. Microwave radiation can also be obtained from Backward Wave Oscillators or by the generation of harmonics from low frequency oscillators[2] and

recently the Gunn diode has been used as a source of microwave radiation in an E.P.R. spectrometer[5].

In the apparatus illustrated in Fig. 6.1 the specimen being investigated is placed in the cavity at a position of maximum microwave magnetic field. The cavity itself is situated between the poles of an electromagnet and generally the direction of the microwave magnetic field is arranged to be perpendicular to the steady magnetic field.

Radiation from the klystron enters the magic-tee junction and divides into the microwave arms 2 and 3. The radiation in arm 2 enters the cavity via a coupling iris and if there is an impedance match between the cavity and the waveguide then the radiation is absorbed in the cavity. Also, if the radiation in arm 3 is absorbed in the matched load then no microwave radiation reaches the crystal in arm 4. However when the resonance condition is achieved in the specimen by adjustment of the steady magnetic field, the impedance in arm 2 changes and microwave radiation is incident on the detector. The output voltage from the detector (the signal) may be displayed on a Cathode Ray Oscilloscope (C.R.O.) or on a pen-recorder as shown in Fig. 6.1. (The advantages of operating a spectrometer with high frequency field modulation will be discussed in section 6.1.3(c).) In practice, the crystal requires a certain steady incident microwave radiation to operate efficiently as a detector and this may be obtained by adjustment of the slide screw tuner in arm 3.

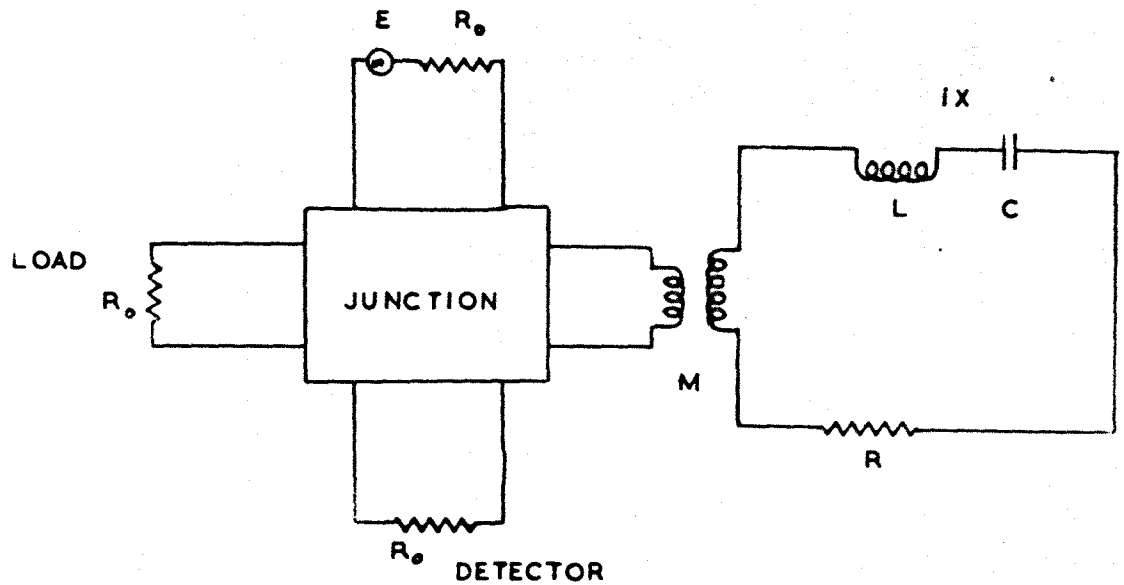

FIG. 6.2 EQUIVALENT CIRCUIT OF A REFLECTION CAVITY SPECTROMETER

The theoretical analysis of the reflection cavity spectrometer can be explained in terms of a low frequency analogue circuit[6] illustrated in Fig. 6.2. If the microwave generator has a voltage output, E, and the waveguide has a characteristic impedance R_o then the microwave radiation incident at the cavity may be represented by a generator of emf, $E/2\sqrt{2}$, in series with a resistance, R_o. The coupling iris is represented by a mutual inductance, M, and the cavity by a series resonant circuit consisting of an inductance L, a capacitance C and a resistance R.

The Q-factor of a cavity, Q, containing a paramagnetic sample may be defined as follows

$$Q = \frac{\omega \cdot \text{Energy stored in cavity}}{\text{Total power dissipated in cavity}} \qquad 6.1$$

(A more detailed discussion of Q-factors is given in section 6.2.2(b).)

When magnetic resonance takes place, microwave radiation is absorbed in the sample, according to the equation 5.13, and the change in Q, δQ, due to this absorption is

$$\delta Q = -Q^2 \chi'' \eta \qquad 6.2$$

where η is the filling factor defined by

$$\eta = \frac{\int_{\text{sample}} b^2 \, d\tau}{\int_{\text{cavity}} b^2 \, d\tau} \qquad 6.3$$

In the low frequency analogue circuit the paramagnetic absorption may be written in terms of a change in the resistance, δR, of the resistive part of the equivalent circuit of the cavity to give:-

$$\frac{\delta R}{R} = -\frac{\delta Q}{Q} = \chi'' \eta Q \qquad 6.4$$

Similarly dispersion may be represented as a change in the reactance of the circuit, δX, giving

$$\frac{\delta X}{R} = \chi' \eta Q \qquad 6.5$$

The voltage at the detector is[6]

$$V_D = \frac{E}{4}\left[\frac{\omega^2 M^2/R_o - R - iX}{\omega^2 M^2/R_o + R + iX}\right] \qquad 6.6$$

and the conditions for V_D to be maximum are

$$\begin{aligned} X &= 0 \\ \frac{\omega^2 M}{R_o} &= R \end{aligned} \qquad 6.7$$

The maximum voltage changes at the detector, resulting from paramagnetic resonance, then become

$$\begin{aligned} (\delta V_D)_{Abs} &= \tfrac{1}{8} E \eta \chi'' Q \\ (\delta V_D)_{Dis} &= i.\tfrac{1}{8} E \eta \chi' Q \end{aligned} \qquad 6.8$$

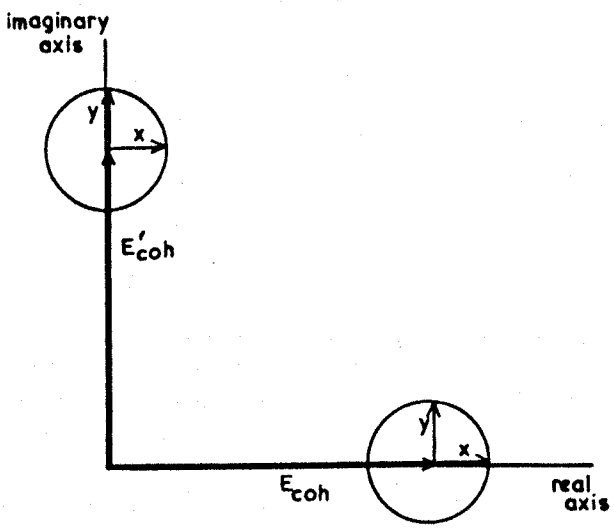

$y = iE\eta x'Q/8$ $\qquad$ $x = E\eta x''Q/8$

FIG. 6.3 THE ADDITION OF COHERENT RADIATION FOR THE DETECTION OF ABSORPTION AND DISPERSION.

magnitude of the vector addition $\underline{E}_{coh} + \underline{x} = E_{coh} + x$

" " " " " $\underline{E}_{coh} + \underline{y} = \sqrt{E_{coh}^2 + y^2}$

$\simeq E_{coh}$

(if $E_{coh} \gg y$)

The conditions given in equation 6.7 indicate that for a maximum change in the microwave radiation at the detector, the cavity must operate at its resonant frequency and must be perfectly matched to the waveguide arm 3.

The information concerning the resonant absorption in the specimen, as detected by the crystal, is the magnitude of the vector sum of $(\delta V_D)_{Abs}$ and $(\delta V_D)_{Dis}$ and this makes the interpretation of the information difficult. The separation of these two signals is achieved by transmitting a coherent (i.e. derived from the same generator) signal to the detector crystal which is large compared to $(\delta V_D)_{Abs}$ or $(\delta V_D)_{Dis}$ and in phase with either one as desired. In Fig. 6.3 the coherent signal, E_{coh}, is shown to be in phase with $(\delta V_D)_{Abs}$ and the absorption of the sample is detected whereas E'_{coh} is in phase with $(\delta V_D)_{Dis}$ and the dispersion of the sample is detected.

The coherent signal can be obtained by the reflection of radiation from arm 3 of the microwave bridge; the phase of the signal can be adjusted by the use of the slide screw tuner. This coherent signal also provides the "biasing" microwave radiation for the detector crystal.

6.1.2 Ideal sensitivity of an E.P.R. spectrometer

The minimum voltage changes, given by equation 6.8, which can be detected by an E.P.R. spectrometer are governed by the electrical noise generated in the microwave and electronic circuits. In an ideal

case this noise will be the Johnson noise due to thermal fluctuations in the characteristic impedance of the microwave circuit and an ideal sensitivity of an E.P.R. spectrometer may be evaluated as outlined by Feher[7].

The r.m.s. Johnson noise voltage, V_N, generated by a resistance R at a temperature T is given by

$$V_N = \sqrt{4kTR\Delta\nu} \qquad 6.9(a)$$

where $\Delta\nu$ is the frequency range (bandwidth) of the detection system.

Applying this to the microwave circuit (of internal resistance R_o) the value of V_N at the output becomes

$$V_N = \tfrac{1}{2}\sqrt{4kTR_o\Delta\nu}$$

$$= \sqrt{kTR_o\Delta\nu} \qquad 6.9(b)$$

The ideal sensitivity may be estimated by assuming that the minimum observable signal at the detector is equal to the r.m.s. noise voltage, i.e. equating $(\delta V_D)_{Abs}$ to V_N.

Hence

$$\chi''_{min} = \frac{\mathcal{G}}{Q\eta}\left(\frac{kT.\Delta\nu}{P_o}\right)^{\frac{1}{2}} \qquad 6.10$$

where P_o is the power from the microwave source.

For an unsaturated Lorentzian resonance line, χ'' is related to the static magnetic susceptibility, χ_o, by the equation[7]

$$\chi_o = \sqrt{3}\,\chi'' \frac{\Delta B}{B_{res}} \qquad 6.11$$

where B_{res} is the value of the steady magnetic field at resonance and ΔB is the linewidth measured between points of maximum slope on the absorption curve.

Also, for an assembly of unpaired electrons the value of χ_o is given by

$$\chi_o = \frac{\mu_o 4\beta^2 NS(S+1)}{3kT} \qquad 6.12$$

where N is the number of unpaired electrons per unit volume

S is the spin quantum number associated with the unpaired electron

β is the Bohr magneton.

For a resonant cavity operating at X band (9 GHz) a value of η is given as[7] $\eta = 0.4\,V_s$ where V_s is the volume of the sample ($in\ cm^3$). Therefore the minimum number of unpaired electrons, N_{min}, which can be detected by an X-band spectrometer is:-

$$N_{min} = \left[\frac{3kT}{4\beta^2 S(S+1)\mu_o}\right]\left[\frac{\Delta B\sqrt{3}}{B_{res}}\right]\cdot\left[\frac{4}{Q\ 0.4}\right]\left[\frac{kT\Delta\nu}{P_o}\right]^{\frac{1}{2}} \qquad 6.13$$

Using the following values for the various parameters, $T = 300^{o}K$, $S = \frac{1}{2}$, $\Delta B = 0.1mT$, $B = 0.35T$, $Q = 5 \times 10^{3}$, $\Delta\nu = 1Hz$, $P_{o} = 100mW$, the value of N_{min} is found to be

$$N_{min} = 1 \times 10^{10}$$

This value is consistent with the analysis given by Wilmshurst et al.[6] and differs from the value given by Feher[7] by a factor of $\sqrt{2}$.

The sensitivity of an E.P.R. spectrometer depends on its operating frequency, f, and it is found[3,7] that $N_{min} \propto f^{-7/2}$. Hence between X-band and Q band, N_{min} should decrease by a factor of $1/125$, other factors in equation 6.13 being equal. A comparison of the measured sensitivity of different commercial instruments, operating with samples at room temperature, is given in Table 6.1.

Table 6.1

Room Temperature Sensitivities of Commercial Spectrometers

Manufacturer	Measured Value of N_{min} for a Resonance of 0.1mT Linewidth	Power Incident on Cavity	Bandwidth of Detection Circuit
X-BAND SPECTROMETERS			
Decca Ltd. (100 KHz Field Modulation)	3×10^{11}	1 mW	1 Hz
Hilger & Watts Ltd. (Microspin) (100 KHz Field Modulation)	2×10^{12}	1 mW	1 Hz
Varian Associates (E.P.R. 3) (100 KHz Field Modulation)	5×10^{10}	100 mW	1 Hz
Q-BAND SPECTROMETERS			
Varian Associates (100 KHz Field Modulation)	5×10^{9}	100 mW	1 Hz
Hilger & Watts Ltd. (Microspin) (100 KHz Field Modulation)	2×10^{12}	1 mW	1 Hz

The values of N_{min} given in Table 6.1 for the X-band spectrometers are seen to be in reasonable agreement with that obtained from equation 6.13. However, the values of N_{min} for the Q-band spectrometers are in disagreement with the theoretical value by more than an order of magnitude. This discrepancy arises from the technical difficulties of manufacturing detector crystals and microwave components which give efficient operation at Q-band frequencies.

If only small samples are available for E.P.R. studies the filling factor, η, depends on the spectrometer operating frequency, f, according to the relationship $\eta \propto f^{+3}$ and hence it is preferable to use the highest operating frequency possible. Since only small samples of n-type GaP were available for the present work it was considered preferable to make the E.P.R. measurements at Q-band rather than X-band.

Other factors affecting the sensitivity of E.P.R. spectrometers can be inferred from equation 6.13; for a maximum sensitivity it follows that:

(a) a high value of cavity Q-factor is required,

(b) a high value of microwave power is required unless saturation of the E.P.R. signal occurs,

(c) a small bandwidth $\Delta\nu$ is required, and

(d) low temperature operation increases the sensitivity.

6.1.3 Noise in an E.P.R. spectrometer

It has been assumed in equation 6.9 that the total noise in an E.P.R. spectrometer is the Johnson noise generated by a resistor, R_o. In an actual spectrometer this assumption is not valid and the r.m.s. noise voltage is generally written as:-

$$V_N = \sqrt{kTR_o \Delta\nu . F} \qquad 6.14$$

where F is a noise figure which takes into account the total noise generated in the spectrometer.

Some of the sources of noise are due to

(a) the klystron,

(b) mechanical vibrations in the microwave circuit and cavity (microphonics),

(c) the detector crystal,

(d) the amplifier.

It has been shown[8] that F may be written in the form

$$F = \left(\frac{N_m}{L} + F_A + t_D - 1\right) \qquad 6.15$$

where N_m is the noise power from the sources listed under (a) and (b) above,

L is the conversion loss of the crystal,

F_A is the noise figure of the amplifier,

t_D is the noise temperature ratio of the crystal.

(The noise temperature ratio of a circuit element is defined as the ratio of the available output noise power to that of an ideal resistor at room temperature.)

For an ideal system $\frac{N_m}{L} = 0$, $F_A = 1$, $t_D = 1$ and hence $F = 1$.

The various sources of noise will now be considered in turn.

(a) Klystron noise

This noise is due to fluctuations in the amplitude (A.M. noise) and frequency (F.M. noise) of the radiation generated by the klystron.

The F.M. noise from a klystron can be minimized by locking the klystron frequency to some fixed frequency and Buckmaster and Dering [9] have shown that a significant reduction in F.M. noise is obtained by "phase-locking" the klystron frequency to a high stability crystal-controlled 1 MHz oscillator. This "phase-locking" system is used in the Decca spectrometer whose sensitivity is shown in Table 6.1. It is more common practice, however, to lock the klystron frequency to the resonant frequency of a microwave cavity.

The A.M. noise from a klystron can be minimized by the use of a balanced mixer detection system and this will be discussed in section 6.2.2(d).

(b) Microphonics

Rigid construction of the spectrometer reduces noise from microphonics and, for low temperature operation, it is advisable to exclude the coolant from the microwave cavity to reduce vibration due to bubbling. The noise due to microphonics in the cavity, however, is reduced by the locking of the klystron frequency to the resonant frequency of the cavity; also the effects of microphonics, which give

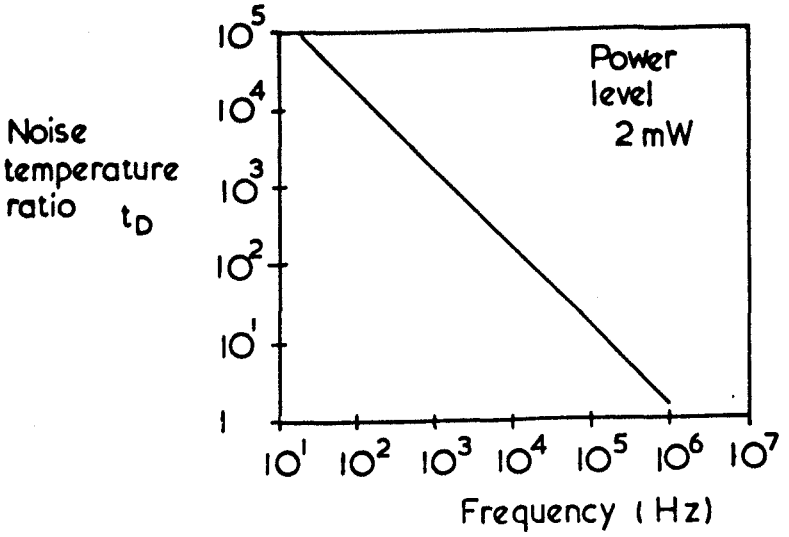

FIG. 6.4. GRAPH SHOWING THE FREQUENCY DEPENDENCE OF THE NOISE TEMPERATURE RATIO OF THE CRYSTAL IN-23 WE (AFTER BUCKMASTER & DERING[11]).

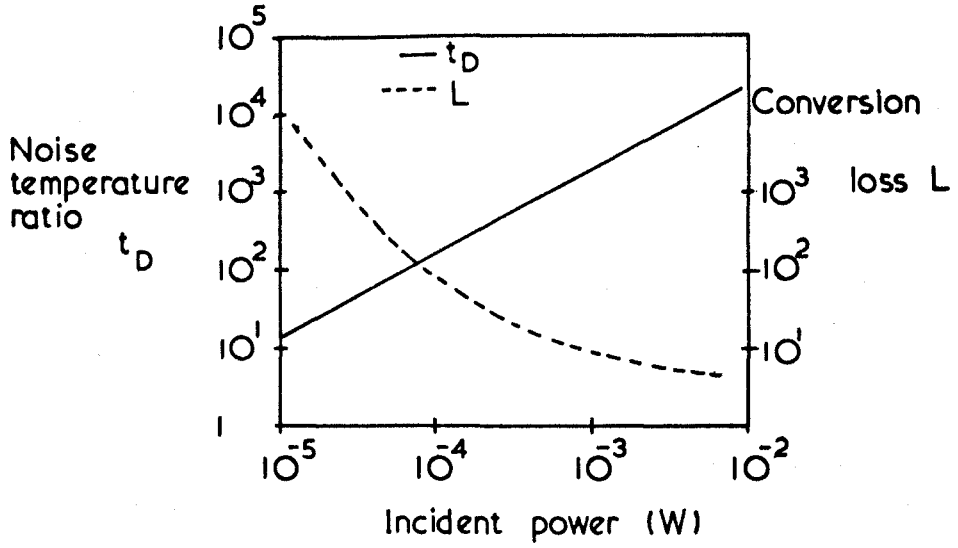

FIG. 6.5. GRAPH SHOWING THE POWER DEPENDENCE OF THE CONVERSION LOSS & NOISE TEMPERATURE RATIO OF THE CRYSTAL IN-23WE AT A MODULATION FREQUENCY OF 400 Hz[11].

rise to low frequency noise, are greatly reduced if a high-frequency magnetic field modulation and detection system is used.

(c) Detector noise

Information concerning the noise temperature ratio, t_D, of silicon detector crystals has been given by numerous authors[8,10,11] and a typical graph showing the frequency dependence of t_D is given in Fig. 6.4 which shows that $t_D \propto 1/\nu$. Such a frequency dependence can be explained in terms of flicker noise in the detector crystal[12].

In order to minimise the effect of t_D on the noise figure given by equation 6.15, a high-frequency magnetic field modulation and detection system must be used. However, a limit to the frequency of the magnetic field modulation is set by the modulation broadening of E.P.R. signals. The frequency commonly used is 100 KHz which results in the broadening of a resonance line, with g = 2, of approximately 0.003 mT.

(N.B. Superheterodyne detection in E.P.R. spectrometers which was pioneered by the work of England and Schneider[13] eliminates the need for high-frequency magnetic field modulation and is therefore extremely useful when narrow E.P.R. lines are to be observed.)

The noise temperature ratio of a crystal also depends on the magnitude of the power incident on the crystal as shown in Fig. 6.5. Also plotted in Fig. 6.5 is the conversion loss, L, of the crystal which gives a measure of the efficiency of the crystal in converting

microwave radiation into an output voltage. It can be seen that L is very high at low values of incident microwave power but is substantially reduced as the microwave power is increased. This suggests that an optimum working point for the detector can be achieved by varying the incident microwave radiation at the detector; in practice this point is determined experimentally by obtaining the best signal-to-noise ratio on a resonance line.

(d) Amplifier noise

The noise figure, F_A, given in equation 6.15, is used to described the overall noise contribution from the electronic circuits of the detection system of the E.P.R. spectrometer. The pre-amplifier, connected to the detector crystal, gives a large contribution to F_A but by careful design this contribution can be minimised[12].

Gambling and Wilmshurst[14] utilized the very low noise properties of an ammonia maser to reduce the value of F_A but the improvement in this noise figure only became evident at low power levels because of the saturation of the maser at high power levels. In a recent analysis, Buckmaster and Dering[15] have indicated that the use of parametric or maser pre-amplifiers in E.P.R. spectrometers is only justified if the spectrometer is to be operated at low power levels (less than 1 μW).

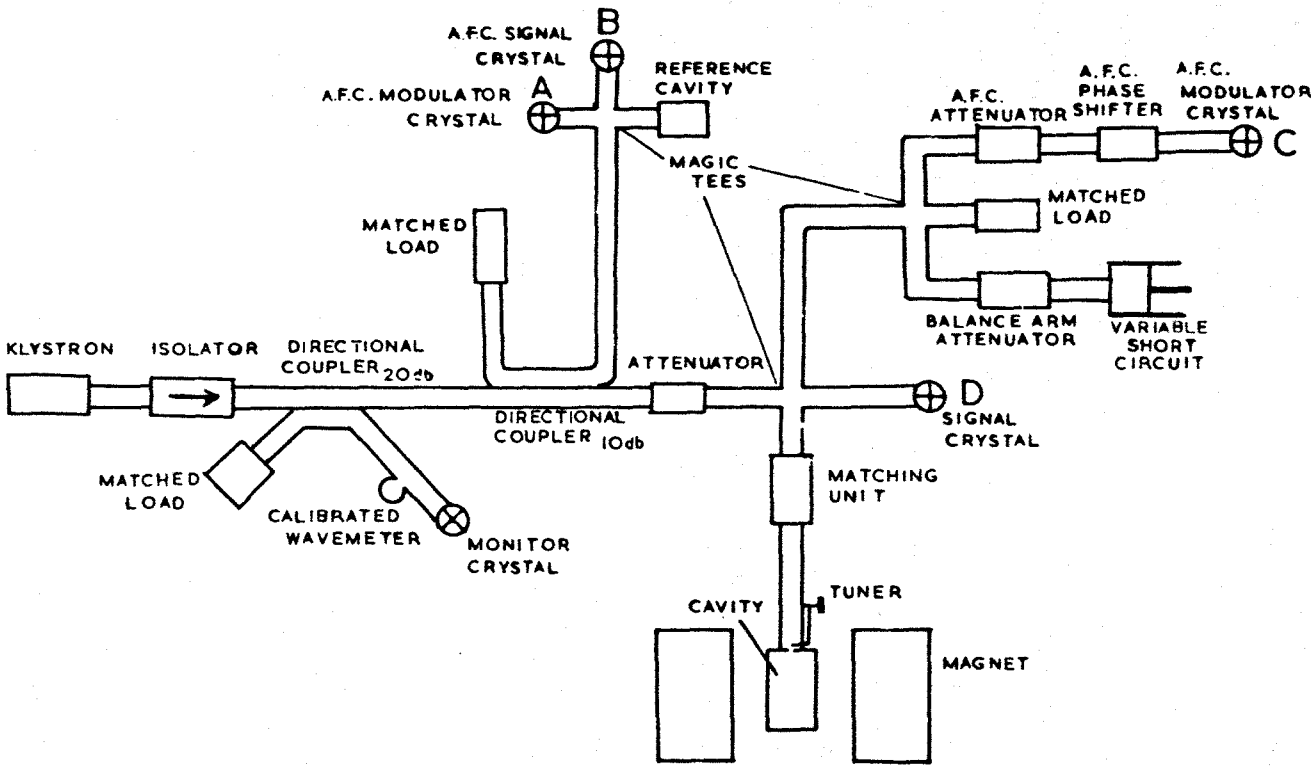

FIG. 6.6 MICROWAVE CIRCUIT DIAGRAM FOR THE "MICROSPIN" SPECTROMETER

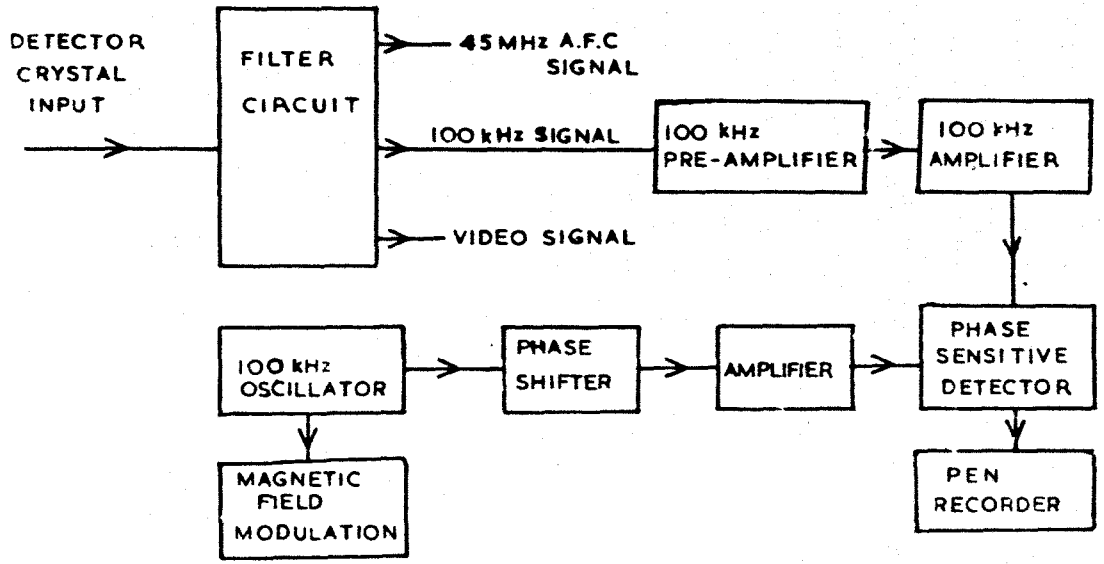

FIG. 6.7 BLOCK DIAGRAM OF THE 100 kHz ELECTRONIC CIRCUITS OF THE 'MICROSPIN' SPECTROMETER

6.2 The "Microspin" Q-band E.P.R. Spectrometer

6.2.1 General description of the "Microspin" spectrometer

The "Microspin" Q-band E.P.R. spectrometer is manufactured by Hilger & Watts Ltd. (now a member of Rank Precision Industries Ltd.) and has a sensitivity at room temperature as given in Table 6.1. The spectrometer has facilities for magnetic field modulation at 100 kHz and an E.P.R. line may be displayed on a C.R.O. or pen-recorder as illustrated in Fig. 6.1.

The general features of the spectrometer are shown in Fig. 6.6. The klystron frequency can be locked to a reference cavity or to the sample cavity by a Pound stabilization system[16] operating at an intermediate frequency (i.f.) of 45 MHz, by using respectively the crystals A and B or C and D. All the crystals, of type S.I.M.8 (manufactured by the General Electric Company), are placed in tunable mounts which can be adjusted for optimum crystal output voltage at a given microwave frequency. The cavity, which was supplied by the manufacturers, is suitable for use at room temperature only. A rotatable magnet with 8 inch diameter pole pieces (Newport Instruments Type D) is used with the spectrometer.

The electronic circuits of the 100 kHz detection system are shown diagrammatically in Fig. 6.7. The filter circuit is so arranged that one crystal can be used to detect the 100 kHz E.S.R. signal, the "video" E.S.R. signal and the 45 MHz signal from the Pound stabilization system. The 100 kHz signal amplifier is a low noise pre-

amplifier and the phase sensitive detector (p.s.d.) is designed according to the circuit given by Schuster[17].

The magnetic field is measured with a magnetometer (manufactured by Newport Instruments) which relies on the nuclear magnetic resonance (n.m.r.) technique[18]. The n.m.r. absorption signal is obtained from an aqueous solution of a lithium salt; over the range of magnetic field 0.2 to 0.6 T the proton resonance is observed and for the range 0.5 to 1.5 T the lithium resonance is observed. The values of the magnetic field in terms of the n.m.r. frequency, $F_{n.m.r.}$, are given as:-

$$B(\text{Tesla}) = 0.023487\ F_{n.m.r.}\ (\text{MHz})$$

in the proton resonance range

$$B(\text{Tesla}) = 0.0604616\ F_{n.m.r.}\ (\text{MHz}) \qquad 6.16$$

in the lithium resonance range.

An assessment of the noise figure, F, for the "Microspin" spectrometer is difficult since no precise data concerning the output noise of the klystron, crystal detector, or pre-amplifier could be obtained from the manufacturers. The low sensitivity of the Q-band "Microspin" spectrometer, as shown in Table 6.1, was confirmed by measurements made in the course of the present work and this low sensitivity indicates that an approximate value for F is 30 db. From the circuit details an estimation of the noise figure of the pre-amplifier was made and a contribution to F of approximately 0.5 db was

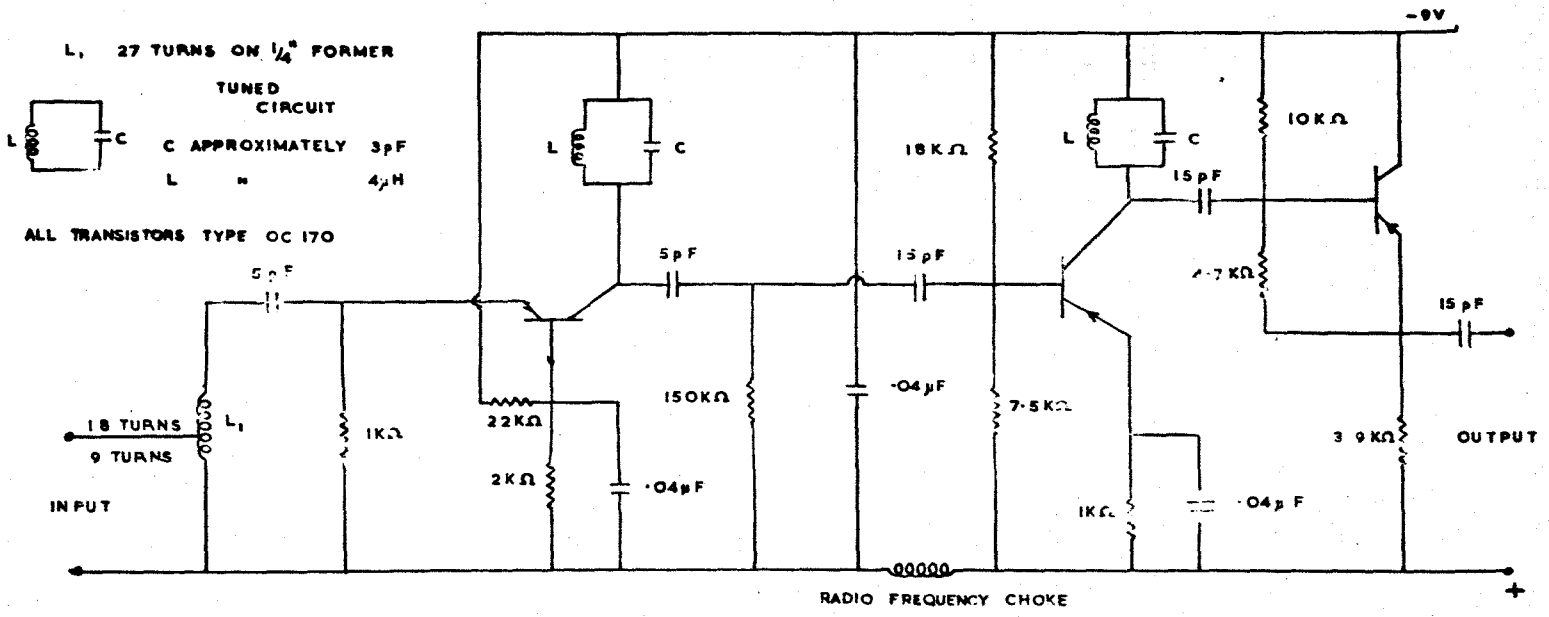

FIG. 6.9 CIRCUIT DIAGRAM OF THE PRE-AMPLIFIER OPERATING AT 45 MHZ

obtained. Provisional data[19] for the S.I.M.8 and S.I.M.9 detector crystals gave a value of noise temperature ratio corresponding to approximately 17 db and therefore this crystal noise was considered to give a major contribution to the value of F. The particular detector crystal which was used in the spectrometer was selected from a number of crystals so that the best signal-to-noise ratio on an E.P.R. line was obtained.

6.2.2 Modifications of the "Microspin" spectrometer

(a) The locking of the klystron frequency to the resonant frequency of the sample cavity

The Pound locking system, on the "Microspin" spectrometer, which was designed to lock the klystron frequency to the resonant frequency of the sample cavity was found to be inadequate. A modified locking system was therefore constructed and this is shown diagrammatically in Figs. 6.8 and 6.9.

The operation of this Automatic Frequency Control (A.F.C.) system may be described as follows. Microwave radiation from the magic-tee 1 proceeds to the sample cavity and a fraction (10 db) of this radiation is coupled into arm 2 of the A.F.C. microwave circuit. This radiation passes through an isolator, divides at the magic-tee 2 and is then modulated at 45 MHz by the A.F.C. modulator crystal. The microwave radiation at frequencies of the carrier frequency ±45 MHz then reaches the A.F.C. signal crystal via a phase shifter. Providing

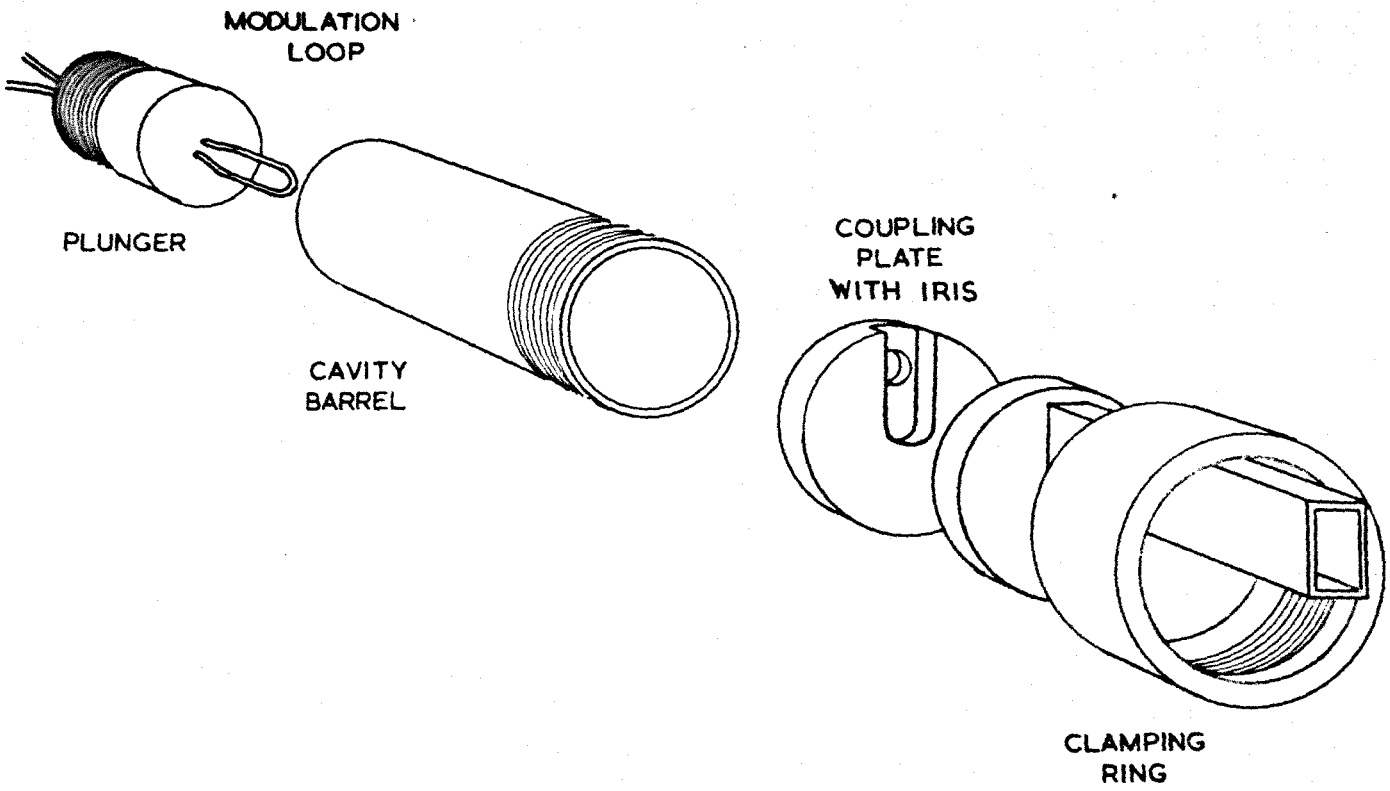

FIG. 6.10 DIAGRAM OF THE SAMPLE CAVITY

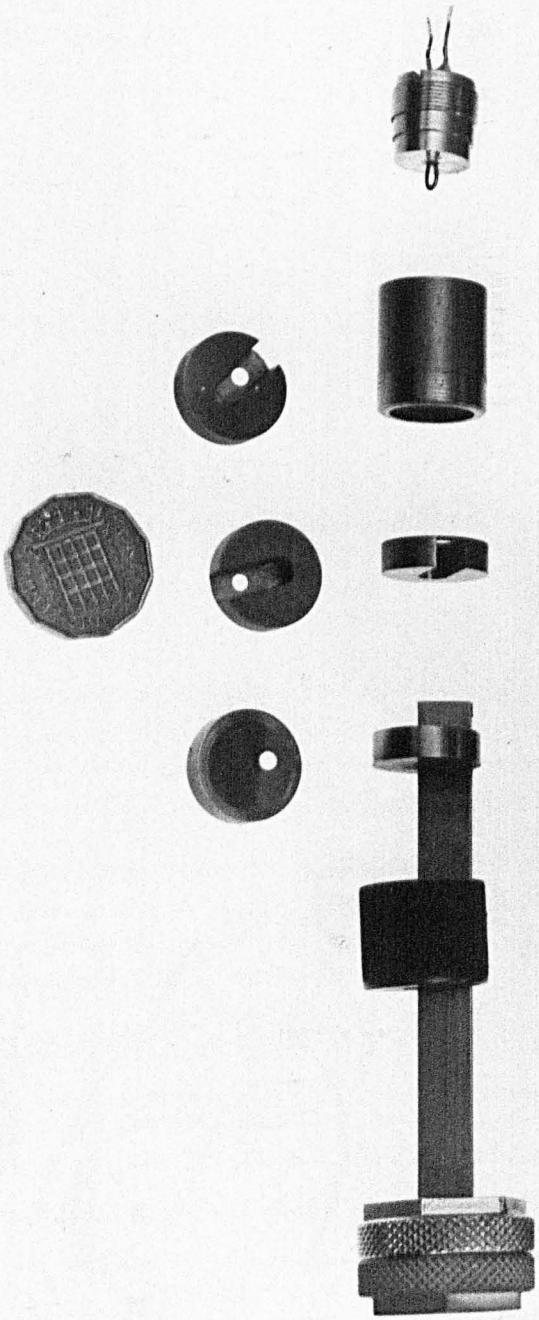

FIG. 6.11

THE SAMPLE CAVITY WITH A SELECTION OF

COUPLING PLATES

no radiation is reflected back from the sample cavity, (i.e. the klystron frequency and the resonant frequency of the cavity are identical) there is no 45 MHz output signal at the A.F.C. signal crystal. However, if the frequency of the klystron is different from the resonant frequency of the cavity, microwave radiation is coupled into arm 1 and a 45 MHz output signal appears at the A.F.C. signal crystal. This 45 MHz signal is amplified, rectified and applied to the reflector of the klystron as a correction voltage.

This modified A.F.C. system gave satisfactory locking of the klystron frequency to the resonant frequency of the sample cavity and was easily incorporated into the "Microspin" spectrometer. With the exception of the 45 MHz pre-amplifier, all the electronic circuits, which are shown in block diagram form in Fig. 6.8, are part of the "Microspin" A.F.C. locking system.

(b) The construction of a sample cavity for operation at low temperatures

The sample cavity which was constructed for use at low temperatures is shown diagrammatically in Fig. 6.10 and is also illustrated in Fig. 6.11. This cavity was designed to operate in the H_{011} mode and for this type of cavity it is unnecessary to achieve good electrical contact between the end plates (the coupling plate and tuning plunger respectively) and the cylindrical cavity walls.

A value for the Q-factor was estimated from measurements of the frequency difference between the half-power points on the cavity absorption curve. The Q-factor of the cavity containing a "non-lossy" sample was found to be approximately 3000 (±5%) at room temperature and 4000 (±10%) at liquid helium temperature. However, in some cases these values were substantially reduced owing to the presence of n-type GaP crystals in the cavity.

The cavity Q-factor, defined by equation 6.1, must take into account all the dissipation of microwave power at the cavity. The major causes of power loss are due to:-

(a) power loss in the walls of the cavity

(b) loss due to power leaking out of the cavity, as determined by the coupling iris,

(c) power loss in the sample.

It is therefore possible to express the Q-factor in the form

$$\frac{1}{Q} = \frac{1}{Q_o} + \frac{1}{Q_E} + \frac{1}{Q_L} \qquad 6.17$$

where Q_o is determined by the wall losses only

Q_E is determined by the power leaking out of the cavity

and Q_L depends on the losses in the sample.

The values of Q_o and Q_E are comparatively constant for a given cavity but the value of Q_L can change substantiallysince it depends on the type of sample in the cavity. For a sample of conductivity, σ,

the losses are due to eddy currents in the sample and an expression for Q_L may be written in the form

$$Q_L = \frac{\omega \int_{\text{cavity}} \frac{b^2}{\mu_o} d\tau}{\int_{\text{sample}} \sigma E^2 d\tau} \qquad 6.18$$

where E is the value of the microwave electric field at the sample. A calculation of Q_L for a Q-band cylindrical cavity operating in the H_{011} mode and containing a sample situated on the axis of the cavity is given in Appendix 2. For a rectangular sample of size 0.55cm x 0.55mm x 100μm and of conductivity 1 mho cm^{-1} the value of Q_L is approximately 5000 (see Fig. A2.1) and therefore the sample losses significantly effect the overall Q-factor of the cavity. The n-type GaP samples used in the present work had values of σ in the range 10^2 mho cm^{-1} to 10^{-4} mho cm^{-1} (see Fig. 7.4) and hence major experimental difficulties were expected to arise from the sample losses.

If a powdered sample is used, however, these difficulties can largely be overcome. The powder is usually dispersed in some non-conducting material and the contact between neighbouring conducting particles is minimal; a high resistance sample is therefore produced and eddy current losses in the sample are reduced. Some of the results given in the final chapter were obtained from powders of high conductivity n-type GaP and the powder was conveniently dispersed in a laboratory wax manufactured by the British Drug Houses Ltd.

The modulation coil for the 100 kHz magnetic field modulation was arranged in the tuning plunger as illustrated in Fig. 6.10. The sample was mounted inside the loop of the coil and it was found that the maximum amplitude of the magnetic field modulation at the sample was of the order of 1 mT. Careful positioning of the coil is required in order to minimise the degradation to the cavity Q-factor.

Attempts were made to devise a variable coupling system for the cavity in a manner similar to that described by Gordon[20]. However these attempts proved to be unsuccessful owing to spurious microwave reflections and it was decided that optimum coupling could best be achieved by having interchangeable coupling plates with irises of different size. The cavity with a selection of coupling plates are illustrated in Fig. 6.11.

(c) Magnetic field calibration

In low temperature E.P.R. experiments, the magnetic field could not be measured with the magnetometer manufactured by Newport Instruments; no n.m.r. absorption line was observed because the probe of the magnetometer was situated outside the cryostat in an inhomogeneous magnetic field. However, a magnetometer with a small probe was constructed, according to the circuit given by Robinson[21], which gave a satisfactory n.m.r. absorption line even when the cryostat was situated between the pole pieces of the magnet. In this magnetometer a Varactor Diode, D, was used as a variable capacitance to facilitate the adjustment of the oscillator frequency[22].

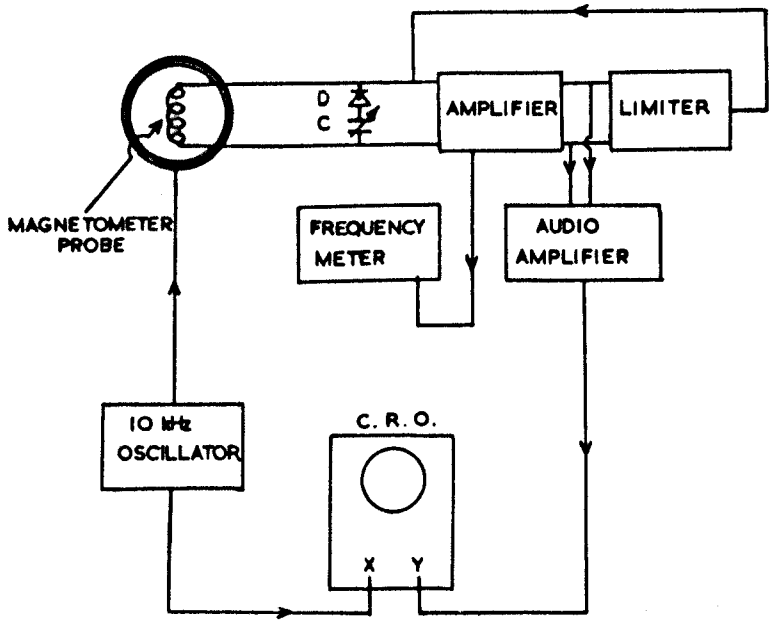

FIG. 6.12. BLOCK DIAGRAM OF THE CIRCUIT ARRANGEMENT FOR THE MAGNETIC FIELD CALIBRATION.

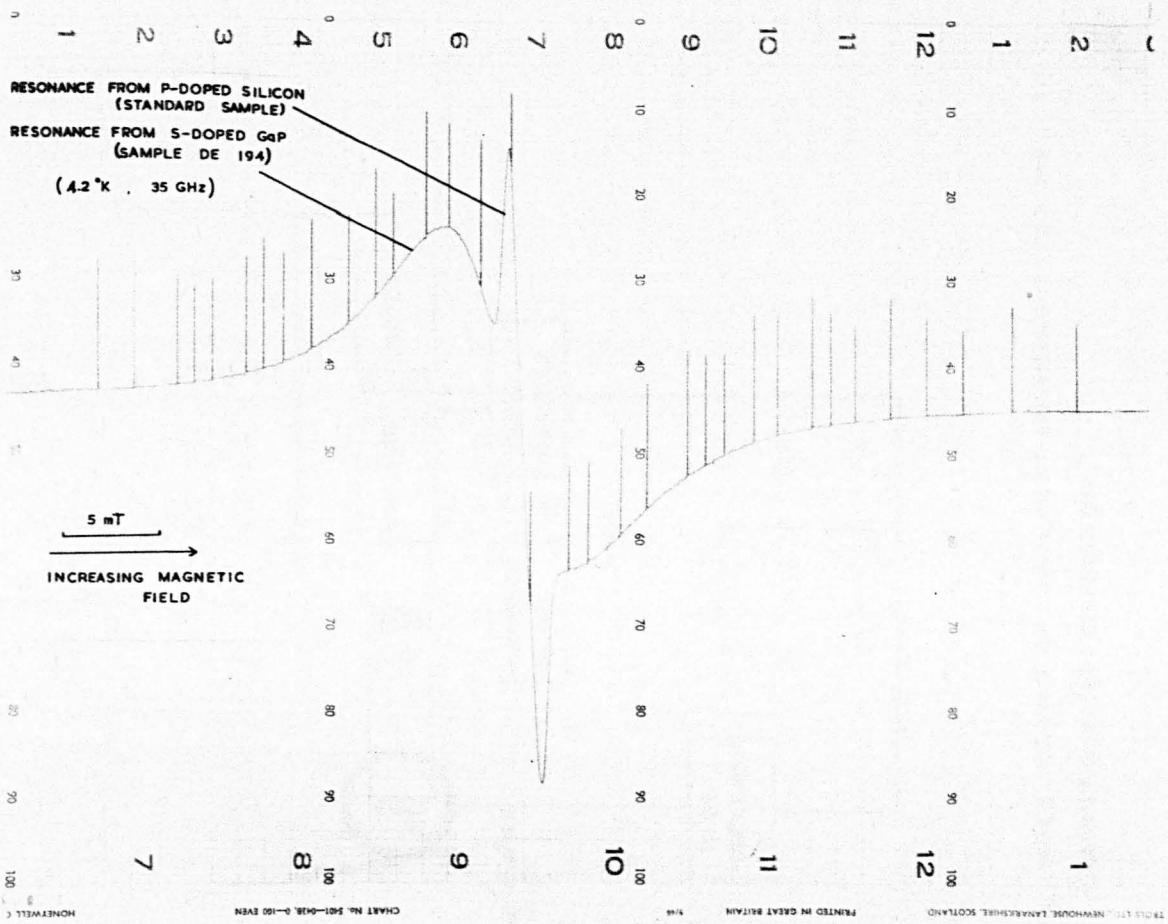

FIG. 6.13. RECORDING OF AN E.P.R RESONANCE FROM S-DOPED GaP SHOWING MAGNETIC FIELD CALIBRATION MARKERS.

Since the E.P.R. resonance from the n-type GaP samples was too weak to be observed using crystal-video detection, it was necessary to put magnetic field markers on the pen-recorder trace of the E.P.R. resonance line and so obtain a magnetic field calibration. The circuit arrangement for this calibration is shown diagrammatically in Fig. 6.12. A magnetic field modulation, of approximate frequency 10 KHz, was applied to the magnetometer probe and the proton resonance absorption line was observed on a C.R.O. (A high frequency, 10 KHz, was used to ensure that the sample in the E.P.R. cavity was well shielded from this magnetic field modulation). The frequency of the magnetometer was monitored with a Marconi Counter/Frequency meter, Type 1417.

Briefly, the method adopted for the calibration was as follows. The magnetic field was swept to display the E.P.R. line and, when the proton resonance signal was observed on the C.R.O., a marker 'pip' was placed on the pen-recorder trace and the reading of the frequency meter was noted. The frequency of the magnetometer was then increased by adjustment of the voltage across the varactor diode, D, and the above procedure was repeated. By this method, a series of magnetic field markers could be recorded and a typical field calibration of an E.P.R. line is shown in Fig. 6.13.

It was estimated that differences in magnetic field could be measured to an accuracy of ±0.05 mT. However, since the magnetometer probe was some distance from the sample situated in the E.P.R. cavity, the actual magnetic field at the sample could not be measured

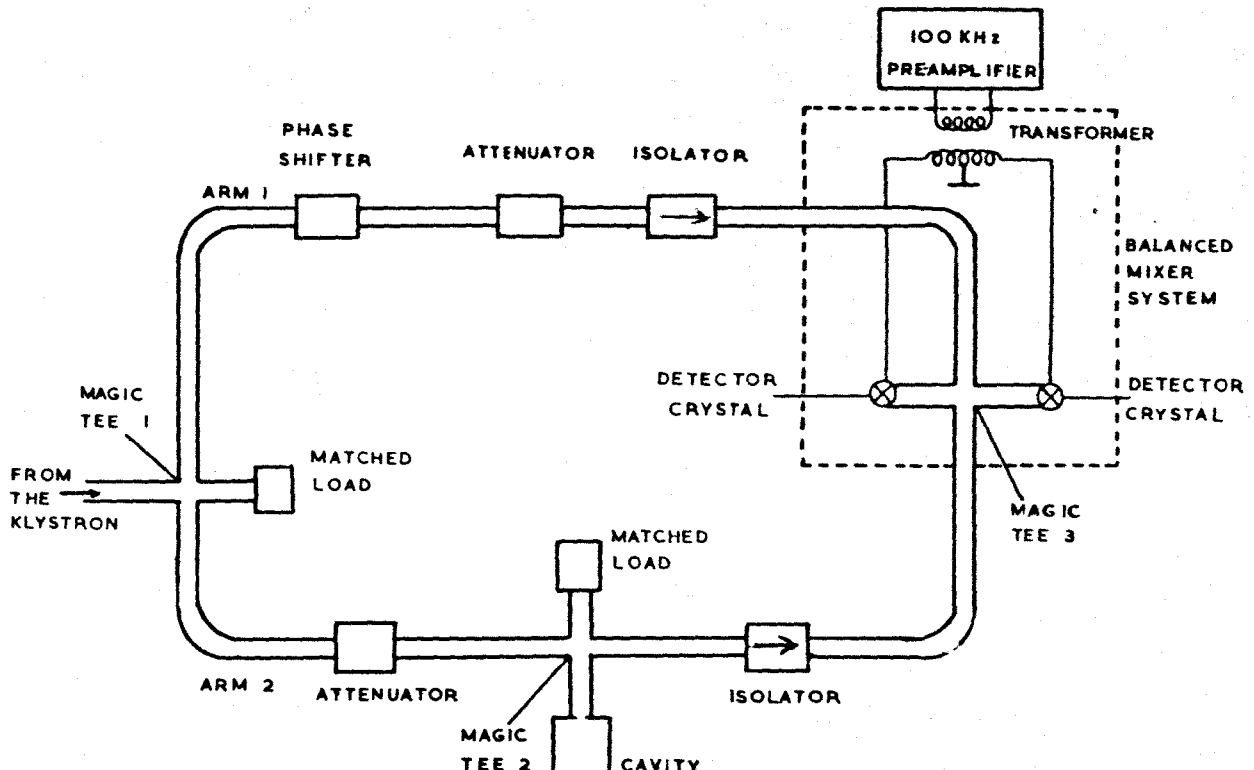

FIG.6.14 DIAGRAM OF THE BALANCED MIXER CIRCUIT

to this accuracy. Measurements of the magnetic field profile between the pole pieces of the magnet were obtained and it was estimated that the magnetic field at the sample could be measured to an accuracy of ±1 mT.

(d) Balanced mixer detection

In an effort to improve the sensitivity of the "Microspin" spectrometer a balanced mixer detection system was constructed in a manner similar to that described by Henning[23]. The general features of this system are shown in Fig. 6.14.

Microwave radiation from the klystron divides at the magic-tee 1 into arms 1 and 2. The radiation in arm 2 proceeds via the sample cavity to the magic-tee 3, whereas the radiation in arm 1 proceeds directly to the magic tee 3. The balanced mixer employs two detector crystals arranged in such a manner that the E.P.R. signal arrives at each of them in phase while the radiation coming directly from the klystron arrives at each crystal with a phase difference of 180°. This detection system, therefore, is useful in minimising the effect of klystron noise arising from fluctuations in amplitude of the microwave radiation.

The E.P.R. spectrometer employing the balanced mixer detection system was found to be approximately $\sqrt{2}$ times less sensitive than the spectrometer whose circuit arrangement is shown in Fig. 6.8. This loss in sensitivity can be explained if it is assumed that the klystron noise is negligibly small compared with other sources of

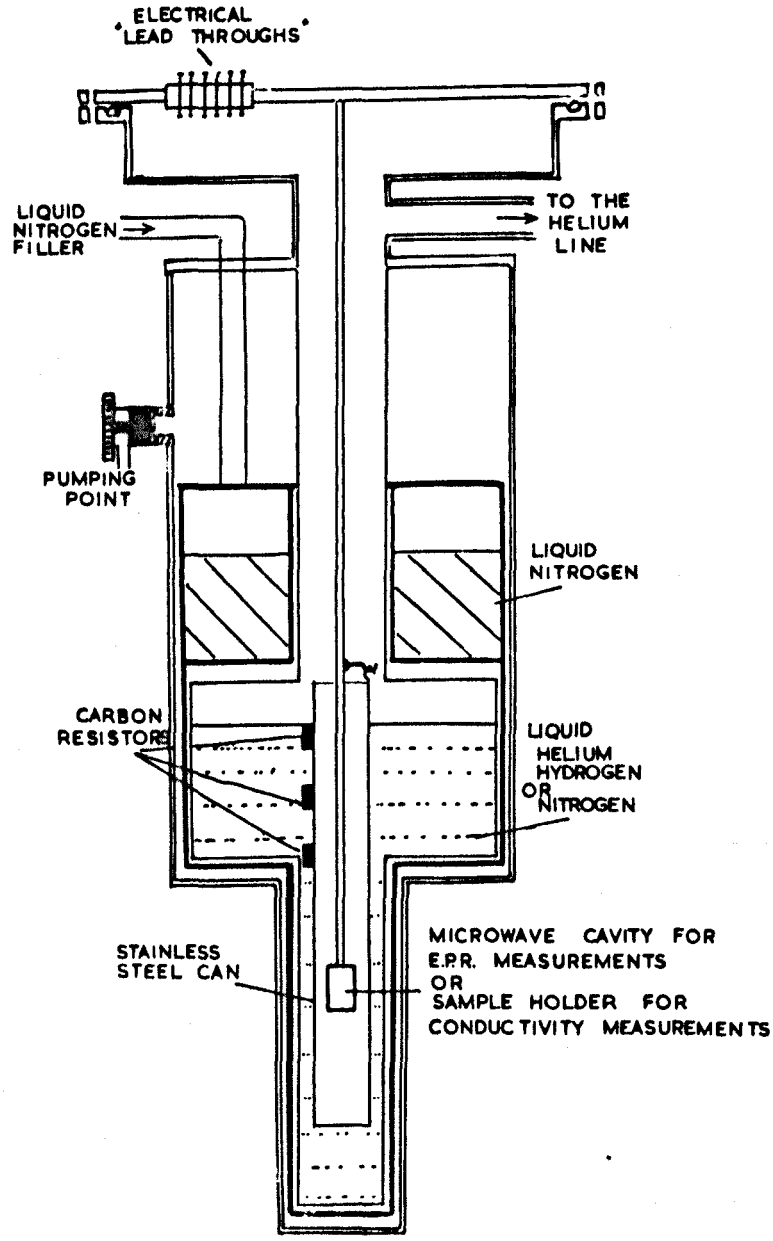

FIG. 6.15 DIAGRAM OF THE METAL CRYOSTAT (not to scale).

noise and that the lower sensitivity is due to the reduction, by a factor of 2, of microwave power at the E.P.R. cavity. It was decided to use the spectrometer with the circuit arrangement as shown in Fig. 6.8 and make use of the balanced mixer detection system in cases where the klystron noise was significantly large.

6.3 Low Temperature Techniques

The investigations on both the paramagnetic resonance and transport properties of electrons in n-type GaP were carried out on samples at temperatures in the range 4.2°K to room temperature (293°K) and in one of the E.P.R. measurements the sample was maintained at a temperature of approximately 2.5°K. Different liquid coolants were used for different temperature ranges as described below and the metal cryostat, which was used for all the low temperature measurements, is shown diagrammatically in Fig. 6.15.

6.3.1 The cryostat

The metal cryostat was manufactured by Oxford Cryogenics Ltd., has an inner container of capacity 1½ litres and requires approximately 1 litre of liquid nitrogen to fill the outer jacket. The liquid coolant was excluded from the sample by a thin walled stainless steel can in both the E.P.R. and conductivity measurements and this enabled the sample to be heated to a temperature above that of the coolant.

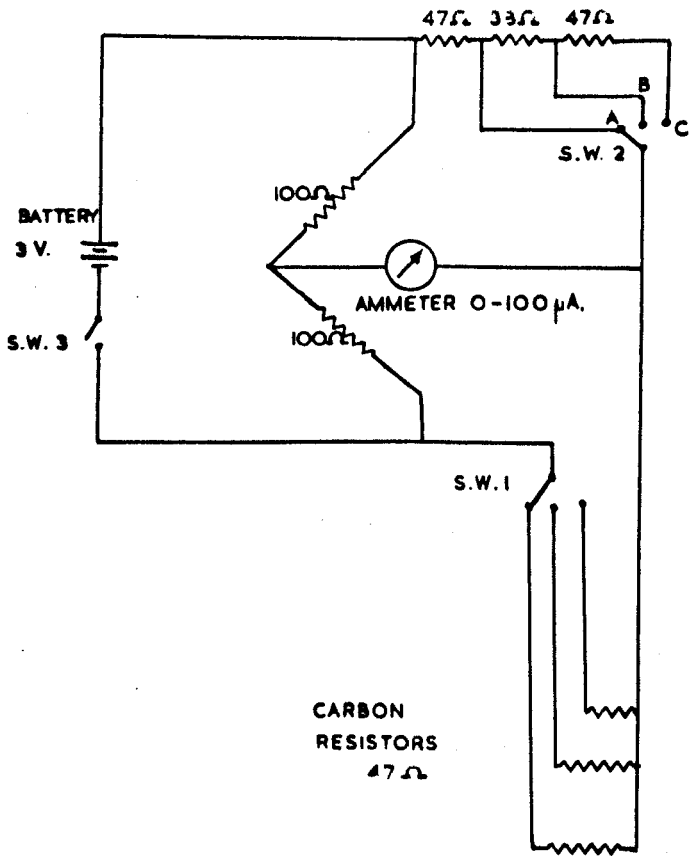

FIG. 6.16. CIRCUIT DIAGRAM OF THE LEVEL INDICATOR.

[POSITIONS OF S.W. 2
A. FOR LIQUID NITROGEN
B. " " HYDROGEN
C. " " HELIUM]

Temperatures in the range 2.5°K to 4.2°K and 4.2°K to 15°K were obtained by using liquid helium coolant. In the first range the sample temperature was lowered from 4.2°K by reducing the pressure of helium gas inside the inner container and in the second range the sample was heated inside the stainless steel can. In a similar manner, temperatures in the range 15°K to 110°K were obtained by using liquid hydrogen or liquid nitrogen coolants. Temperatures in the range 110°K to 293°K were obtained with only gaseous nitrogen in the inner container and liquid nitrogen in the outer jacket.

The level of the liquid coolant inside the cryostat was monitored by means of a simple bridge-circuit as shown in Fig. 6.16. Three carbon resistors were mounted at different positions on the outside of the stainless steel can as illustrated in Fig. 6.15. The switch S.W.1 (in Fig. 6.16) allows any one of the three resistors to be connected to the bridge circuit; the switch S.W.2 allows the level indicator to be used with helium, hydrogen, or nitrogen liquid coolants. The bridge was approximately balanced, on each range, for a resistor in the liquid coolant and a marked out of balance current was observed when the resistor was in the gas above the coolant. Hence the level of liquid coolant was monitored with respect to the positions of the carbon resistances.

6.3.2 Temperature measurement

Several types of thermometer can be used in the measurement of low temperatures[24,25]. Unfortunately no single thermometer can be used to make accurate temperature measurements over the range 4.2°K to 293°K and, in the present work, two types of thermometer were used, namely, a copper-constantan thermocouple and a carbon resistor.

The copper-constantan thermocouple was found to be suitable for temperature measurements in the range 20°K to 293°K. The e.m.f., E_{th}, from the thermocouple was measured with a "CROPICO" potentiometer (Croydon Precision Instrument Co.) and was calibrated at the following temperatures: 4.2°K, 20°K, 77°K and 293°K. The dependence of E_{th} on the temperature, T, was assumed to be of the form[26]

$$E_{th} = A + BT + CT^2 \qquad 6.19$$

and the values of the constants A, B, C were obtained by fitting the calibration measurements to this equation. The temperature measurements with the thermocouple, in the range 20°K to 293°K, were found to be accurate to ±0.5°K.

The carbon resistance thermometer was found to be suitable for temperature measurements in the range 2.5°K to 77°K. Resistors manufactured by the Allen-Bradley Resistor Company have been found to give reproducible temperature measurements and were therefore used. A constant current of 10μA was passed through the resistor during all temperature measurements since this low current was found to give no

measurable heating effect of the resistor. The potential difference across the resistor was measured with the "CROPICO" potentiometer and hence the resistance was obtained. The Allen-Bradley resistors were calibrated by measurements at 2.5°K, 4.2°K, 20°K and 77°K and the results were fitted to an equation of the form[27]

$$T = \frac{\ln R}{(D + E \ln R)^2} \qquad 6.20$$

where D and E are constants.

The temperature measurements with the resistor were accurate to ±0.1°K in the range 2.5°K to 10°K and ±0.5°K in the range 10°K to 77°K.

6.3.3 Temperature control

In discussing the control of the sample temperature two situations can be distinguished. Firstly, there is the situation in which the desired sample temperature is at or below the normal boiling point of the liquid coolant and the temperature can be controlled by the adjustment of the pressure of the vapour above the liquid coolant. Secondly, there is the situation in which the desired sample temperature is above the normal boiling point of the liquid coolant. In this case the sample is placed in poor "thermal contact" with the coolant and its temperature may then be controlled by supplying heat to the sample.

In the former situation a manostat was used to control the pressure of the vapour above the liquid coolant and the temperature of

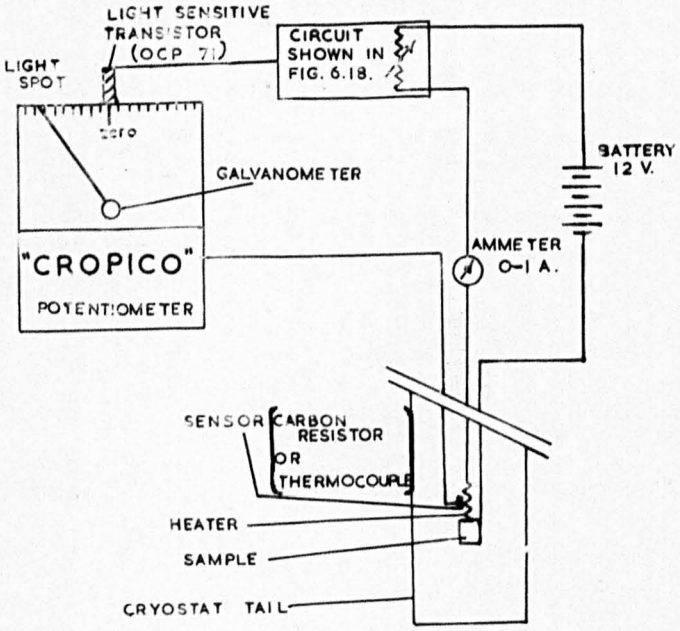

FIG. 6.17. DIAGRAM OF THE TEMPERATURE CONTROL SYSTEM.

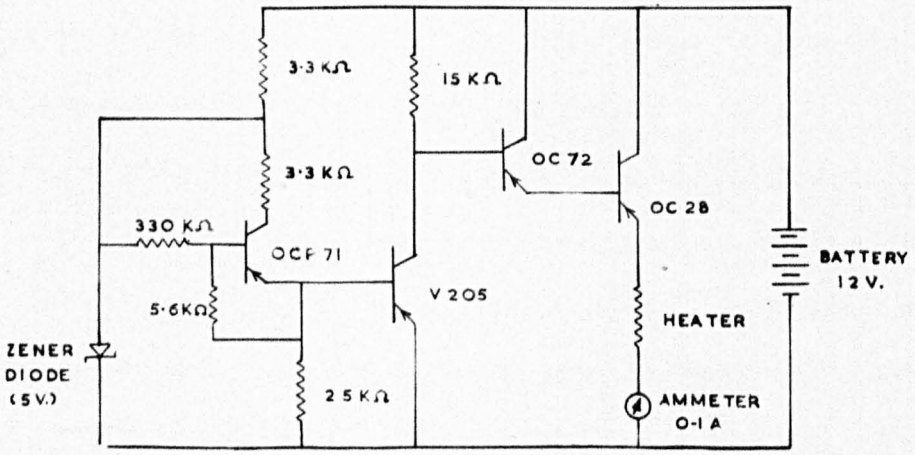

FIG. 6.18. DIAGRAM OF THE ELECTRONIC CIRCUIT SHOWN IN FIG. 6.17.

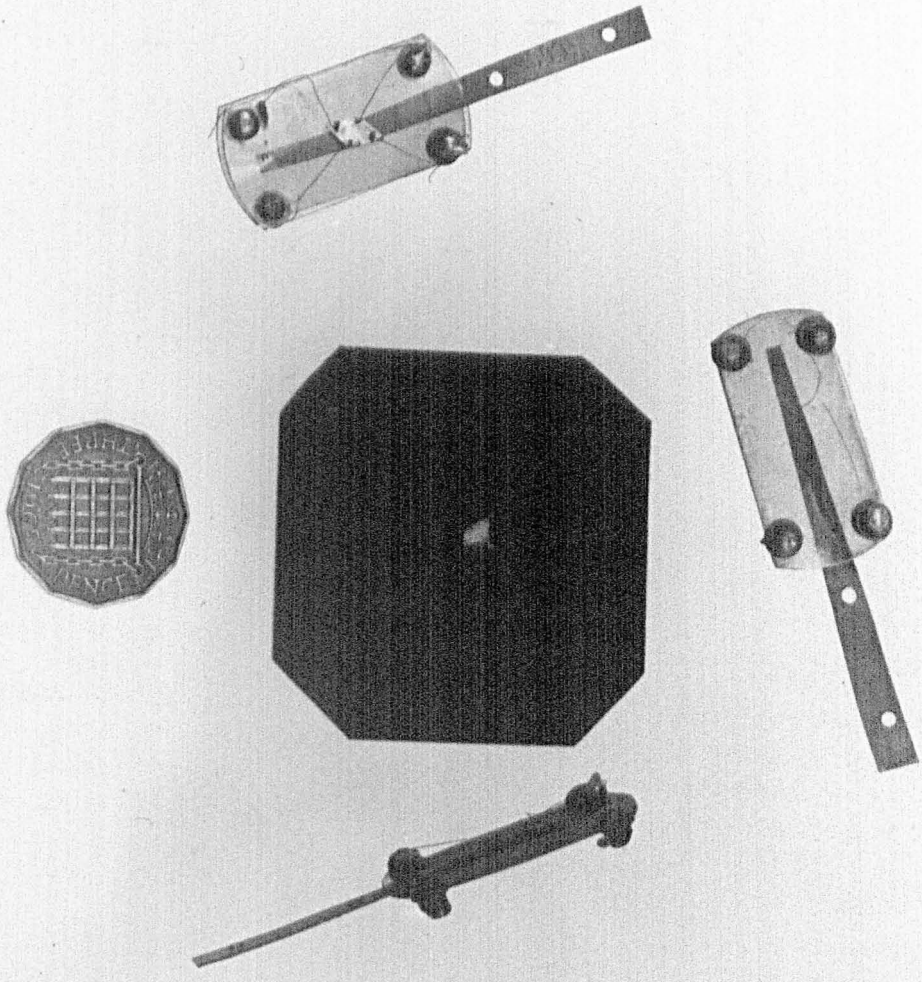

FIG. 6.19

SAMPLES AND SAMPLE HOLDERS USED FOR HALL EFFECT

AND CONDUCTIVITY MEASUREMENTS

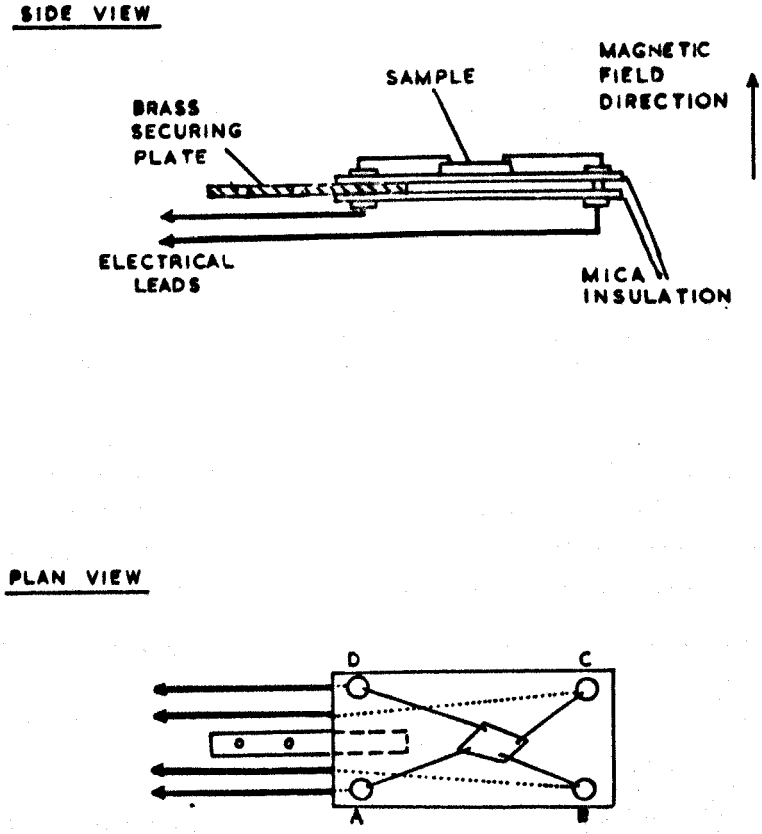

FIG. 6.20. DIAGRAM OF THE SAMPLE ARRANGEMENT FOR HALL EFFECT & CONDUCTIVITY MEASUREMENTS.

the liquid was estimated from the pressure measurements[24,25]. In the latter situation a system, shown diagrammatically in Figs. 6.17 and 6.18, was found to control the sample temperature adequately.

The operation of this control system is as follows. If the temperature at the sensor (a thermocouple or resistor) is below a desired temperature, a current is supplied to the heater and the sensor temperature increases. As the sensor temperature approaches the desired temperature the light spot on the "CROPICO" potentiometer moves to the zero mark, illuminates a photo-transistor, causes the heater current to be reduced and hence stabilizes the sensor temperature. Since the sensor was placed very close to the sample, a steady temperature was also obtained in the sample and the sample temperature was controlled to approximately $\pm 0.5^{\circ}K$ in the range $2.5^{\circ}K$ to $10^{\circ}K$ and $\pm 1.0^{\circ}K$ in the range $10^{\circ}K$ to $293^{\circ}K$.

6.4 Conductivity and Hall Effect Measurements

For the present work only small thin samples of n-type GaP were available (approximate size 4mm x 4mm x 100μm) and therefore the Van der Pauw method, described in section 4.2, was used for the measurements of Hall effect and conductivity. The samples were mounted on a former, as illustrated in Figs. 6.19 and 6.20 and this former was then fixed to a rod so that the sample could be positioned in the cryostat in the magnet gap. At low temperatures the resistance of the samples was of the order of $10^{7}\Omega$ and so care was necessary to prevent leakage between the four electrical leads to the sample.

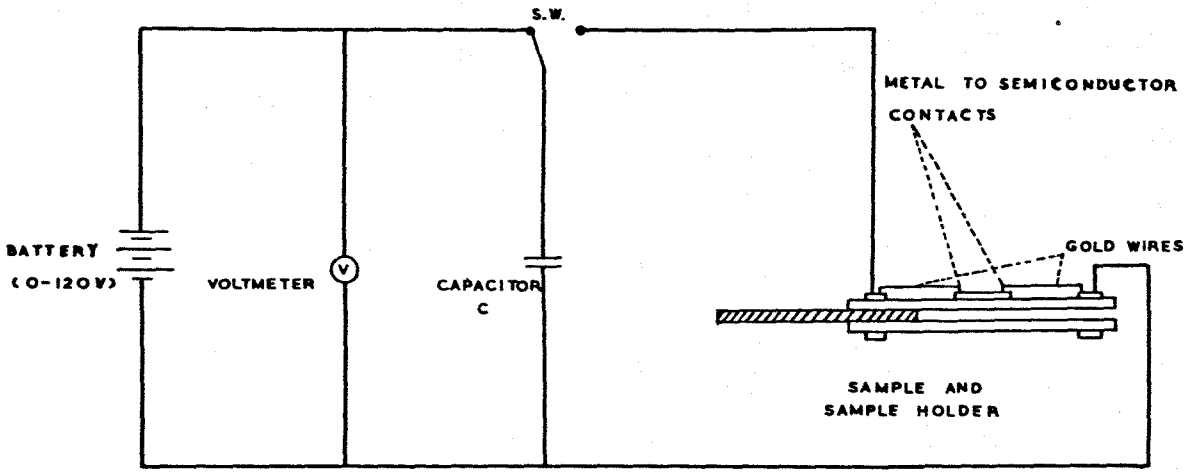

FIG. 6.21. THE CIRCUIT ARRANGEMENT FOR THE SPOT-WELDING OF CONTACTS ONTO THE SAMPLES

6.4.1 Electrical contacts

An important aspect of electrical conductivity measurements is the making of suitable contacts to the specimen. These should be of low resistance and of small area compared with the size of the specimen so that they do not disturb the uniformity of the current flow. Some of the more important types of contacts are as follows:-

(a) pressure contacts

(b) soldered or brazed contacts

(c) spot-welded contacts

(d) alloyed contacts

(e) diffused contacts

(f) evaporated contacts

(g) plated contacts

(h) painted contacts.

Only two of the above types of contacts will be discussed; namely, the spot-welded and alloyed contacts.

The spot-welding technique is widely used for making electrical contacts to samples; such contacts can have very small areas and be accurately located. Since the time required for the spot-welding process is short, the contamination of the specimen is minimised.

A simple circuit which was used in the making of spot-welded contacts to the n-type GaP samples is shown diagrammatically in Fig. 6.21. Gold wires of approximately 0.1mm diameter were pressed lightly onto the sample and connections were made to the capacitor C.

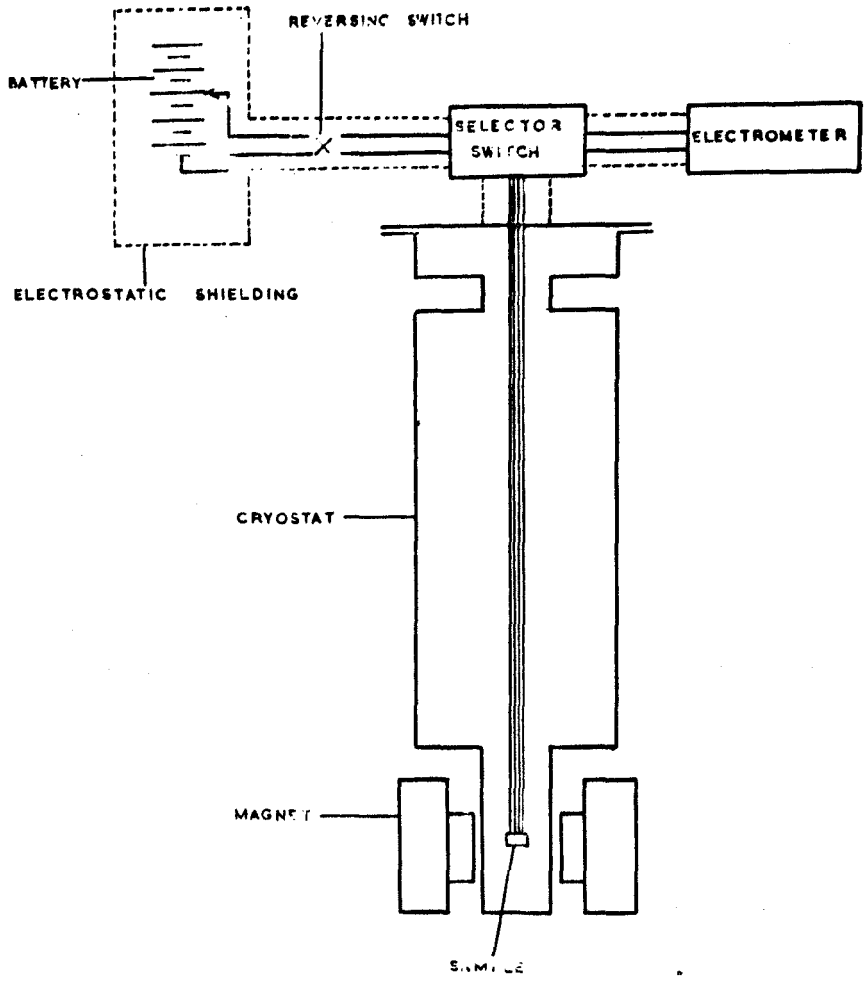

FIG. 6.22. THE CIRCUIT ARRANGEMENT FOR THE MEASUREMENT OF HALL EFFECT & CONDUCTIVITY

The capacitor was charged from a battery and a spark discharge from C fused the gold wires to the sample. Typical values of C and V were 50μf and 20 volts respectively.

Alloyed contacts are prepared by placing small pieces of an alloy metal, of low melting point, onto the sample and then heating the sample in an inert atmosphere. Some samples of n-type GaP complete with alloyed contacts were obtained from the Plessey Company, the following procedure for making the contacts being followed. Small pieces of an indium/tin alloy, approximately 0.5mm in diameter, were placed on a sample which had been etched with hot trichlorethylene and methanol. The sample was then heated to approximately 800°K for one second in an atmosphere of dry, deoxygenated hydrogen whereupon some of the alloy dissolved into the specimen to form a contact.

These alloyed contacts were of larger area than the spot-welded contacts but were much less fragile and details of the conductivity measurements on samples with both these types of contacts are given in the final chapter.

6.4.2 Measuring circuit and procedure

The arrangement of the measuring circuit for the Hall effect and conductivity is shown in Fig. 6.22. The electrometer was a micro-volt-ammeter (Model 150B, Keithley Instruments Inc.) which had an input resistance of $10^8\Omega$ when used on the 0 - 30μV scale. The current through the sample was obtained from the measurement of the voltage

across a standard resistance and the magnetic field at the sample was measured with a proton resonance magnetometer. (Details of the magnetometer are given in section 6.2.2.(c).)

Because of an unavoidable asymmetry in the position of the contacts B and D on the sample (see Fig. 6.20), there was always a steady potential difference (p.d.) between these contacts when current was passed through the sample and the Hall voltage, also measured between these contacts, was often much smaller than this steady p.d. However, the microvolt-ammeter had provisions for zero suppression and thus the Hall voltage could be measured with the steady p.d. suppressed. Electrostatic "pick-up" was found to give induced voltages which affected the Hall voltage measurements and hence it was found to be necessary to shield the apparatus as illustrated in Fig. 6.22.

REFERENCES

1. D.J.E. Ingram, "Spectroscopy at Radio and Microwave Frequencies" (Butterworth 1967).
2. C.P. Poole, "Electron Spin Resonance" (Wiley 1966).
3. T.H. Wilmshurst, "Electron Spin Resonance Spectrometers" (Hilger & Watts Monograph 1967).
4. E.A. Faulkner, J. Sci. Inst., 39 135 (1962).
5. E.A. Faulkner, Nature, 218 670 (1968).
6. T.H. Wilmshurst, W.A. Gambling, D.J.E. Ingram, J. Elect. & Control, 13 339 (1962).
7. G. Feher, Bell Syst. Tech. J., 36 449 (1957).
8. H.C. Torrey and C.A. Whitmer, "Crystal Rectifiers" M.I.T. Radiation Laboratory Series, 15 34 (1948).
9. H.A. Buckmaster and J.C. Dering, Can. J. Phys., 45 1)7 (1967).
10. B.G. Bosch, W.A. Gambling and T.H. Wilmshurst, Proc. I.R.E., 49 1226 (1961).
11. H.A. Buckmaster and J.C. Dering, Can. J. Phys., 43 1088 (1965).
12. R. King, "Electrical Noise" (Chapman & Hall 1966), F.N.H. Robinson, "Noise in Electrical Circuits" (O.U.P. 1962).
13. T.S. England and E.E. Schneider, Nature, 166 437 (1950).
14. W.A. Gambling and T.H. Wilmshurst, Proc. 3rd Int. Conf. on Quantum Electronics (Ed. P. Grivet and N. Bloembergen) p.401 (1964).

15. H.A. Buckmaster and J.C. Dering, J. Sci. Inst., 44 430 (1967).

16. R.V. Pound, Proc. I.R.E., 35 1405 (1946);
R.V. Pound, "Microwave Techniques" M.I.T. Radiation Laboratory Series, 17 490 (1946).

17. N.A. Schuster, Rev. Sci. Inst., 22 254 (1951).

18. F.N.H. Robinson, J. Sci. Inst., 36 481 (1959).

19. Provisional data for S.I.M.8, S.I.M.9 silicon mixer diodes, The General Electric Company.

20. J.P. Gordon, Rev. Sci. Inst., 32 658 (1961).

21. F.N.H. Robinson, J. Sci. Inst., 42 653 (1965).

22. G. Lancaster and A.G. Smallman, J. Sci. Inst., 42 341 (1965).

23. J.C.M. Henning, Rev. Sci. Inst., 32 35 (1961).

24. A.C. Rose-Innes, "Low Temperature Techniques" (E.U.P. 1964).

25. G.K. White, "Experimental Techniques in Low Temperature Physics" (O.U.P. 1968).

26. A.J. Hall, Practical Thermometry (Inst. of Physics 1953).

27. J.R. Clement et al., Advances in Cryogenic Engineering, 2 (1956).

CHAPTER 7

RESULTS AND DISCUSSION

The results which are given in this chapter are concerned with the E.P.R. and transport properties of electrons from the shallow donor impurity atoms (S, Te and Si) in GaP. During the course of this work results concerning the E.P.R. and electron transport properties of n-type GaP were published by other workers and these will also be discussed.

All the crystals which were used in the present work were supplied by The Plessey Company and were grown by the epitaxial deposition of GaP on 111B faces of GaAs substrates. The transport properties of electrons in these crystals will first be discussed and this will be followed by a discussion of the E.P.R. results. Finally, recommendations for future work will be given.

7.1 Hall Effect and Conductivity Measurements

Since it was only possible to obtain small thin samples of n-type GaP, the Van der Pauw method[1] of measuring Hall effect and conductivity was found to be most convenient. Some preliminary measurements were first made on the samples and these will now be discussed.

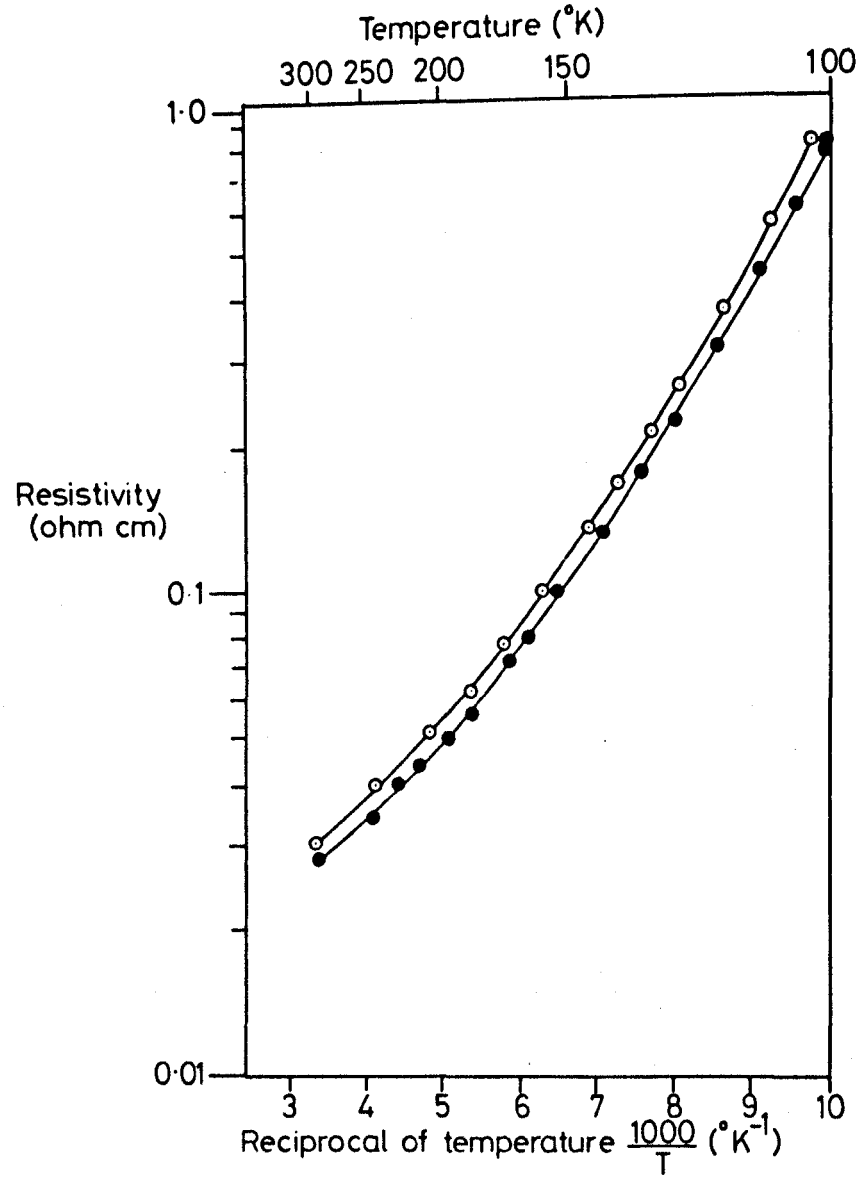

FIG. 7.1 GRAPH SHOWING THE EFFECTS OF DIFFERENT CONTACTS ON THE RESISTIVITY MEASUREMENTS OF SAMPLE DE194.

[• Data points for the crystal with alloyed contacts.
o Data points for the crystal with spot-welded contacts.]

7.1.1 Preliminary measurements

(a) The effect of different contacts on the resistivity measurements

Measurements of resistivity were made on two crystals of a particular S-doped GaP sample (DE 194). On one of the crystals alloyed contacts were made and on the other, the contacts were formed by the spot-welding technique. The variation of resistivity with temperature for the two crystals is shown in Fig. 7.1. The difference between the measured resistivities of the crystals was found to be outside the experimental error (± 1% approximately). This discrepancy is thought to be due to differences between the contact size of the alloyed and spot-welded contacts (the respective contact diameters were approximately 50 microns and 10 microns).

Although the spot-welded contacts are preferable to the alloyed contacts in that a more accurate measure of the resistivity of a sample can be obtained, (the Van der Pauw analysis is strictly applicable to point contacts), it was found that the former contacts were very fragile and often became "open-circuit". Therefore, samples with alloyed contacts were used in the measurements of Hall effect and conductivity, these being provided, complete with contacts, by The Plessey Company. It is desirable, where possible, to use samples of the "clover-leaf" shape (see Fig. 4.2(b) to minimise the effect of contact size on resistivity and Hall effect measurements. However, samples of this shape were not used since they could not be easily fabricated from the extremely small samples.

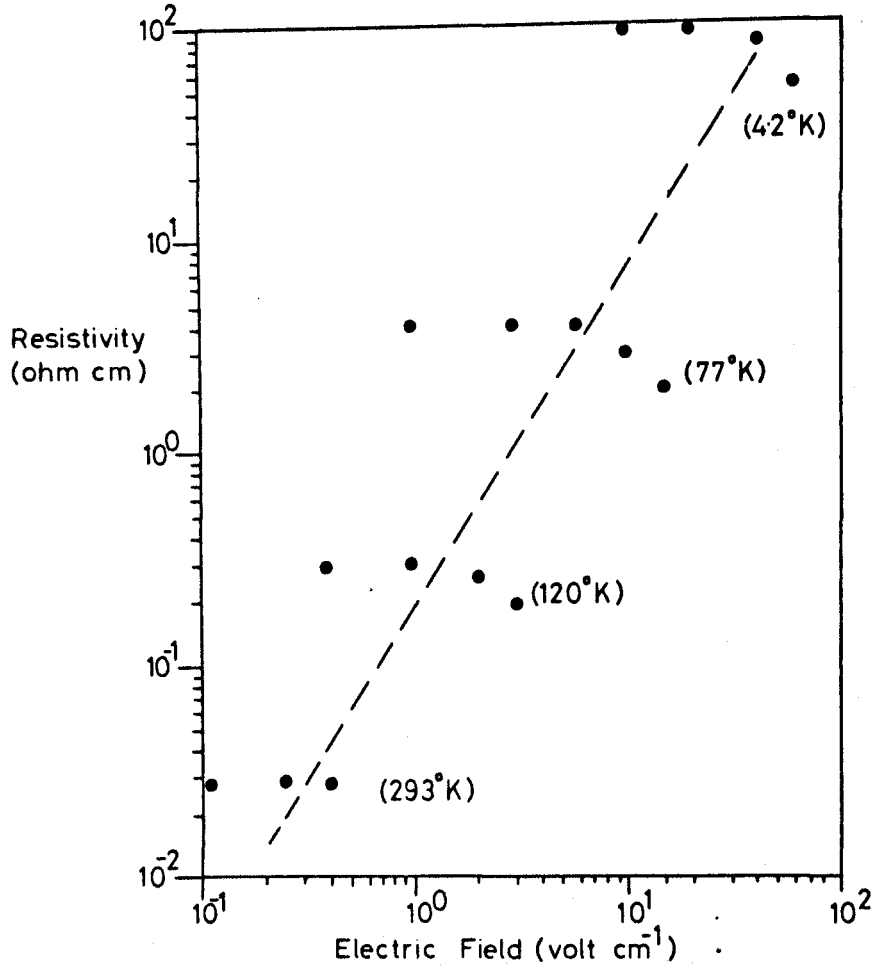

FIG 7.2 GRAPH SHOWING CHANGES OF THE RESISTIVITY OF THE SAMPLE DE194 FOR VARIATIONS OF THE ELECTRIC FIELD ACROSS THE SAMPLE.

[---- Shows the power dissipation in the sample of 1mW]

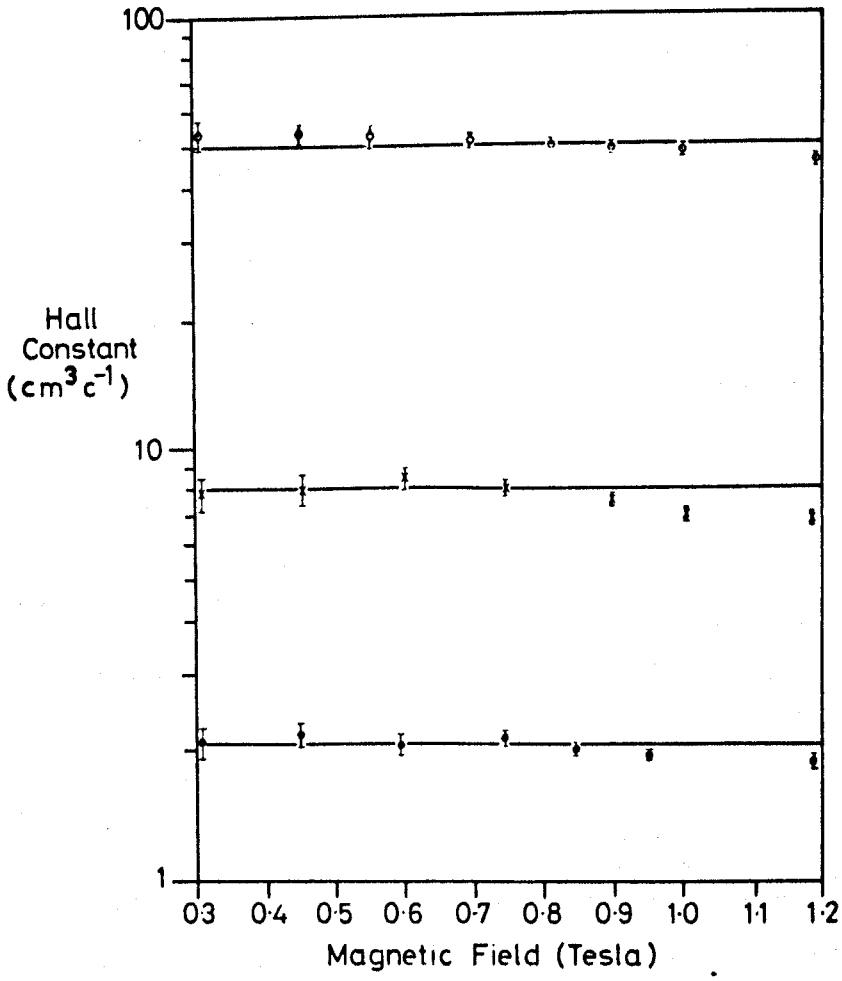

FIG. 7.3 VALUES OF THE HALL CONSTANTS FOR SAMPLES AT DIFFERENT MAGNETIC FIELDS (temperature = 293°K)

[o DE223, S-doped GaP
x DE161, Si-doped GaP
• DE194, S-doped GaP]

(b) The effect of the electric field variation on the resistivity measurements

In Fig. 7.2 the changes of the resistivity of the S-doped sample (DE 194) are shown as a function of the electric field applied to the sample. The observed deviation from ohmic behaviour in n-type GaP at high electric fields was not investigated in detail but is presumably due to "hot electron" effects. The measurements of Hall effect and conductivity were therefore carried out on samples in which the power dissipation was less than 1 milliwatt.

(c) The variation of Hall constant with magnetic field

The Hall constants for the S-doped GaP samples (DE 194, DE 223) and the Si-doped GaP sample (DE 161) were measured at room temperature at different magnetic fields, the results being shown in Fig. 7.3. For each sample the differences in the values of the Hall constants measured at different magnetic fields were found to be within the experimental errors (±10% to ±5%) for the field range 0.3 to 0.6 Tesla. In the higher field range, 0.6 to 1.2 Tesla, a slight reduction in the values of the Hall constants was observed which indicated a non-linear relationship between the Hall constant and magnetic field. It was therefore decided that magnetic fields of approximately 0.6 Tesla would be used in these measurements.

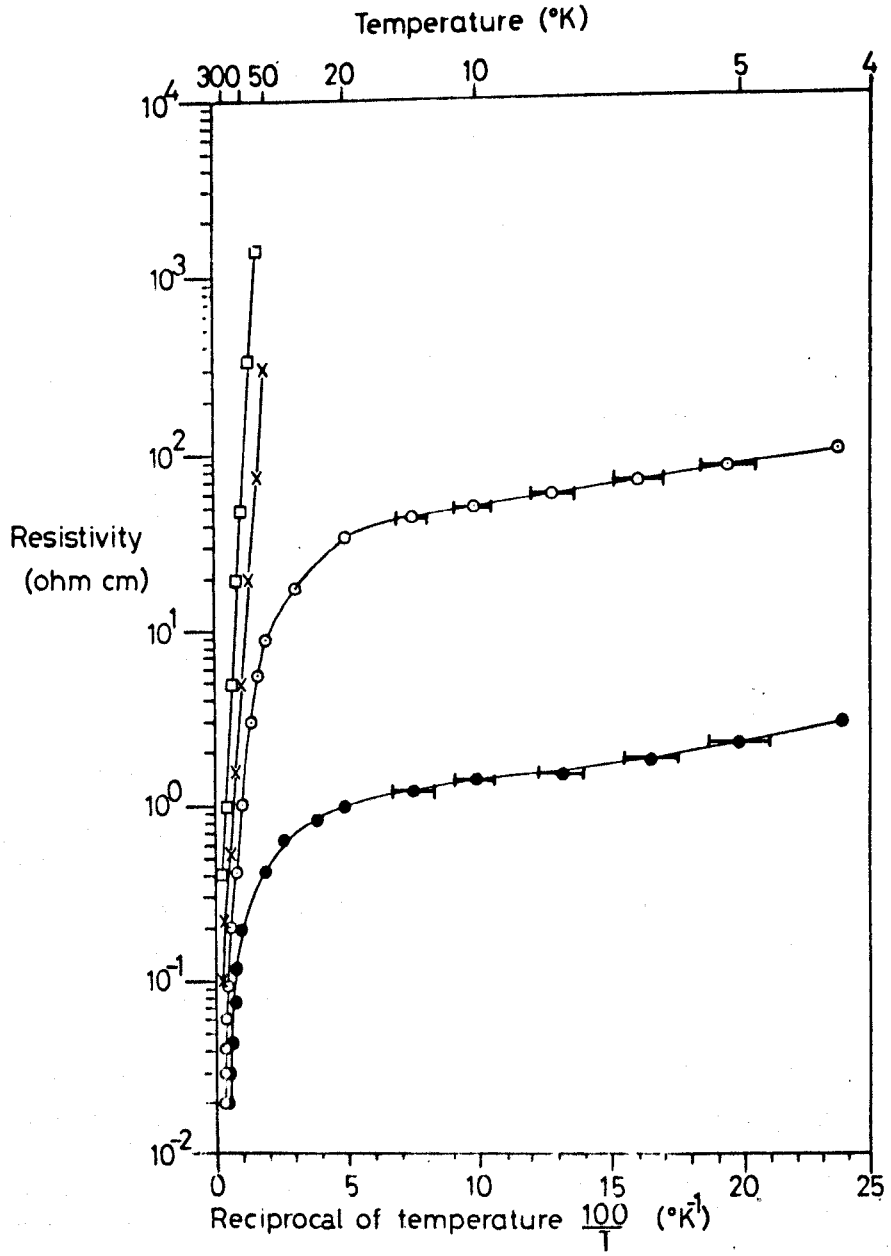

FIG 7.4 TEMPERATURE VARIATION OF THE RESISTIVITY OF THE S-DOPED GaP SAMPLES

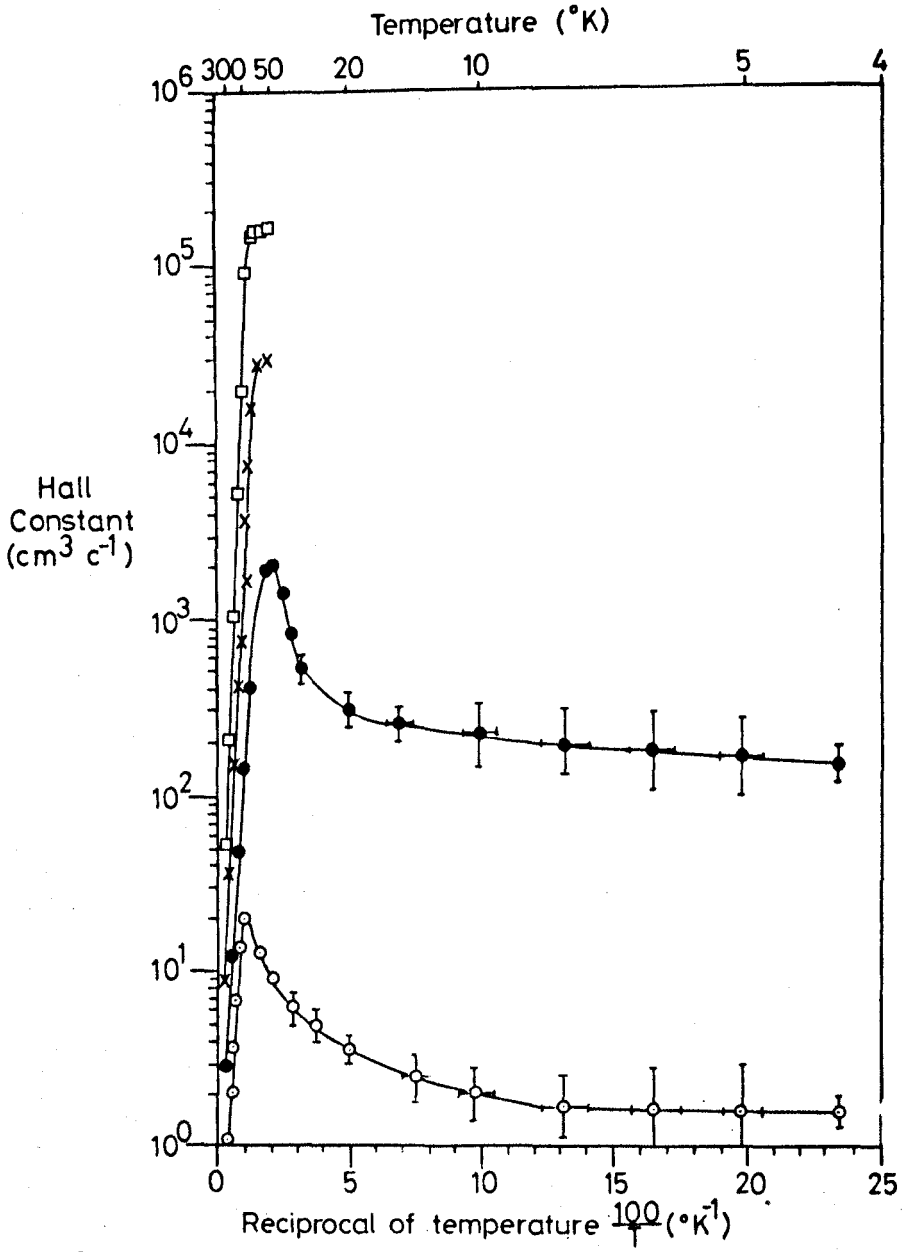

FIG 7.5 TEMPERATURE VARIATION OF THE HALL CONSTANT OF THE S-DOPED GaP SAMPLES.

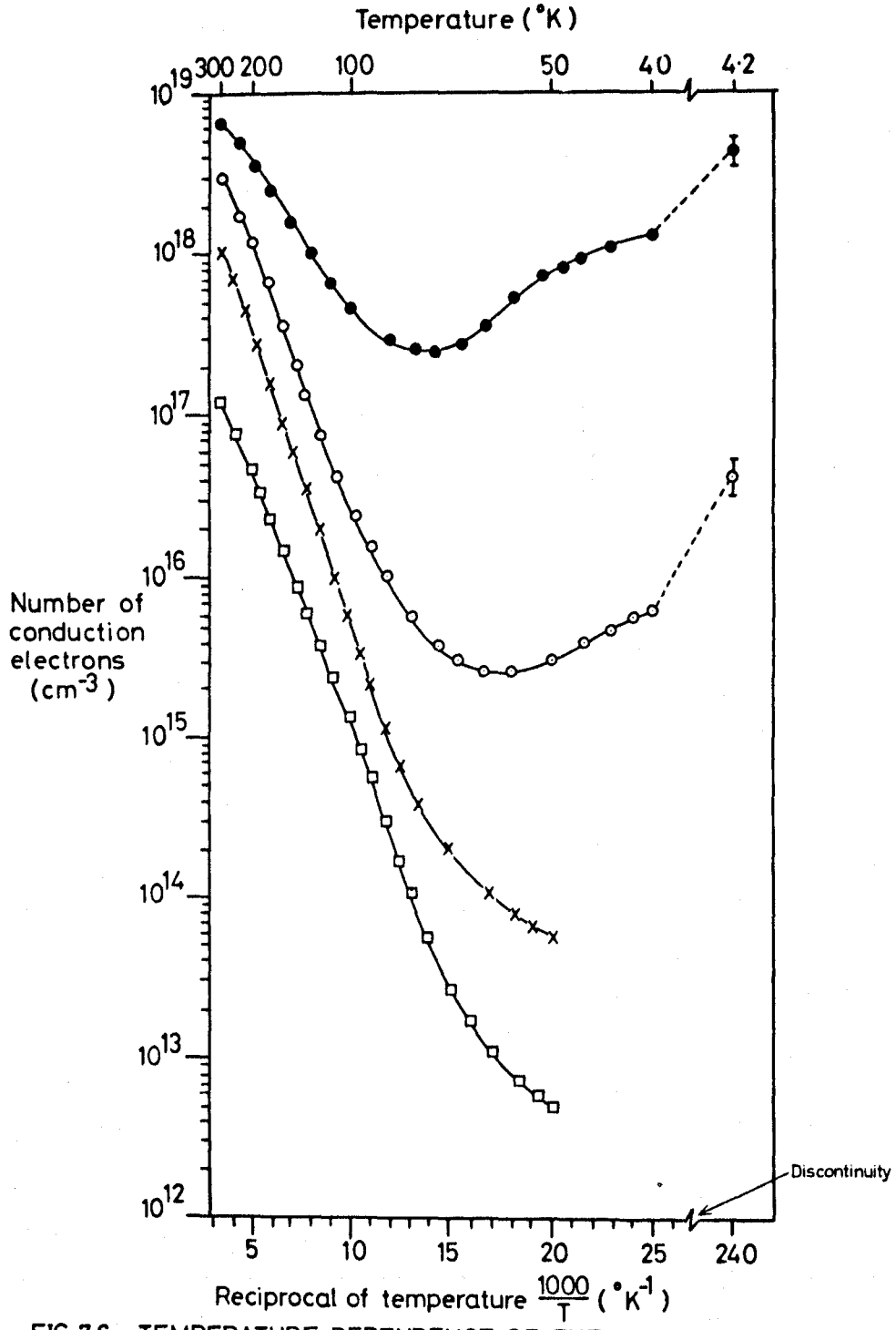

FIG 7.6 TEMPERATURE DEPENDENCE OF THE NUMBER OF CONDUCTION ELECTRONS IN S-DOPE GaP SAMPLES.

- ● DE 178
- ⊙ DE 194
- × DE 209
- □ DE 223

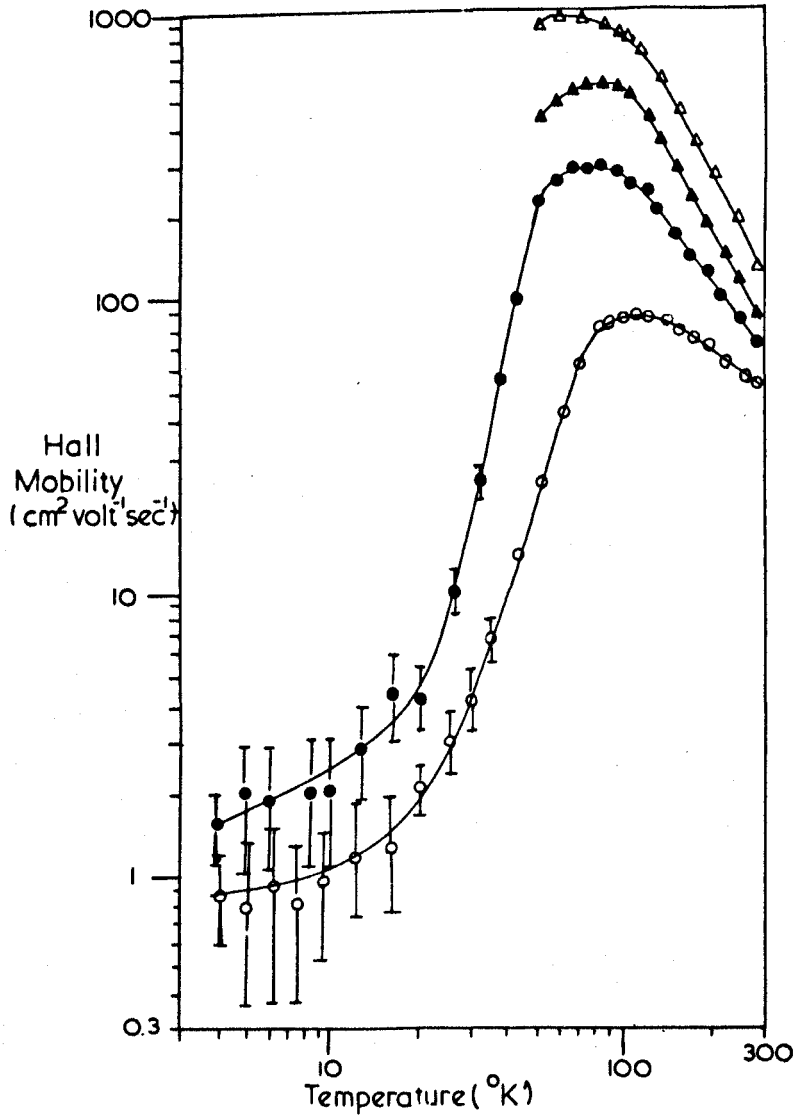

FIG. 7.7(a) MEASURED HALL MOBILITY OF ELECTRONS IN S-DOPED GaP

DE 223
DE 209
DE 194
DE 178

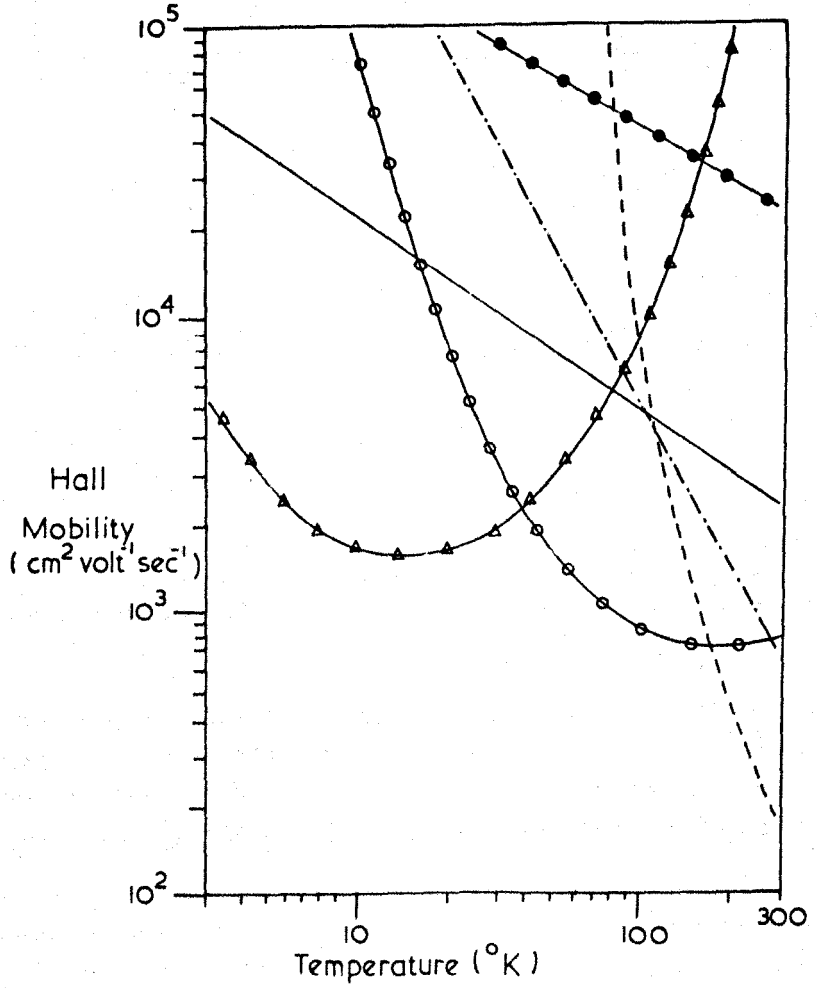

FIG. 7.7(b) CALCULATED MOBILITIES OF ELECTRONS IN n-TYPE GaP

[----- μ_O ——●—— μ_D —o—o— μ_I ($N_I = 10^{18} cm^{-3}$)
—·—·— μ_A ——— μ_S —▲—▲— μ_I ($N_I = 10^{16} cm^{-3}$)]

7.1.2 Results from the S-doped GaP Samples

The temperature dependence of the resistivity and Hall constant for S-doped GaP samples are shown in Fig. 7.4 and Fig. 7.5 respectively. Measurements in the temperature range 4.2°K to 50°K were made on two samples (DE 178, DE 194) but not on the other two samples (DE 209, DE 223) owing to the lack of liquid helium and hydrogen coolants. For clarity some of the experimental data points have been omitted from the graphs shown in Fig. 7.4 and Fig. 7.5. The experimental errors are labelled on some of the points on these graphs and are approximately ±5% if not specified.

The number of conduction electrons in the samples may be calculated by the use of equation 4.3. Since the carrier scattering processes in n-type GaP are in some doubt, the Hall factor, r, was assumed to be unity throughout this analysis. The temperature dependence of the number of conduction electrons is shown in Fig. 7.6. The values for the Hall mobilities for the S-doped samples, as calculated from equation 4.5 are shown in Fig. 7.7(a). The calculated values of the mobilities as limited by various scattering mechanisms are shown in Fig. 7.7(b) and these will be discussed in section 7.1.2(c).

(a) Impurity conduction

The impurity band conduction process has been discussed in section 4.3. The occurrence of this type of conduction process is generally inferred from the temperature dependence of the Hall constant.

If the Hall constant has a maximum value for some temperature, T, such that $kT < E_D$, then impurity band conduction is likely to take place in samples at temperatures lower than T. The temperature variation of the Hall constant, illustrated in Fig. 7.5, shows a maximum value of the Hall constant for the S-doped samples, DE 178, DE 194 and DE 209 and hence it is likely that impurity band conduction occurs in these samples. This is further substantiated by a marked change in the slope of the curves of resistivity versus reciprocal temperature for the samples DE 178 and DE 194 at temperatures below $20^{o}K$ as shown in Fig. 7.4.

An analysis of the impurity band conduction process for sample DE 178 has been carried out as follows. For a sample with electrons in the conduction and impurity band, the Hall constant is given by equation 4.17. The Hall factor, r, is assumed to be unity in the present analysis and equation 4.17 can therefore be rewritten as

$$R_H = \frac{1}{e}\left[\frac{n_c\mu_c^2 + n_i\mu_i^2}{(n_i\mu_c + n_i\mu_i)^2}\right] \qquad 7.1$$

If n_{exh} is defined as the total electron density (i.e. the electron density in the conduction band when all the electrons are excited from the impurity band) a Hall constant, $(R_H)_{exh}$, can be defined by

$$(R_H)_{exh} = \frac{1}{n_{exh}e} = \frac{1}{(n_c + n_i)e} \qquad 7.2$$

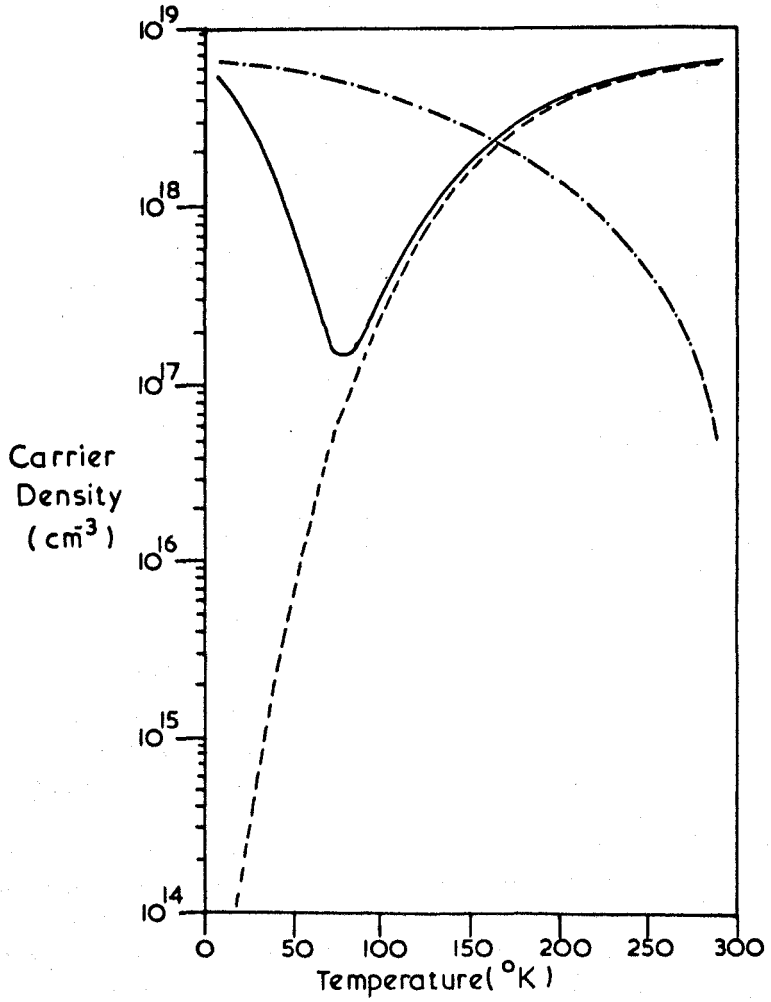

FIG. 7.8. CARRIER DENSITIES IN THE CONDUCTION AND IMPURITY BANDS. (sample DE 178)

[—— carrier density ,n, measured from the Hall constant.
------ " " , n_c in the conduction band.
—·—·— " " , n_i , in the impurity band.]

Equation 7.1 can then be written in the form:-

$$\frac{R_H}{(R_H)_{exh}} = \frac{(b^2 + x)(x + 1)}{(b + x)^2} \qquad 7.3$$

where $x = \frac{n_i}{n_c}$ and $b = \frac{\mu_c}{\mu_i}$

Since the value of b is more weakly dependent on temperature than the value of x, the maximum Hall constant can be obtained by differentiating equation 7.3 with respect to x to give:[2]

$$\frac{(R_H)_{max}}{(R_H)_{exh}} = \frac{(b + 1)^2}{4b} \qquad 7.4$$

The values of b and x may therefore be obtained from a graph showing the Hall constant as a function of temperature by the use of equations 7.3 and 7.4.

For the sample DE 178 the value of $(R_H)_{exh}$ is assumed to be equal to the Hall constant at 293°K. The foregoing analysis then gives the value of b as 100 (±10) and the values of n_c and n_i are as shown in Fig. 7.8. The carrier density, n, for sample DE 178, which is plotted in Fig. 7.6, is also shown in Fig. 7.8. In the temperature region 100°K to 300°K the value of n_c is approximately equal to n. Hence, in this temperature region the conductivity and Hall constant can be considered to depend on the values of n_c and μ_c. Although the values of n_i are appreciable in this region the values of μ_i are small

($b = \frac{\mu_c}{\mu_i} \approx 100$) and therefore the carriers in the impurity band do not contribute significantly to the conductivity or Hall constant. In the temperature region below approximately 20°K however, the value of n_c becomes very small and the conductivity and Hall constant depend on the values of n_i and μ_i. In the temperature range 4.2°K to 20°K the measured values of the mobilities in samples DE 178 and DE 194 are considered to give values for μ_i.

In the preceding analysis concerning impurity band conduction the value of $(R_H)_{exh}$ has been taken as the value of R_H at 293°K. This is not a valid approximation for even the most highly doped sample, namely DE 178, and is a less valid approximation for the other S-doped samples. Hence, an analysis of impurity band conduction was not carried out for the latter samples. Values of $(R_H)_{exh}$ may be obtained by measuring the Hall constant of samples at temperatures above 293°K but such measurements were not taken in the present work.

The analysis does show, however, that in the temperature range 100°K to 293°K the electron density, as measured from the Hall constant, is approximately equal to the density of electrons in the conduction band. With this fact established, a further analysis can be made on the results from the S-doped GaP samples as described in the section 7.1.2(b).

One further point, concerning the electrical resistivity, ρ, of the samples DE 178 and DE 194 at temperatures below 20°K, will be discussed. The resistivity of the samples in this temperature range has

a temperature dependency given approximately by the relationship $\rho \propto e^{E_h/kT}$ and the measured value of E_h for either sample is $4.0\ (\pm 0.5) \times 10^{-4}$eV. On the assumption that the conduction process in this temperature range is due to a hopping process, the value of E_h may be calculated from equation 4.15. Anticipating the results given in Table 7.1, the calculated values of E_h for samples DE 178 and DE 194 are $2.5\ (\pm 1.0) \times 10^{-2}$eV and $1.5\ (\pm 1.0) \times 10^{-2}$eV respectively. From the large differences between the calculated and measured values of E_h it can be inferred that the conduction process at low temperatures in these samples is unlikely to arise from a hopping mechanism. It has not been possible, however, to explain the exponential temperature dependence of ρ in terms of other conduction mechanisms.

(b) Donor impurity ionization energies and electron effective masses

The number of electrons in the conduction band of a semiconductor, which contains donor and acceptor impurity atoms, has been given in equation 2.29. If a graph is plotted of the expression

$$\ln\left[\frac{n(n + N_A)}{(N_D - N_A - n)N_c'}\right]$$

against $1/T$, then the gradient of the graph will correspond to the value E_D/k and the intercept, at $1/T = 0$, will be equal to Y where

$$Y = \left[\frac{m_n^*}{m}\right]^{3/2} D_n^{-1}$$

Since it has been shown in section 7.1.2(a) that the electron concentration, obtained from Hall constant measurements, can be

identified with the electron concentration in the conduction band, n, in the temperature range 100°K to 293°K, the above analysis may be carried out.

The values of n for the S-doped GaP samples are shown in Fig. 7.6 and a marked curvature is observed for the curves of ln n versus $^1/T$ in the temperature range 100°K to 293°K. In the expression

$$\ln\left[\frac{n(n + N_A)}{(N_D - N_A - n)N_i}\right]$$

N_d and N_A are varied by successive approximation until the relationship between

$$\ln\left[\frac{n(n + N_A)}{(N_D - N_A - n)N_i}\right] \quad \text{versus } {}^1/T$$

is <u>linear</u>; the values of E_D and Y can then be calculated[3].

A summary of the characteristics of the S-doped GaP samples is given in Table 7.1.

Table 7.1

Characteristics of the S-doped GaP samples

Sample	$N_D(cm^{-3})$	$N_A(cm^{-3})$	$E_D(eV)$	Y	$r_i(\text{Å})$	λ
DE 178	$1.0\times10^{19}(\pm10\%)$	$5.0\times10^{17}(\pm10\%)$	0.05(±0.01)	1.5(±0.5)	28(±1)	1.9(±0.2)
DE 194	$7.0\times10^{18}(\pm5\%)$	$3.0\times10^{16}(\pm5\%)$	0.075(±0.005)	0.8(±0.2)	32(±1)	2.1(±0.2)
DE 209	$3.0\times10^{18}(\pm5\%)$	$3.0\times10^{16}(\pm5\%)$	0.085(±0.005)	0.5(±0.2)	43(±1)	2.8(±0.2)
DE 223	$5.0\times10^{17}(\pm5\%)$	$1.0\times10^{16}(\pm5\%)$	0.075(±0.005)	0.5(±0.2)	79(±2)	5.0(±0.4)
			Mean	0.8(±0.5)		

Here $r_i = \left[\frac{3}{4\pi N_D}\right]^{1/3}$, $\lambda = \frac{r_i}{a_i}$, $a_i = \varepsilon(\frac{m}{m^*})a_H$.

In view of the fact that measurements have only been made on four S-doped samples, information concerning the concentration dependence of the various parameters is limited. However, it is evident from Table 7.1 that the donor ionization energy decreases with increasing donor impurity concentration. For the elemental semiconductors, silicon and germanium, it has been reported that E_D is inversely proportional to the cube root of the donor concentration[4] but further measurements are necessary to see if this relationship applies to n-type GaP.

The values of the donor ionization energy as given in Table 7.1 are in agreement with those given by Montgomery and Feldman[5], who have also determined the value of E_D from measurements of the Hall constant and found values of E_D in the range 0.05 (±0.01)eV to 0.01 (±0.01)eV for samples having comparable values of N_A and N_D. From data obtained in optical experiments[6] a value of E_D has been given as E_D = 0.11 (±0.01), but the donor concentration was not specified and therefore this value cannot be correlated with the present results.

The mean distance between donor impurities, r_i, can be calculated from the relationship, $r_i = (3/4\pi N_D)^{1/3}$ and values of r_i for the S-doped samples are shown in Table 7.1. The effective "Bohr radius", a_i, of the orbit of an electron around an impurity atom has

been defined by equation 4.13. Using the following values, $\varepsilon = 10.2$[7], $m^* = 0.35m$[8] and $a_H = 0.53\text{Å}$ the value of a_i is 15.4Å. A parameter, λ, may be defined such that $\lambda = r_i/a_i$ and the values of λ for the S-doped samples are shown in Table 7.1. According to Mott and Twose[9], semiconducting samples are expected to show impurity band conduction if $\lambda \leq 3$. For each of the samples DE 178, DE 194 and DE 209, $\lambda \leq 3$ and the observed maximum of the respective Hall constants is consistent with impurity band conduction processes occurring in these samples.

The effective masses of electrons in n-type GaP was analysed as follows. The "density of states" effective mass, m_n^*, can be related to the longitudinal and transverse effective masses (m_ℓ and m_t respectively) by the equation

$$m_n^* = M^{2/3}(m_\ell m_t^2)^{1/3} \qquad 7.5(a)$$

where M is the number of equivalent minima (valleys) in the conduction band.

The actual value of m_n^* was obtained from the relationship

$$Y = \left[\frac{m_n^*}{m}\right]^{-3/2} D_n^{-1} \qquad 7.5(b)$$

where the mean value of Y is given in table 7.1.

Moss et al.[8] have measured an effective mass, m^*, from a Faraday rotation experiment and have shown that the relationship between m_ℓ, m_t and m^* is

$$m^* = \frac{m_\ell(2m_\ell + m_t)}{(2m_t + m_\ell)} \qquad 7.6(a)$$

They obtained a value for m^* as

$$m^* = 0.35m \qquad 7.6(b)$$

With the assumptions that $M = 3$ and $D_n = 1$, values of m_ℓ and m_t were evaluated from equations 7.5(a), 7.5(b), 7.6(a) and 7.6(b) to be

$$\frac{m_\ell}{m} = 1.5\ (\pm 0.5) \qquad \frac{m_t}{m} = 0.2\ (\pm 0.1) \qquad 7.7(a)$$

The value, $M = 3$ is appropriate for the assumption that the conduction band minima occur at the edge of the Brillouin zone and this assumption is substantiated by data obtained from optical experiments[10]. The value, $D_n = 1$ is appropriate for impurity centres whose electronic wavefunctions have a significant overlap[2] and from the present Hall constant measurements it can be inferred that such an overlap is likely to occur in samples DE 178, DE 194 and DE 209.

Values of the effective masses of electrons in GaP have also been given by Montgomery[11] as

$$\frac{m_\ell}{m} = 1.7\ (\pm 0.5) \quad , \quad \frac{m_t}{m} = 0.20\ (\pm 0.10) \qquad 7.7(b)$$

and these values are in agreement with the values given in the present work. However there are large inaccuracies in both values of m_ℓ and m_t and further experimental measurements are necessary to verify these values.

(c) Charge carrier scattering processes

A variety of charge carrier scattering processes were discussed in general terms of section 4.4, and the temperature dependence of the mobility of the charge carriers, as limited by these various processes, was given. For n-type GaP, the expressions for calculating the mobilities of electrons (in the units $cm^2 volt^{-1} sec^{-1}$) are as follows[12,13]:

$$\mu_A = \frac{7 \times 10^8}{T^{3/2} D_u^2} \qquad 7.8$$

$$\mu_o = 2.45 T^{\frac{1}{2}} F\left(\frac{580}{T}\right) \left[\exp\left(\frac{580}{T}\right) - 1\right] \qquad 7.9$$

$$\mu_I = \frac{4 \times 10^{17} . T^{3/2}}{N_i \left[\ln(1 + b) - \frac{b}{1 + b} \right]} \qquad 7.10$$

where $b = \frac{3.8 \times 10^{14} T^2}{n}$

$$\mu_s = 5.4 \times 10^9 . T^{-\frac{1}{2}} (N_s A)^{-1} \qquad 7.11$$

$$\mu_D = 2.0 \times 10^9 . T^{-\frac{1}{2}} (R.N) \qquad 7.12$$

The values of the mobilities, calculated from the equations 7.8 to 7.12 are shown in Fig. 7.7(b). The following values of the various parameters were used, $D_u = 12.7 eV$[12] $(N_s A) = 10^5 cm^{-1}$[12], $R = 3 \times 10^{-5} cm$[14], $N = 1.0 \times 10^8 cm^{-2}$[15]. These calculated values of the mobilities of electrons in GaP will now be compared with the

experimentally determined Hall mobilities of electrons in S-doped GaP, the latter being shown in Fig. 7.7(a).

In the temperature range 120°K to 293°K the Hall mobility of electrons in each of the S-doped samples decreases with increasing temperature according to the relationship, $\mu_H \propto T^x$, the experimentally determined values of x being given in Table 7.2.

Table 7.2

Temperature dependence of the Hall mobility of electrons in S-doped GaP at temperatures in the range 120°K - 293°K

Sample	Values of x in the relationship $\mu_H \propto T^x$
DE 178	-0.65 (±0.05)
DE 194	-1.35 (±0.05)
DE 209	-1.50 (±0.05)
DE 223	-1.55 (±0.05)

These values of x are in general agreement with the values obtained by other workers [16,17,18] who give values in the range -0.50 (±0.05) to -1.80 (±0.05). This suggests that the conduction electron mobility is predominantly determined by the scattering by acoustic phonons since, theoretically, it is predicted that $\mu_A \propto T^{-1.5}$. But the magnitude of μ_A, as calculated from equation 7.8 using the value D_u = 12.7eV, is higher than the experimentally determined Hall mobility by a factor of

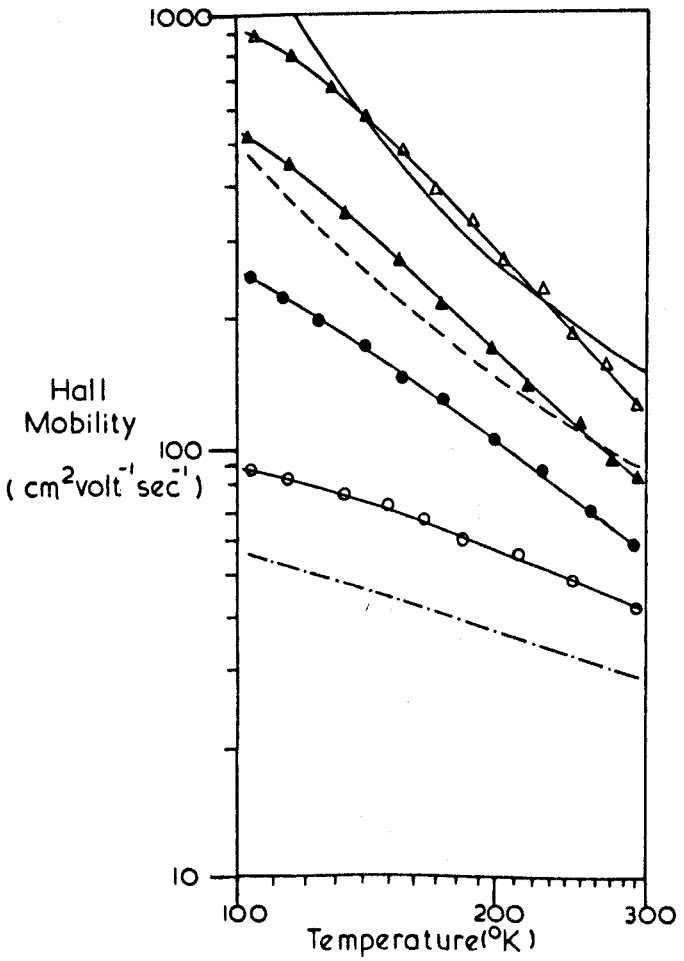

FIG. 7.9. HALL MOBILITY OF ELECTRONS IN S-DOPED GaP TOGETHER WITH THE CALCULATED MOBILITY OF ELECTRONS SCATTERED BY OPTICAL PHONONS & LATTICE DEFECTS.

DE 178 DE 209

DE 194 DE 223

Calculated mobility

$N_S A = 10^5 cm^{-1}$

$N_S A = 10^6 cm^{-1}$

$N_S A = 10^7 cm^{-1}$

approximately 10. However, since the measured values for D_u lie in the range 8.2eV to 55eV[12] there is a large uncertainty in the calculated value of μ_A.

It is thought that an alternative electron scattering process, in this temperature range, could involve the combined scattering of electrons by lattice defects and optical phonons. In Fig. 7.9 the calculated mobility, limited by this combined scattering, is compared with the Hall mobilities of electrons in S-doped GaP. The calculated mobility and experimentally determined Hall mobilities are in order of magnitude agreement for values of $(N_s A)$ in the range $10^5 cm^{-1}$ to $10^7 cm^{-1}$. However, precise experimental measurements of $(N_s A)$ could not be obtained for the samples used in the present work to substantiate the occurrence of this scattering process.

In the temperature range 77°K to 120°K it is thought that the electron mobility in GaP is likely to be limited by ionized impurity scattering. The agreement between the calculated mobility and the experimentally determined Hall mobility for samples DE 223, DE 194 and DE 209 (as shown in Fig. 7.7(a) and 7.7(b) respectively) is to within ±10%.

The abrupt decrease in the Hall mobility of electrons in S-doped GaP at temperatures below 77°K can be explained in terms of impurity band conduction. It has been shown in section 7.1.2(a) that, for sample DE 178, the ratio of the Hall mobilities of electrons in the impurity band to those in the conduction band is approximately

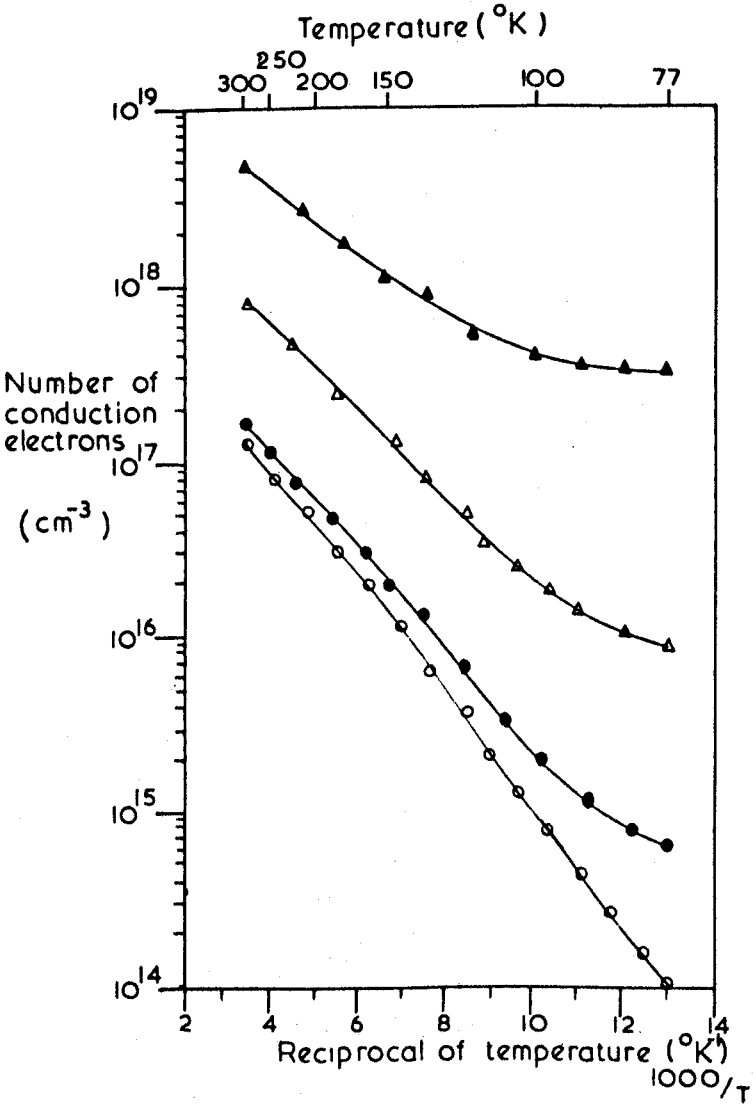

FIG. 7.10 TEMPERATURE DEPENDENCE OF THE NUMBER OF CONDUCTION ELECTRONS IN Te-DOPED & Si-DOPED GaP.

- ▲ DE 156 Si-DOPED
- △ DE 161 Si-DOPED
- ● DE 158 Si-DOPED
- ○ Te-DOPED

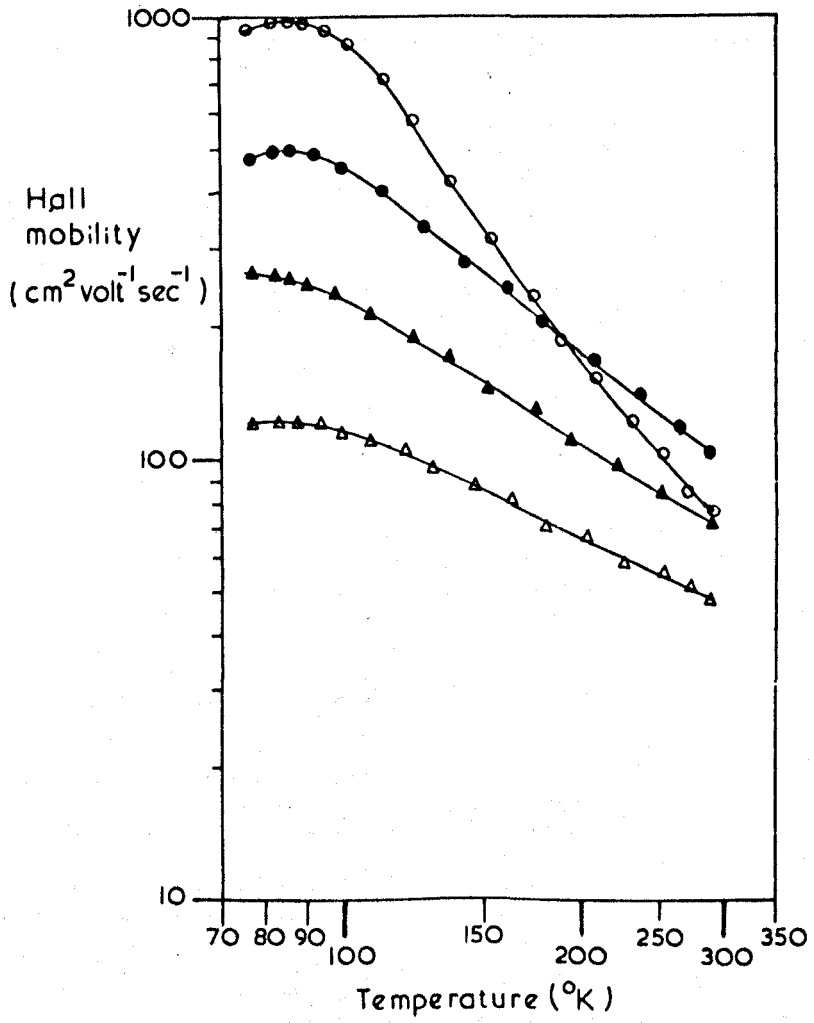

FIG. 7.11. TEMPERATURE DEPENDENCE OF THE HALL MOBILITY OF ELECTRONS IN Te-& Si-DOPED GaP.

△ DE 156 Si-DOPED GaP
▲ DE 161 Si-DOPED GaP
● DE 158 Si-DOPED GaP
○ Te-DOPED GaP

$^1/100$. The low Hall mobility can therefore be explained by assuming that, at temperatures, T, such that $kT << E_D$, the majority of electrons are in the impurity band.

7.1.3 Results from the Si-doped and Te-doped GaP samples

Only one sample of Te-doped GaP and three samples of Si-doped GaP were available for the measurements of Hall effect and conductivity in the present work. The temperature dependence of the number of conduction electrons and the Hall mobility of these electrons are shown in Fig. 7.10 and Fig. 7.11 respectively.

(a) Impurity band conduction

Since the results for the Te-doped and the Si-doped GaP samples were only obtained from samples at temperatures in the range 77^oK to 293^oK, the analysis of impurity band conduction cannot be made. However, since the number of conduction electrons in each of the Si-doped samples tends towards a minimum value at temperatures of approximately 77^oK, (see Fig. 7.10), it is likely that impurity band conduction will occur in these samples at temperatures less than 77^oK. In the case of the Te-doped GaP sample no such minimum is observed and it is impossible to predict the type of conduction process which will occur in this sample at low temperatures.

(b) Donor impurity ionization energies and electron effective masses

The analysis of the donor impurity ionization energies and electron effective masses was made on the Si-doped and Te-doped GaP

samples in the manner outlined in section 7.1.2(b). A summary of the characteristics of the Si-doped and Te-doped GaP samples is given in Table 7.3.

Table 7.3

Characteristics of the Si-doped and Te-doped GaP samples

Sample	$N_D(cm^{-3})$	$N_A(cm^{-3})$	$E_D(eV)$	Y	$r_i(\text{Å})$	λ
DE 156 Si-doped GaP	$2\times10^{19}(\pm10\%)$	$2\times10^{18}(\pm10\%)$	0.04(±0.01)	1.4(±0.5)	23(±1)	1.5(±0.2)
DE 161 Si-doped GaP	$5\times10^{18}(\pm5\%)$	$2\times10^{17}(\pm5\%)$	0.05(±0.01)	0.5(±0.2)	37(±1)	2.5(±0.2)
DE 158 Si-doped GaP	$1\times10^{18}(\pm5\%)$	$5\times10^{16}(\pm5\%)$	0.06(±0.01)	0.5(±0.2)	62(±1)	4.0(±0.2)
			Mean	0.8(±0.5)		
Te-doped GaP	$4\times10^{17}(\pm5\%)$	$1\times10^{16}(\pm5\%)$	0.07(±0.01)	0.7(±0.1)	84(±2)	5.5(±0.2)

$$Y = \left[\frac{m_n^*}{m}\right]^{3/2} D_n^{-1}$$

$$r_i = (3/4\pi N_D)^{1/3}$$

$$\lambda = \frac{r_i}{a_i} \quad \text{where } a_i = \epsilon\left(\frac{m}{m^*}\right)a_H.$$

From Table 7.3 it can be seen that the values of E_D for the Si-doped GaP samples also decrease with increasing impurity concentration. These values are consistent with data obtained in similar experiments by Montgomery and Feldman[5] in which values of E_D are in the range 0.04 (±0.01) eV to 0.08 (±0.01) eV. A value of E_D = 0.08 (±0.01) eV was obtained from optical measurements[19] but, since no specification was given regarding the donor impurity concentrations, this value of E_D cannot be correlated with the present results.

For the Te-doped GaP sample the value of E_D given in Table 7.3 is in agreement with the value E_D = 0.070 (±0.005) given by Montgomery[11].

In the present results, it is observed that the compensation factor, K, (where $K = \frac{N_A}{N_D}$) is greater in the Si-doped samples than in the S-doped samples. One possible cause of this may arise from the amphoteric nature of the Si atom as an impurity in Group III - V compounds. This type of behaviour has also been reported for silicon impurity atoms in GaAs[20].

The parameter, Y, associated with the Si-doped samples has a mean value of 0.8. The effective mass analysis is, therefore, the same as that given for the S-doped samples but further measurements are necessary to substantiate the values of the effective masses as given in section 7.1.2(b).

(c) Charge carrier scattering processes

The temperature dependence of the Hall mobility of electrons in the Si-doped and Te-doped GaP samples, in the temperature range

120°K to 293°K, has been found to have the form $\mu_H \propto T^x$ where the values of x are given in Table 7.4.

Table 7.4

Temperature dependence of the Hall mobility of electrons in Si-doped and Te-doped GaP samples at temperatures in the range 120°K to 293°K

Sample	Value of x in the relationship $\mu_H \propto T^x$
DE 156 Si-doped GaP	x = -0.9 (±0.1)
DE 161 Si-doped GaP	x = -1.2 (±0.1)
DE 158 Si-doped GaP	x = -1.5 (±0.1)
Te-doped GaP	x = -2.1 (±0.1)

The temperature dependence of the electron mobility for the Si-doped and Te-doped GaP samples is similar to that of the S-doped samples and hence the carrier scattering processes are thought to be similar to those discussed for the S-doped samples.

7.2 E.P.R. Measurements

E.P.R. measurements have been made on the n-type GaP samples as indicated in Table 7.5. The low temperature apparatus used with the Q-band "Microspin" spectrometer which allowed the sample temperatures

to be controlled in the range 2.5°K to 293°K was described in section 6.3. In the case of the measurements at X-band frequencies (9 GHz) the sample was cooled by a helium gas flow system and this allowed the sample temperature to be controlled in the range 20°K to 293°K. For the measurements made with the 70 GHz spectrometer it was necessary to use a superconducting magnet and the sample temperature was fixed at 4.2°K.

Table 7.5

E.P.R. measurements on the n-type GaP samples

Sample		Details of the E.P.R. measurement
S-doped GaP	DE 178	70 GHz, sample temperature 4.2°K Q band, " " 2.5°K to 100°K X band, " " 20°K to 100°K
	DE 194	Q band, " " 4.2°K to 100°K
	DE 209	Q band, " " 4.2°K to 100°K
	DE 223 epitaxially grown crystal	Q band, " " 4.2°K to 100°K
	DE 223 "whisker"	Q band, " " 4.2°K to 100°K
Si-doped GaP	DE 156	Q band, " " 4.2°K
	DE 161	Q band, " " 4.2°K
	DE 158	Q band, " " 4.2°K
Te-doped GaP		Q band, " " 4.2°K to 100°K X band, " " 20°K to 100°K

7.2.1 Measurement procedures

In each of the measurements on the GaP samples, which have been listed in Table 7.5, the E.P.R. resonance consisted of a single broad line with a narrower line superimposed upon it. The latter E.P.R. line was found to be greatly reduced when the samples were etched and was, therefore, considered to be due to a surface effect. The broad E.P.R. line was considered to be due to electrons from donor impurity atoms and the following characteristics of this line were investigated:-

(a) the linewidth

(b) the g-value and g-value anisotropy

(c) the number of unpaired electrons associated with E.P.R. line

(d) the lineshape.

The measurement procedures for investigating the above characteristics will now be discussed in more detail.

(a) The measurement of linewidth

The linewidth, ΔB, of an E.P.R. resonance may be defined as the difference in magnetic field between points of maximum slope of the E.P.R. absorption line. Since most spectrometers give a chart recording of the derivative of the absorption line, the linewidth is measured between the maximum and minimum points on the recorder trace of an E.P.R. line. The procedure for calibrating an E.P.R. recording in terms of magnetic field has been described in section 6.2.2(c) and this allows magnetic field differences to be measured to an accuracy of ± 0.1mT.

(b) The measurement of the g-value and g-value anisotropy

Since the g-value of the resonance from electrons in n-type GaP was found to be approximately 2, it was measured by a comparison of the E.P.R. resonance from n-type GaP with that from a standard sample of P-doped silicon[21]. An illustration of the chart recording of the two superimposed spectra has been shown in Fig. 6.13. The g-value of the standard sample is 1.99875(±0.00010)[21] and the differences between the g-values of the two resonance lines, δg, may be obtained from the formula

$$\delta g = -g\frac{\delta B}{B} \qquad 7.13$$

where δB is the magnetic field difference between the two resonance lines

and B is the magnetic field at the two samples.

Since the g-value of the standard sample is isotropic[21], any g-value anisotropy in the resonance from the n-type GaP samples can be observed as a change in the value of δg.

(c) The measurement of the number of unpaired electrons

The number of unpaired electrons in the GaP sample, N, which contribute to the E.P.R. resonance can be calculated from the relationship

$$N = N' \left[\frac{\Delta B_{GaP}}{\Delta B_{standard}}\right]^2 \frac{A_{GaP}}{A_{standard}} \qquad 7.14$$

where N' is the number of unpaired electrons in the standard sample and is a known quantity[21],

ΔB_{GaP} and $\Delta B_{standard}$ are the measured linewidths,

A_{GaP} and $A_{standard}$ are the amplitudes of the resonance line.

The equation 7.14 is only valid if the positioning of the GaP and standard samples is such that the filling factor and the amplitude of the 100 KHz magnetic field modulation are the same for each sample.

(d) The measurement of the lineshape

Details of the lineshapes of E.P.R. resonances in semiconductors have been given in section 5.2.2. According to the theory given by Dyson[22] significant distortion of a resonance line occurs if the sample thickness is greater than 4δ, where δ is the skin depth of the sample. The value of δ may be calculated from the equation

$$\delta = (\pi.\sigma.f.\mu\ \mu_o)^{-\frac{1}{2}} \qquad 7.15$$

where f is the frequency of the microwave radiation

σ is the conductivity of the sample

μ is the permeability of the sample

μ_o is the permeability of free space.

It is seen from Fig. 7.4 that the maximum conductivity of the most highly doped n-type GaP sample is approximately 100 mho cm^{-1} at 293°K. For microwave radiation of frequency, f = 35 GHz, the value of δ is approximately 100 microns in such a sample at a temperature of 293°K. The samples used in the present E.P.R. measurements were approximately 100 microns in thickness and hence a Dysonian lineshape is not expected to occur in the E.P.R. resonance at or below 293°K.

The two other lineshapes which are discussed in section 5.4 are of the Gaussian and Lorentzian form. In n-type GaP the former type of lineshape could possibly arise from the hyperfine interaction between the magnetic moments of the electrons and the nuclear magnetic moments of the Ga and P nuclei and would be expected to occur in samples with "isolated" donor impurity centres (the electronic wavefunctions associated with "isolated" centres do not give rise to a significant overlap). A lineshape of the latter type could result from motional effects of the electrons or the "exchange" interaction between electrons. Also, electron-phonon interactions can significantly affect the E.P.R. lineshape. An analysis of the lineshape can, therefore, give information about the extent of the delocalization of the electrons and the significance of the electron-phonon interactions and this information can be compared with data obtained from Hall effect and conductivity measurements.

The lineshapes of the E.P.R. resonance lines were analysed numerically on a digital computer with the aid of the programme shown in Appendix 3. Since the sweep of the steady magnetic field was non-linear with respect to the measurement of displacements on the recorder chart, the proton resonance field markers were used to calibrate the field axis of the recording of the resonance line and the amplitude of the resonance line was measured from the recording at the position of each of these markers. The digital computer was programmed to calculate the area under the resonance line from the above data and compare this

with the areas under the standard Lorentzian and Gaussian resonance lines of the form given by equations 5.16 and 5.17 respectively. The final result from the computer programme gives the lineshape in terms of a percentage of the Lorentzian form.

7.2.2 Results from the S-doped and Te-doped GaP samples

The results from the S-doped and Te-doped GaP samples at a temperature of 4.2°K, which were obtained with the Q-band "Microspin" spectrometer, are given in Table 7.6 below.

Table 7.6

Results from the S-doped and Te-doped GaP samples at 4.2°K obtained with the Q-band spectrometer

Sample	Linewidth ΔB (mT)	g-value	Number of unpaired electrons (cm^{-3})	Lineshape	Value of N_D from Hall effect measurements (cm^{-3})
DE 178 S-doped GaP	5.6(±0.2)	1.9996 (±0.0002) isotropic	$1x10^{19}$(±20%)	95% Lorentzian (±10%)	$1x10^{19}$(±10%)
DE 194 S-doped GaP	5.5(±0.2)	1.9997 (±0.0002) isotropic	$5x10^{18}$(±20%)	95% Lorentzian (±10%)	$7x10^{18}$(±5%)
DE 209 S-doped GaP	5.8(±0.2)	1.9996 (±0.0002) isotropic	$1x10^{18}$(±20%)	90% Lorentzian (±10%)	$3x10^{18}$(±5%)
DE 223 S-doped GaP "Whisker"	5.6(±0.2)	1.9996 (±0.0002) isotropic	$4x10^{17}$(±20%)	80% Lorentzian (±20%)	
DE 223 S-doped GaP epitaxial	5.7(±0.2)	1.9997 (±0.0002) isotropic	$5x10^{17}$(±20%)	85% Lorentzian (±20%)	$5x10^{17}$(±5%)
Te-doped GaP	6.0(±0.2)	1.9995 (±0.0002) isotropic	$2x10^{17}$(±20%)	50% Lorentzian (±40%)	$4x10^{17}$(±5%)

Also included in Table 7.6 is the concentration of donor impurity atoms, N_D, obtained from Hall effect data.

The results from the S-doped GaP sample, DE 178, at a temperature of 4.2°K, which were obtained with the spectrometer operating at 70 GHz, are given in Table 7.7.

Table 7.7

Results from the sample DE 178 at 4.2°K obtained with the spectrometer operating at 70 GHz

Sample	Linewidth ΔB (mT)	g-value	Number of unpaired electrons (cm^{-3})	Lineshape	Value of N_D
DE 178 S-doped GaP	7.0(±1.0)	1.999 (±0.001) isotropic	$1x10^{19}$(±20%)	No analysis	$1x10^{19}$(±10%)

The magnetic field in the superconducting magnet was determined from the measurement of the current through the solenoid.

In the case of the results from the S-doped and Te-doped GaP samples obtained with the X-band spectrometer the lowest attainable sample temperatures were approximately 20°K and the results at this temperature are given in Table 7.8.

Table 7.8

Results from the S-doped and Te-doped samples at 20°K obtained with the X-band spectrometer

Sample	Linewidth ΔB (mT)	g-value	Number of unpaired electrons (cm^{-3})	Lineshape	Value of N_D
DE 178 S-doped GaP	4.5(±0.2)	1.9990 (±0.0005) isotropic	$1x10^{19}$(±20%)	100% Lorentzian (±10%)	$1x10^{19}$(±10%)
DE 223 S-doped GaP "Whisker"	4.5(±0.2)	1.9995 (±0.0005) isotropic	$5x10^{17}$(±20%)	80% Lorentzian (±10%)	
Te-doped GaP	4.8(±0.2)	1.9990 (±0.0005)	$2x10^{17}$(±20%)	50% Lorentzian (±20%)	$4x10^{17}$(±5%)

As the temperature of the samples was varied a measurable change in the linewidth of the E.P.R. resonance was observed. There was also a marked reduction in the cavity Q-factor in the E.P.R. measurements on single crystals of the samples at temperatures above 77°K. This degradation of the Q-factor was minimised by the use of powdered samples (the size of each crystallite was approximately 50 microns in diameter) in these measurements and, since each of the E.P.R. spectra consisted of a single isotropic line, the same spectrum was obtained from a sample in powdered or single crystal form. However, it was found necessary to etch the powders (a suitable etchant was found to be a 10% solution of Bromine

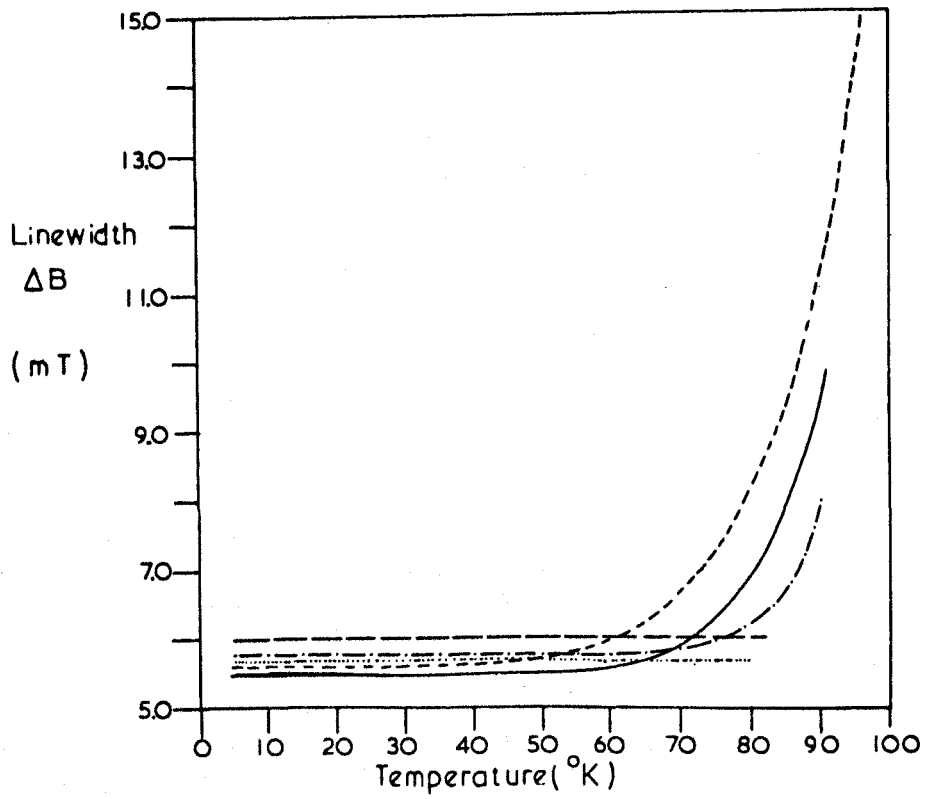

FIG. 7.12(a) TEMPERATURE DEPENDENCE OF THE LINEWIDTH OF THE E.P.R. RESONANCE (at Q-band) FROM THE S-DOPED & Te-DOPED SAMPLES.

---- DE 178 —·— DE 209 ——— Te-DOPED

—— DE 194 ····· DE 223

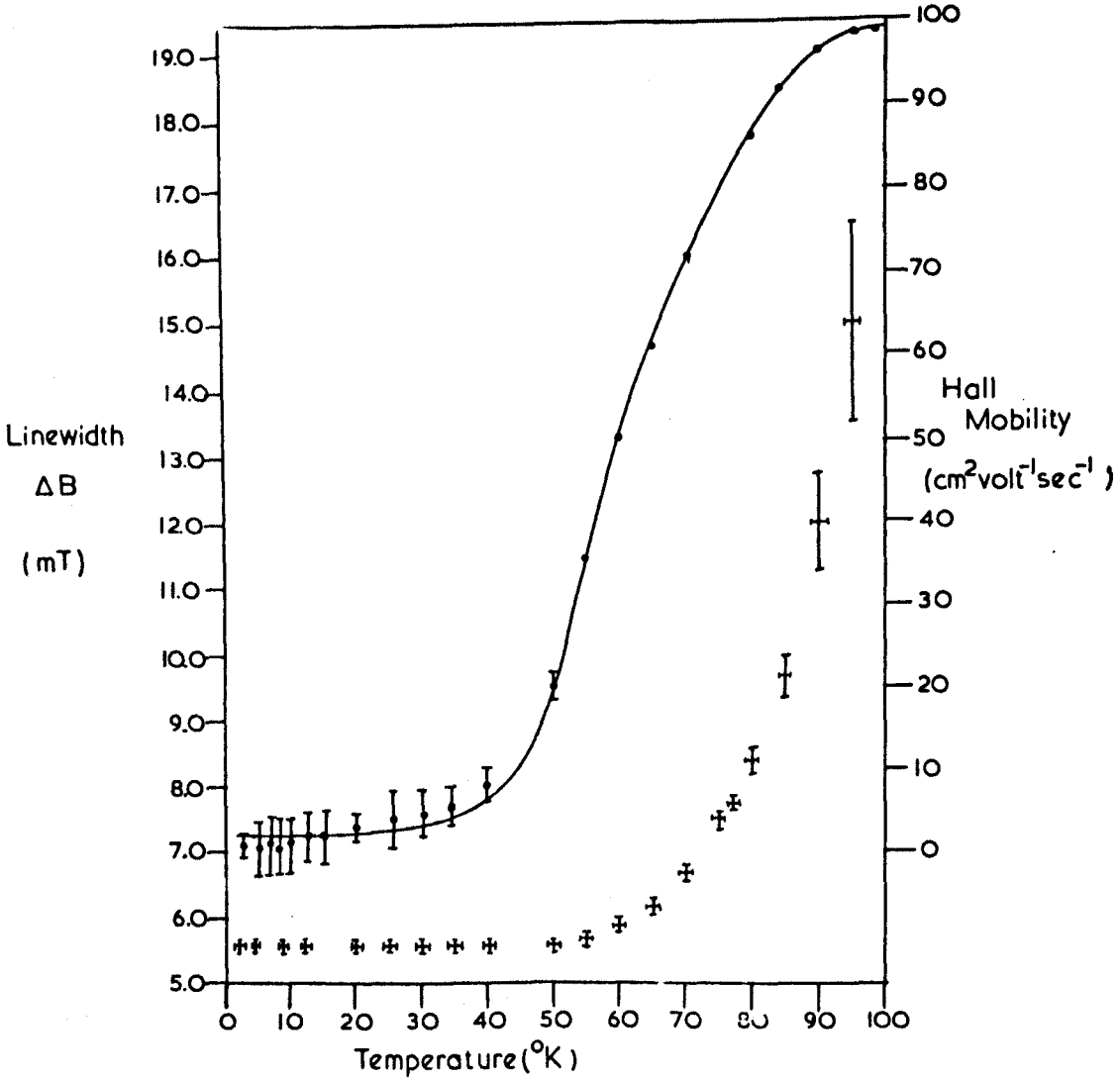

FIG. 7.12 (b) TEMPERATURE DEPENDENCE OF THE HALL MOBILITY & THE LINEWIDTH OF THE E.P.R. RESONANCE (at Q band) OF ELECTRONS IN S-DOPED GaP (sample DE 178)

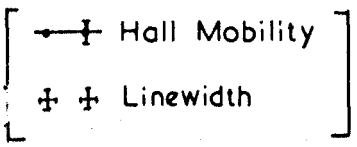

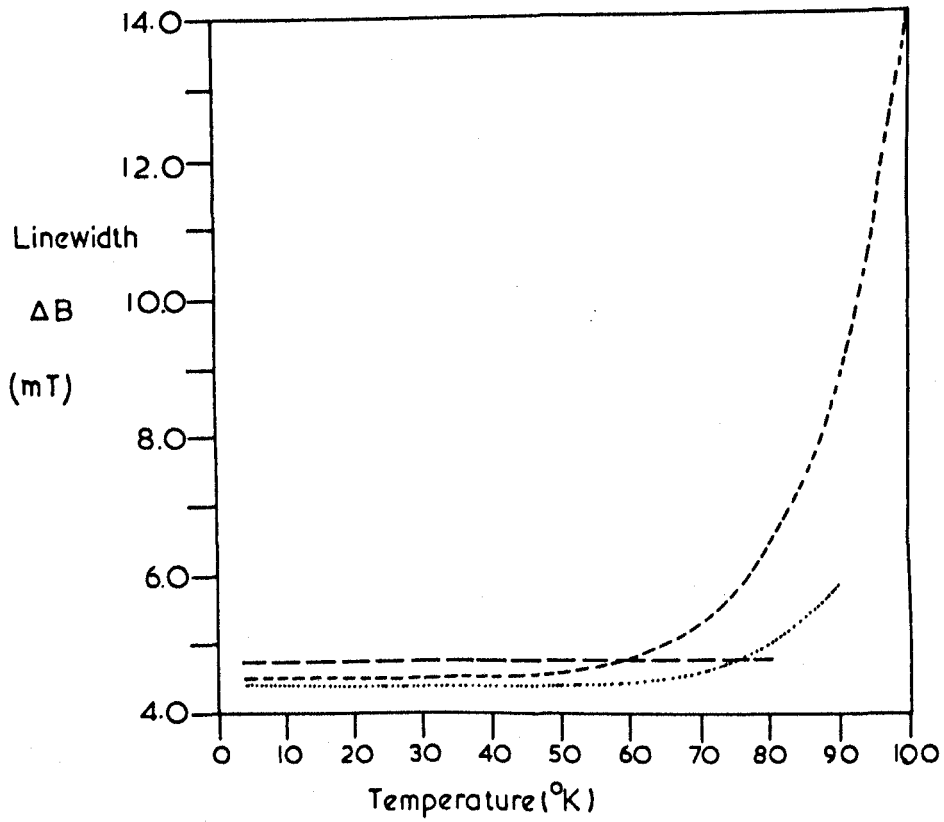

FIG. 7.12(c) TEMPERATURE DEPENDENCE OF THE LINEWIDTH OF THE E.P.R. RESONANCE (at X-band) FROM THE S-DOPED & Te-DOPED SAMPLES.

[----- DE 178
..... DE 223
———— Te-DOPED GaP]

in methanol), otherwise the E.P.R. resonance due to surface effects was significantly large.

The temperature dependence of the linewidth of the resonance for Te- and S-doped samples, obtained from measurements on the Q-band spectrometer, is shown in Fig. 7.12(a). For clarity the experimental errors associated with each of the data points are not recorded on the graphs. In Fig. 7.12(b) the linewidth versus temperature curve is shown for sample DE 178; the experimental errors in the linewidth measurement are shown on this curve and are typical of those for the other S-doped and Te-doped samples. Also shown in Fig. 7.12(b) is the temperature dependence of the Hall mobility for sample DE 178 which was given in Fig. 7.7(a). A comparison between these two curves will be made in section 7.2.2(d). The temperature dependence of the resonance linewidth for the S-doped and Te-doped GaP samples, obtained from measurements on the X-band spectrometer, is shown in Fig. 7.12(c).

The above results will now be discussed.

(a) g-value

It is observed from the results that, to within experimental error, the g-values of electrons from the donor impurities, sulphur and tellurium, are isotropic and constant with respect to changes of sample temperature and impurity concentration. Also, no measurable change of g-value was observed from the measurements made at different frequencies. These g-values are in agreement with those given by Title[23].

The g-values may be calculated from the formulae derived by Roth[24] which are given in section 5.2. Assuming that the equations 5.6 and 5.7 are applicable to electrons from shallow donor impurities in GaP the calculated values of $g_{||}$ and $g_{\perp}$ are 2.028 and 1.976 respectively. For an unstrained crystal the conduction band minima have equal populations of electrons and the g-value is expected to be isotropic and given by the relationship

$$g = \tfrac{1}{3}g_{||} + \tfrac{2}{3}g_{\perp} \qquad 7.16$$

Hence the calculated g-value is 1.994 and is in approximate agreement with the observed value.

Actual values of $g_{||}$ and $g_{\perp}$ have been observed experimentally in n-type Si by E.P.R. measurement on crystals to which a stress is applied but this type of measurement has not been carried out in this present work on n-type GaP.

(b) The number of unpaired electrons

The inaccuracy in the values of the number of unpaired electrons, obtained from E.P.R. measurements, is within ±20%. To within this experimental error there is agreement between the values of the number of unpaired electrons and the values of the donor impurity concentrations which were obtained from conductivity and Hall effect measurements.

(c) Lineshape analysis

From the analyses of the E.P.R. resonance from S-doped GaP samples it is found that the lineshape is predominantly Lorentzian and this suggests that the electrons are not localized at "isolated" donor centres. This suggestion is in agreement with the conductivity data in which impurity band conduction is observed at low temperatures.

In the case of the Te-doped GaP sample the analysis shows that the lineshape is not totally Lorentzian and the E.P.R. resonance may be partly due to electrons from "isolated" donor centres. Unfortunately the conductivity data for Te-doped GaP does not extend to low temperatures to substantiate this supposition.

(d) Linewidths

The temperature dependence of the linewidth, ΔB, of the E.P.R. resonances from the S-doped and Te-doped GaP samples has been shown in Fig. 7.12(a), (b), (c). At temperatures below approximately $60^{\circ}K$ the E.P.R. linewidths are constant at a value, $\Delta B_{constant}$, which is independent of the donor impurity concentration.

The temperature dependence of the linewidth was analysed as follows. The value of $\Delta B_{constant}$ was subtracted from the total linewidth, ΔB, to give a temperature dependent parameter $\Delta B'$. In an attempt to determine an analytical relationship between $\Delta B'$ and T the measured values of $\Delta B'$ were fitted to relationships of the form $\Delta B' \propto \exp\frac{\Delta E}{kT}$ and $\Delta B' \propto T^{n}$. The values determined for ΔE and n are shown in Table 7.9.

Table 7.9

Temperature dependence of the linewidths of the E.P.R. resonance from S-doped and Te-doped samples

Sample	Temperature independent region		Temperature dependent region		
	$\Delta B_{constant}$ (mT)	Temperature range (°K)	Temperature range (°K)	ΔE (eV)	n
Q-band measurements					
DE 178 S-doped GaP	5.6(±0.2)	2.5 to 50	50 to 95	0.05(±0.01)	7(±2)
DE 194 S-doped GaP	5.5(±0.2)	4.2 to 55	55 to 90	0.06(±0.01)	9(±2)
DE 209 S-doped GaP	5.8(±0.2)	4.2 to 60	60 to 90	0.07(±0.02)	11(±3)
DE 223 Epitaxial S-doped GaP	5.7(±0.2)	4.2 to 77	No analysis possible owing to the weak E.P.R. resonance		
DE 223 "Whisker" S-doped GaP	5.6(±0.2)	4.2 to 77			
Te-doped GaP	6.0(±0.2)	4.2 to 77			
X-band measurements					
DE 178 S-doped GaP	4.5(±0.2)	20 to 50	50 to 100	0.05(±0.01)	7(±2)
DE 223 S-doped GaP "Whisker"	4.5(±0.2)	20 to 70	70 to 90	0.06(±0.02)	10(±3)
Te-doped GaP	4.8(±0.2)	20 to 77	No analysis possible owing to the weak E.P.R. resonance		

(e) Interpretation of the temperature dependence of the linewidth

A number of possible sources of the width of E.P.R. lines will now be discussed in an attempt to explain the observed linewidths in GaP.

It is expected that for electrons bound to "isolated" donor impurities in GaP, the linewidth of the E.P.R. would be governed by the hyperfine interaction between the magnetic moments of the electrons and the nuclear magnetic moments of the Ga and P nuclei and may, therefore, be calculated from the equation 5.18. Although the value of η (which is a factor describing the "peaking" of the conduction band wavefunctions at a lattice site) in this equation was not known, it was thought that it must lie between the values for Si and Ge and a value equal to the mean of these values was used. The resultant calculated values for the linewidths were then found to be approximately 8mT and 10mT for the conduction band minima occurring, respectively, at or inside the Brillouin zone boundary. These values are in order of magnitude agreement with the observed linewidths which are in the range 4.5(±0.2)mT to 6.0(±0.2)mT.

However, it is expected that a resonance line from electrons bound to "isolated" donor impurities would have a Gaussian lineshape and the observed lineshape of the resonance in the S-doped samples was found to be predominantly Lorentzian. Therefore it was thought that the observed linewidth of the E.P.R. in these samples was caused by either life-time broadening (i.e. $\Delta B \propto \frac{1}{T_1}$ where T_1 is the spin lattice

relaxation time) or the "motional averaging" of the hyperfine interaction which produces a resonance line of Gaussian shape. For the Te-doped sample, however, the shape of the E.P.R. line is approximately 50% Lorentzian, 50% Gaussian and it is thought likely that the observed linewidth could be due to hyperfine interaction.

The "motional averaging" could occur as a result of electrons hopping between impurity centres and the calculated reduction in the linewidth would be obtained from equation 5.19; the hopping frequency, W, in this equation may be determined from equation 4.14. From these equations it can be inferred that the width of an E.P.R. line from a sample, in which "motional averaging" occurs, will increase as the temperature and impurity concentration decrease. Since the observed linewidth in the present n-type GaP samples does not have these characteristics it is thought that "motional averaging" is not a significant source of the linewidth. This supposition is supported by data concerning the electrical conductivity of the S-doped samples, given in section 7.1.2(a), in which electron hopping is shown to be unlikely to occur.

According to the theoretical analysis given by Elliott[26] the linewidth, ΔB, of a life-time broadened E.P.R. line is related to the electrical mobility, μ, according to the relationship $\Delta B \propto \frac{1}{\mu}$. From Fig. 7.12(b) it is seen that, over a temperature range 0 to 30°K, the mobility and linewidth observed in sample DE 178 are both constant with respect to changes in temperature and hence the relationship

$\Delta B \propto \frac{1}{\mu}$ is satisfied. Also, from equations 5.20 and 5.21, the spin-lattice relaxation time, T_1, may be determined from the mobility measurements and a value $T_1 = 5(\pm 1) \times 10^{-9}$secs was obtained for sample DE 178. The magnitude of T_1 obtained from the linewidth measurement was $2.0(\pm 0.1) \times 10^{-9}$sec and therefore it appears that this type of life-time broadening is a possible cause of the linewidth for this sample at temperatures between 0 to 30°K. For the sample DE 194 at these temperatures, the agreement between the values of T_1, obtained from the two types of measurements, was found to be within an order of magnitude but for the other S-doped samples (DE 209, DE 223) the correlation between the E.P.R. and mobility measurements could not be obtained owing to insufficient data.

For the samples DE 178 and DE 194 at temperatures in the range 30°K to 60°K the relationship $\Delta B \propto \frac{1}{\mu}$ is not obeyed since the E.P.R. linewidth is constant and the mobility increases with increasing temperature. Also, for the S-doped samples at temperatures above 60°K the linewidth, which has a temperature dependence of the form $\Delta B' \propto T^n$, (the values of n are in the range 7 to 11) cannot be explained according to the theories given by Elliott[26] and Yafet[27] and further sources of the linewidth must be considered.

From the exponential temperature dependence of $\Delta B'$ it is thought that the so-called "Orbach" relaxation process[28] may occur. In such a process the value of the activation energy ΔE must be less than the energy corresponding to the Debye temperature θ; for GaP

the value of θ is $580^{\circ}K$[12] and the corresponding energy is approximately 0.05eV. The values of ΔE, given in Table 7.9, are in the range 0.4(±0.1)eV to 0.7(±0.2)eV and are therefore consistent with the above restriction and hence the Orbach relaxation process may be a source of the width of the observed resonance line in the Te-doped and S-doped samples.

One other feature of the linewidth measurement is that the linewidth shows a dependence on the magnetic field, B, at which the E.P.R. resonance is observed. The observed results in GaP can be fitted to the relationship $\Delta B \propto B^{1/n}$ where $n \simeq 4$. There are no reported spin-lattice relaxation processes which could give such a dependence and at present these results cannot be explained.

Title[23] has suggested that the observed linewidth and lineshape of the E.P.R. line in n-type GaP is due to motional effects caused by the hopping of electrons between donor impurities. This suggestion, which is based on the measurements on samples at a single temperature, namely $77^{\circ}K$, is in disagreement with the present results which show that motional effects are unlikely to be important. The dependence of the linewidth on impurity concentration in the n-type GaP samples at $77^{\circ}K$, which was obtained in the present work (see Figs. 7.12(a) and 7.12(b)), is similar to that given by Title, but the observed increase in linewidth with respect to increasing concentration is inconsistent with the suggested dependence of the linewidth on motional effects[23]. It is hoped that further measurements on samples containing

a wider range of impurity concentrations ($10^{16}cm^{-3}$ to $10^{20}cm^{-3}$) will help to elucidate the concentration dependence of the linewidth.

7.2.3 Results from the Si-doped GaP samples

The E.P.R. resonance from the Si-doped GaP shows a marked difference from that obtained from GaP doped with Group VI impurities. E.P.R. was not observed from samples DE 161 and DE 158 but a resonance line was observed from the sample DE 156. The linewidth of the resonance line was 12 (±2)mT and the g-value was isotropic and had a magnitude of 1.9950 (±0.0005). The lineshape could not be analysed owing to the small signal to noise ratio. Also, the resonance was not observed at temperatures above $4.2^{o}K$.

Owing to the lack of data it is difficult to make a comprehensive analysis of the E.P.R. from Si-doped GaP. The above g-value is in agreement with the value g = 1.994 calculated in terms of the formula given by Roth[24] (see section 7.2.2(a)) but in this calculation it is assumed that the wavefunction of an electron at an impurity atom corresponds to a singlet state. In section 2.4 it has been shown that electrons from Group IV atoms may occupy a triplet state and the calculated g-values of these electrons has not been obtained in the present work. Also the cause of the large value of the linewidth has not been explained.

7.3 Conclusions

(a) Electron transport properties in samples at temperatures in the range 100°K to 293°K

The results of the conductivity and Hall effect measurements of electrons in samples of n-type GaP, at temperatures in the range 100°K to 293°K are in agreement with data recently published by other workers[5,10,12,13]. The analysis of the donor ionization energy gives values of E_D which compare with those given by other workers[5,12] but the dependence of E_D on the donor impurity concentration has not been firmly established from the present results because of the limited number of samples on which measurements were made.

The present values of the effective masses m_ℓ and m_t are in agreement with those given by Montgomery[10]. However the inaccuracies in these values are approximately (±50%) and hence further measurements are necessary to substantiate these values.

From the temperature dependence of the mobility of electrons in the n-type GaP samples, at temperatures in the range 120°K to 293°K, it can be inferred that two types of electron scattering processes are likely to be significant, namely acoustic phonon scattering and the combined scattering from lattice defects and optical phonons. The relative importance of these two processes cannot be assessed at present owing to insufficient data concerning the deformation potential, D_u, and the lattice defect structure in GaP. However, in order to assess the importance of the lattice defect structure, it is hoped to make

further measurements of the mobility of electrons in n-type GaP and to correlate these with studies of the defect structure in GaP as observed by electron microscopy.

(b) Electron transport properties in samples at temperatures below 50°K

The Hall effect and conductivity of electrons in one S-doped GaP sample (DE 178) at low temperatures has been analysed in terms of impurity band conduction processes. The ratio, b, of the mobility of electrons in the conduction band to their mobility in the impurity band has been found to be approximately 100. Other information concerning the value of b in n-type GaP has not been obtained by other workers, but Basinski and Oliver[29] have found values of b in the range 2.48 to 25.8 for n-type GaAs.

More detailed measurements are necessary to make a comprehensive analysis of impurity band conduction processes in n-type GaP. In particular the Hall effect data, obtained in the present work, should be extended to include measurements on the samples at temperatures of up to approximately 500°K, since these measurements would provide a reliable value of the parameter $(R_H)_{exh}$. Also, the present Hall effect data for samples at low temperatures (below 50°K) was very inaccurate and this was thought to arise from inadequate control of the sample temperature. With the present system sample temperature was controlled to within ±1°K, but with a commercial controller it would be possible to control the sample temperature to within ±1/10°K.

(c) Electron transport properties in samples at temperatures in the range 50°K to 100°K

The conductivity and Hall effect measurements of electrons in n-type GaP samples at temperatures in the range 50°K to 100°K are in agreement with those obtained recently by Hara and Akasaki[13]. The temperature dependence of the electron mobility shows an abrupt decrease in mobility for sample temperatures of approximately 60°K and below and this has been explained in terms of impurity band conduction processes. For samples at temperatures in the range 80°K to 100°K it is proposed that the electron mobility is limited by ionized impurity scattering.

(d) E.P.R. of electrons in GaP containing S and Te impurities

The g-values of the resonances from electrons in S-doped and Te-doped GaP have been explained in terms of the theory given by Roth[24]. There is however a small discrepancy between the measured and calculated g-values and a similar discrepancy has been observed for electrons in n-type silicon. The theoretical calculation of the g-values for electrons in n-type silicon have been revised by Liu[30] and these g-values have been found to be in excellent agreement with the experimental values. However, there is insufficient data concerning the band structure of GaP for such a calculation to be made for the g-values of electrons in n-type GaP.

It is hoped to make future measurements which will include the determination of the values of the g-tensor, $g_{\parallel}$ and $g_{\perp}$. These values can be obtained from E.P.R. measurements involving the application of a stress to the GaP sample and can provide an estimation of the effective masses m_{ℓ} and m_t. It would then be possible to correlate the values of m_{ℓ} and m_t obtained from E.P.R. and conductivity and Hall effect measurements.

Several interpretations have been given of the magnitude of the linewidth of the resonance line observed in the n-type GaP samples. For the samples with a low impurity concentration (e.g. the Te-doped sample in which $N_D \simeq 2 \times 10^{17} cm^{-3}$) it is thought that the hyperfine interaction between the magnetic moments of the electrons and the nuclear magnetic moments of the Ga and P nuclei is a possible source of the linewidth. However, in the sample DE 178 ($N_D = 1 \times 10^{19} cm^{-3}$) at low temperatures (less than $30^{\circ}K$) the magnitude of the linewidth can be explained in terms of life-time broadening[26] and at higher temperatures (above $60^{\circ}K$) the Orbach relaxation process[28] is thought to give rise to a significant broadening of the E.P.R. lines.

The above interpretations are not conclusive since it is difficult to state precisely whether the electrons are at isolated donor impurities, in an impurity band, or in the conduction band. Table 7.10 is given in an attempt to clarify and summarise the evidence pertaining to the source of the E.P.R. line in the S- and Te-doped samples. The two features which are hardest to resolve are the

Lorentzian shaped line being independent of temperature and impurity concentration at low temperatures and the temperature dependence of the linewidth at higher temperatures.

Table 7.10

Evidence for the origin of the observed E.P.R. lines in S- and Te-doped GaP

	Electrons localized at donor impurity atoms	Electrons in the impurity band at all temperatures at which E.P.R. is observed	Electrons in the impurity band at low temperatures and the conduction band at high temperatures
Lineshape	X *	✓	✓
Temperature independence of $\Delta B_{constant}$ at "low" temperature	✓	✓	✓
Concentration independence of $\Delta B_{constant}$ at "low" temperatures	✓	✓ ** X †	✓ ** X †
Magnitude of $\Delta B_{constant}$	✓	✓	✓
T^n dependence of ΔB at "high" temperatures	✓	X	X
exp $\Delta E/kT$ at "high" temperatures	✓	✓	X
Comparison of the concentration of electrons with N_D	✓	✓	X

✓ explanation possible

X explanation not possible

* Lineshape is 50% Lorentzian for the Te-doped sample

** if scattering from defects is dominant, ✓ is appropriate

† if scattering from impurities is dominant, X is appropriate.

The weight of the evidence is slightly towards the unpaired electrons being localized at the donor impurity atoms for the most lightly doped sample (Te-doped GaP) but it is likely that the electrons in the highly doped sample (DE 178) occupy an impurity band.

The present limitations on the E.P.R. measurements were due to the small size of the samples and to the restricted sensitivity of the E.P.R. spectrometer. The recent production of large single crystals of GaP[31] is likely to alleviate the first of these limitations and it will be possible to extend the E.P.R. measurements to include (a) the E.P.R. on samples of n-type GaP with donor concentrations lower than those examined in the present work, and (b) the E.P.R. on samples at temperatures greater than those used in the present work.

(e) E.P.R. of electrons in GaP containing silicon impurity

Little information has been gained from the E.P.R. results obtained from the Si-doped GaP. The marked difference between the E.P.R. from the Si-doped GaP and S-doped and Te-doped GaP is chiefly in the magnitude of the linewidth of the resonance line in the samples at 4.2°K (12 (±2)mT for the Si-doped sample and between 4.5(±0.2) and 6.0(±0.2) for the S- and Te-doped samples). This difference has not been explained in the present results but it is hoped that future E.P.R. measurements on GaP containing germanium or carbon impurities may provide useful information.

(f) New materials

Very recently large single crystals of GaP have been grown by the liquid encapsulation Czochralski method[31] and it is hoped that future measurements will include the E.P.R. and transport properties of electrons in these crystals. The results from such crystals containing shallow donor impurities could then be compared with the present results which were obtained from crystals grown by the epitaxial deposition technique. Also, other impurities could be introduced into the large crystals by diffusion processes (e.g. transition metal impurities) and the electrons associated with these impurities could be investigated by the E.P.R. techniques.

Finally, there has recently been a great deal of interest shown in the mixed Group III - V semiconductors with a view to obtaining semiconductors with a direct band gap corresponding to optical transitions. Since the E.P.R. from electrons associated with shallow donor impurities in semiconductors gives information about the band structure it is thought that such measurement on mixed Group III - V semiconductors will provide valuable information about their band structures. To date, only E.P.R. data on the mixed elemental semiconductors, Si/Ge has been reported[32] and it is hoped to make E.P.R. measurements in the future on electrons from shallow donor impurities in GaP/GaAs mixed semiconductors.

REFERENCES

1. G.J. Van der Pauw, Philips Res. Repts., 13 1 (1958).
2. O.V. Emel'yanenko et al., Soviet Phys. Solid State, 7 1063 (1965).
3. A.R. Hutson, Phys. Rev., 108 222 (1957).
4. G.L. Pearson and J. Bardeen, Phys. Rev., 75 865 (1949).
5. H.C. Montgomery and W.L. Feldman, J. Appl. Phys., 36 3228 (1966).
6. M. Gershenzon et al., Phys. Rev., 133, 269 (1964).
7. D.A. Kleinman and G. Spitzer, Phys. Rev., 118 110 (1960).
8. T.S. Moss, A.K. Walton and B. Ellis, Proc. Int. Conf. on Semiconductors (Exeter), Inst. of Phys. and Phys. Soc., p.295 (1962).
9. N.F. Mott and W.D. Twose, Adv. in Phys., 13 107 (1961).
10. T.N. Morgan, Phys. Rev. Letts., 21 819 (1968).
11. H.C. Montgomery, J. Appl. Phys., 39 2002 (1968).
12. A.S. Epstein, J. Phys. Chem. Solids, 27 1611 (1966).
13. T. Hara and I. Akasaki, J. Appl. Phys. 39, 285 (1968).
14. R.A. Smith, "Semiconductors" (C.U.P. 1961).
15. W.G. Oldham, J. Appl. Phys., 36 2887 (1965).
16. C. Frosh et al., Symposium, Battelle Memorial Institute (1959).
17. H.F. Flicker et al., J. Appl. Phys., 35 2959 (1964).
18. T. Miyauchi et al., Jap. J. of Appl. Phys., 6 1409 (1967).
19. P.J. Dean et al., J. Appl. Phys., 39 5631 (1968).
20. J.M. Whelan et al., Proc. Int. Conf. on Physics of Semiconductors (Prague) p.943 (1960).

21. E.A. Gere, Private communication.

22. F. Dyson, Phys. Rev., 98 349 (1955).

23. R.S. Title, Phys. Rev., 154 668 (1967).

24. L.M. Roth, Phys. Rev., 118 1534 (1960).

25. D.K. Wilson and G. Feher, Phys. Rev., 124 1068 (1961).

26. R.J. Elliott, Phys. Rev., 96 266 (1954).

27. Y. Yafet, Solid State Phys., 14 90 (Academic Press 1963).

28. R. Orbach, Proc. Phys. Soc. (London), A77 821 (1960).

29. J. Basinski and R. Oliver, Can. J. Phys., 45 119 (1967).

30. L. Liu, Phys. Rev., 126 1317 (1962).

31. S.J. Bass and P.E. Oliver, Proc. 2nd Int. Conf. on Crystal Growth, 3,4 286 (1968).

32. I.G. Gverdtsiteli et al., Soviet Phys. Solid State, 9 1328 (1967).

APPENDIX I

Wavefunctions of electrons bound to shallow donor impurities in GaP (or other indirect band-gap semiconductors)

In section 2.4 the wavefunctions for shallow donor electrons in GaP have been given as

$$\psi^{i}_{\underline{k}}(\underline{r}) = \sum_{j} \alpha^{i}_{j} F_{j}(\underline{r}) e^{i\underline{k}^{j}_{o}\cdot\underline{r}} u^{j}_{\underline{k}_{o}}(\underline{r}) \qquad \text{A.1.1}$$

By applying Group Theoretical methods[1] it can be shown that these wavefunctions must form a basis for the irreducible representations of the Tetrahedral Group, T_d, whose character table is given in Table A.1.

Table A.1 : Character table of the Tetrahedral Group

Irreducible Representations \ Group Element operators	E	$8C_3$	$3C_2$	$6\sigma_d$	$6S_4$
A_1	1	1	1	1	1
A_2	1	1	1	-1	-1
E	2	-1	2	0	0
T_1	3	0	-1	1	-1
T_2	3	0	-1	-1	1

The energy band structure of GaP has been shown in Fig. 2.6. If the conduction band minima occur inside the Brillouin zone boundary there are six distinct minima along (100)-type directions; if the minima occur at the Brillouin zone boundary there are only three distinct minima. In both these cases the symmetry of the wavefunctions associated with a conduction band minima can be s-like or p-like, as described in section 2.4.

By applying the Group Element operators to the wavefunctions given in equation A.1.1 the representations, carried by these functions, are obtained. The following notation will be used:-

$$(\Gamma_\Delta)_s \quad (\Gamma_\Delta)_p \quad (\Gamma_x)_s \quad (\Gamma_x)_p$$

denoting respectively the representations carried by wavefunctions associated with, the six conduction band minima having s-like symmetry, the six conduction band minima having p-like symmetry, the three conduction band minima having s-like symmetry and the three conduction band minima having p-like symmetry.

The characters of the representations defined above are shown in Table A2.

Table A.2 : Characters of the representations carried by wave-functions given by equation A.1.1

Representations \ Group Element operators	E	$8C_3$	$3C_2$	$6\sigma_d$	$6S_4$
$(\Gamma_\Delta)_s$	6	0	2	0	2
$(\Gamma_\Delta)_p$	6	0	2	0	2
$(\Gamma_x)_s$	3	0	3	1	1
$(\Gamma_x)_p$	3	0	-1	-1	1

(Note The wavefunctions associated with the conduction band minima transform like, x, -x, y, -y, z, -z under the Group Element operators[1].)

By Group Theoretical methods[1] it can be shown that the representation, Γ_ψ, carried by any function, ψ, can be decomposed into irreducible representations by the use of the equation

$$\Gamma_\psi = \sum_\Gamma a_\gamma \Gamma \qquad \text{A.1.2}$$

where Γ extends over all the irreducible representations and a_γ is the coefficient for the corresponding irreducible representation.

The value of a_γ is obtained from the equation:-

$$a_\gamma = \frac{1}{h} \sum_R \chi_{\Gamma_\psi}(R).\chi_\Gamma(R) \qquad \text{A.1.3}$$

where h is the order of the Group

and R extends over all the Group Element operators.

The representations, given in Table A.2, decompose as follows:-

$$\begin{aligned} (\Gamma_\Delta)_s &\rightarrow A_1 \,,\; E \,,\; T_2 \\ (\Gamma_\Delta)_p &\rightarrow A_1 \,,\; E \,,\; T_2 \\ (\Gamma_x)_s &\rightarrow A_1 \,,\; E \\ (\Gamma_x)_p &\rightarrow T_2 \end{aligned} \qquad \text{A.1.4}$$

The wavefunctions of electrons from shallow donor impurities in GaP must, therefore, be of the symmetry types shown in A.1.4 and these wave functions may give rise to different energy levels. However, Group Theoretical methods cannot be used to determine the energies of these levels; further theoretical calculation or experimental measurements are necessary.

Explicit forms of the wavefunctions of the symmetry types shown in A.1.4 may be obtained by the use of projection operators. A projection operator has the form:

$$P_\Gamma = \frac{1}{h} \sum_R \chi(\Gamma)R \qquad \text{A.1.5}$$

and the wavefunction, ψ_Γ, for the representation Γ is given by

$$\psi_\Gamma = P_\Gamma \psi^i_{\underline{k}}(\underline{r}) \qquad \text{A.1.6}$$

where $\psi^i_{\underline{k}}(\underline{r})$ is given in equation A.1.1.

The linearly independent functions of the symmetry types shown in A.1.4 are given in terms of the coefficients $\alpha_j^{\,i}$ as follows:

$$
\begin{aligned}
A_1 \text{ singlet} \quad & \alpha_j^{\,1} = 1/\sqrt{6} \quad (1, 1, 1, 1, 1, 1) \\
E \text{ doublet} \quad & \alpha_j^{\,2} = 1/\sqrt{12} \quad (1, 1, 1, 1, -2, -2) \\
& \alpha_j^{\,3} = \tfrac{1}{2} \quad (1, 1, -1, -1, 0, 0) \\
T_2 \text{ triplet} \quad & \alpha_j^{\,4} = 1/\sqrt{2} \quad (1, -1, 0, 0, 0, 0) \\
& \alpha_j^{\,5} = 1/\sqrt{2} \quad (0, 0, 1, -1, 0, 0) \\
& \alpha_j^{\,6} = 1/\sqrt{2} \quad (0, 0, 0, 0, 1, -1)
\end{aligned}
\qquad \text{A.1.7}
$$

$$
\begin{aligned}
A_1 \text{ singlet} \quad & \alpha_j^{\,1} = 1/\sqrt{3} \quad (1, 1, 1) \\
E \text{ doublet} \quad & \alpha_j^{\,2} = \tfrac{1}{2} \quad (1, -2, 1) \\
& \alpha_j^{\,3} = 1/\sqrt{2} \quad (1, 0, -1)
\end{aligned}
\qquad \text{A.1.8}
$$

$$
\begin{aligned}
T_2 \text{ triplet} \quad & \alpha_j^{\,4} = (1\ 0\ 0) \\
& \alpha_j^{\,2} = (0\ 1\ 0) \\
& \alpha_j^{\,3} = (0\ 0\ 1)
\end{aligned}
\qquad \text{A.1.9}
$$

The wavefunctions of the symmetry types shown in A.1.7, A.1.8 and A.1.9 correspond respectively with those given by the equations 2.21, 2.22 and 2.23.

Reference

(1) Falicov, "Group Theory and its Physical Applications" (Chicago University Press, 1962)

APPENDIX 2

The effect of a sample, of conductivity σ, on the Q factor of a cavity operating in the H_{011} mode.

In equation 6.18 a value of Q_L has been given as

$$Q_L = \frac{\omega \int_{\text{cavity}} \frac{b^2}{\mu_o} \tau}{\int_{\text{sample}} \sigma E^2 d\tau} \qquad \text{A.2.1}$$

For a cavity operating in an H_{011} mode the electromagnetic field configuration is given by[1]

$$B_r = \frac{b_o J_o'(K_c r) \cos(\pi z/d)}{\left[1 + \{(k_c a)\frac{d}{\pi a}\}^2\right]^{\frac{1}{2}}} \qquad \text{A.2.2}$$

$$B_z = \frac{b_o J_o(K_c r) \sin(\pi z/d)}{\left[1 + \{\pi a/(k_c a)d\}^2\right]^{\frac{1}{2}}} \qquad \text{A.2.3}$$

$$E = \left(\frac{1}{\mu\mu_o\varepsilon\varepsilon_o}\right)^{\frac{1}{2}} b\, J_o'(k_c r) \sin(\pi z/d) \qquad \text{A.2.4}$$

where $k_c = 2\pi/\lambda_c$ and $\lambda_c = 1.64a$

a and d are the radius and length of the cavity respectively.

and the cylindrical axes are shown in Fig. A.2.1.

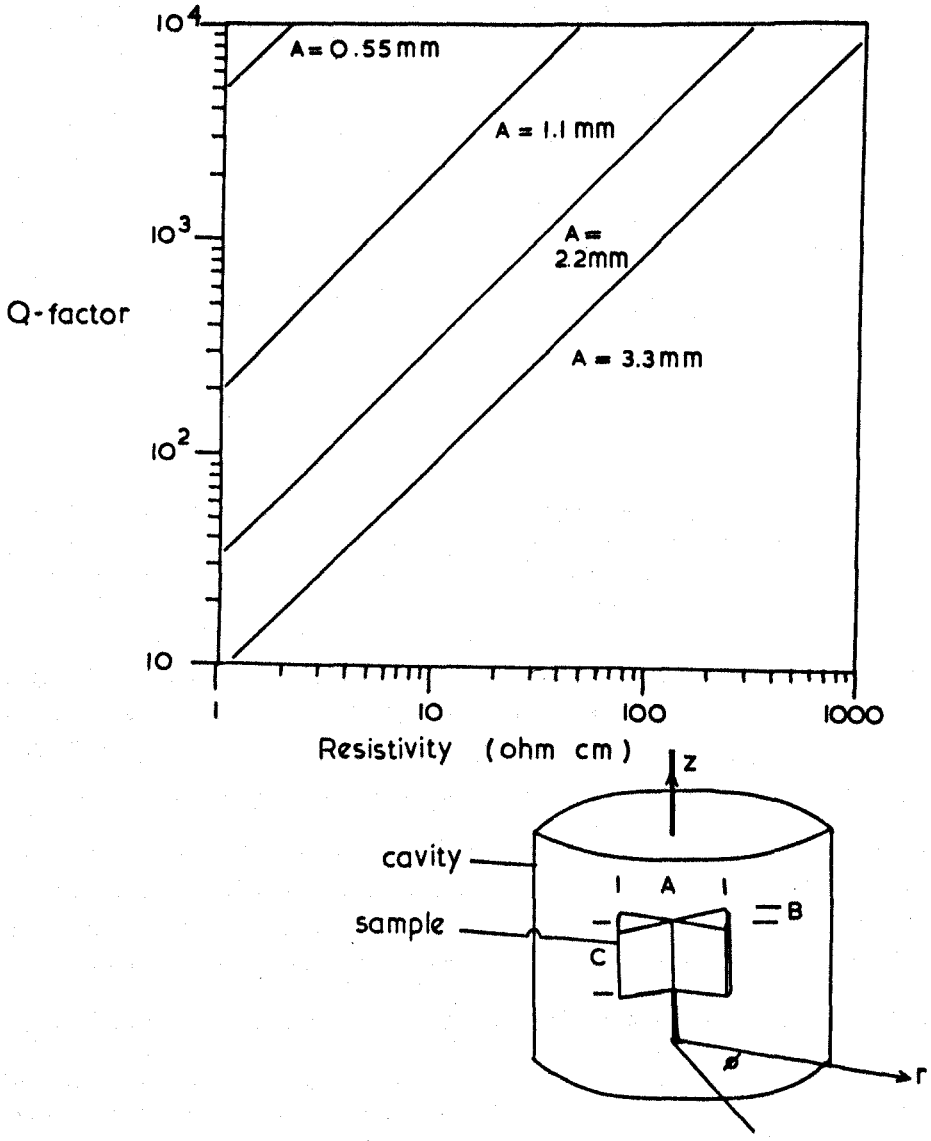

FIG. A 2.1 DIAGRAM SHOWING THE EFFECT OF A_1 SAMPLE ON THE CAVITY Q FACTOR

For an axially situated cylindrical sample of radius r_s and length $\frac{1}{2}d$, the value of Q_L becomes[1]:-

$$Q_l = \frac{\omega\varepsilon\varepsilon_o}{\sigma} \frac{0.0811\ (\pi a^2 d)\ b_o^2}{\pi(0.41d)\ r_s^2\{f(J)\}\ b_o^2} \qquad \text{A.2.5}$$

where $f(J) = J_o^2(k_c r_s) - \frac{2}{k_c r_s} J_o(k_c r_s)\ J_1(k_c r_s) + J_1^2(k_c r_s)$

N.B. This calculation ignores any perturbation of the electromagnetic field configuration arising from the presence of a sample of relatively high conductivity in the cavity.

The samples which were used in the present E.P.R. measurements were thin wafers and therefore values of Q_L were calculated for samples of the shape illustrated in Fig. A.2.1. The dimensions of the samples were as follows:

A = 0.55mm, 1.1mm, 2.2mm, 3.3mm.

B = 100μm.

C = 0.55cm.

The dependence of Q_L on the sample conductivity, for the different values of A, is shown in Fig. A.2.1.

Reference

(1) C.P. Poole, "Electron Spin Resonance" (Wiley 1966).

```
   4 CONTINUE
     FMAX=FINT(1)
     LMAX=LORENT(1)
     GMIN=GAUSS(1)
     LMIN=LORENT(1)
     GMAX=GAUSS(1)
     DO 5 K=2,NPNT
     IF(GAUSS(K).LT.GMIN) GMIN=GAUSS(K)
     IF(LORENT(K).LT.LMIN) LMIN=LORENT(K)
     IF(FINT(K).GT.FMAX) FMAX=FINT(K)
     IF(LORENT(K).GT.LMAX) LMAX=LORENT(K)
   5 IF(GAUSS(K).GT.GMAX) GMAX=GAUSS(K)
     WRITE(2,1022) LMAX,LMIN,GMAX,GMIN
1022 FORMAT(4F10.4)


     DO 6 K=1,NPNT
     LORENT(K)=FMAX*(LORENT(K)-LMIN)/(LMAX-LMIN)
     GAUSS(K)=FMAX*(GAUSS(K)-GMIN)/(GMAX-GMIN)
     WRITE(2,1021) LORENT(K),GAUSS(K),FINT(K)
1021 FORMAT(1H ,3F10.4,10X,F10.4)
   6 CONTINUE
     DO 7 K=2,NPNT
     SLOREN(K)=0.5*(LORENT(K)+LORENT(K-1))*(PR(K)-PR(K-1))+SLOREN(K-1)
   7 SGAUSS(K)=0.5*(GAUSS(K)+GAUSS(K-1))*(PR(K)-PR(K-1))+SGAUSS(K-1)
     WRITE(2,1005) SLOREN(NPNT),SGAUSS(NPNT)
1005 FORMAT(1H0,10X,25HLORENTZIAN INTEGRAL IS = ,F10.4//10X,22HGAUSSIAN
    1INTEGRAL IS = ,F10.4)
     XLOREN=1.02*SLOREN(NPNT)
     XGAUSS=0.98*SGAUSS(NPNT)
     IF(CSINT.GT.XLOREN.OR.CSINT.LT.XGAUSS) GO TO 10
     PERL=(100.*CSINT-100.*SGAUSS(NPNT))/(SLOREN(NPNT)-SGAUSS(NPNT))
     WRITE(2,1006) PERL
1006 FORMAT(1H0,30HPERCENTAGE LORENTZIAN SHAPE = ,F10.4)
     GO TO 11
  10 WRITE(2,1007)
1007 FORMAT(1H0,10X,32HINTEGRAL OUTSIDE PERMITTED LIMIT)
     GO TO 13
  11 CALL ORIGIN(200,1)
     CALL MOVE(0,2200)
     DO 12 K=1,NPNT
     DLOREN(K)=-2.*(PR(K)-ARMAX)*LORENT(K)*LORENT(K)
  12 DGAUSS(K)=-4.*(PR(K)-ARMAX)*GAUSS(K)/(FDMAX-FDMIN)*(FDMAX-FDMIN)
     CALL SCALE(PR,10.0,NPNT,1)
     CALL SCALE(POS,8.0,NPNT,1)
     CALL SCALE(DLOREN,8.0,NPNT,1)
     CALL SCALE(DGAUSS,8.0,NPNT,1)
     CALL LINE(PR,POS,NPNT,1,0,1)
     CALL LINE(PR,DLOREN,NPNT,1,1,3)
     CALL LINE(PR,DGAUSS,NPNT,1,1,4)
   1 CALL MOVE(2500,0)
  13 CONTINUE
     STOP
     END
```